2003

Analysis and design of a calcium-based sulfur sorbent for applications in integrated gasification combined cycle energy systems

David Johann Ludwig Hasler
Iowa State University

Analysis and design of a calcium-based sulfur sorbent for applications in Integrated Gasification Combined Cycle energy systems

by

David Johann Ludwig Hasler

A dissertation submitted to the graduate faculty

in partial fulfillment of the requirements for the degree of

DOCTOR OF PHILOSOPHY

Major: Chemical Engineering

Program of Study Committee:
Thomas D. Wheelock, Co-major Professor
Kristen P. Constant, Co-major Professor
Laxmangudi K. Doraiswamy
Thomas D. McGee
Brent H. Shanks

Iowa State University

Ames, Iowa

2003

ProQuest Information and Learning Company
300 North Zeeb Road
P.O. Box 1346
Ann Arbor, MI 48106-1346

Graduate College
Iowa State University

This is to certify that the doctoral dissertation of

David Johann Ludwig Hasler

has met the dissertation requirements of Iowa State University

Signature was redacted for privacy.

Co-major Professor

Signature was redacted for privacy.

Co-major Professor

Signature was redacted for privacy.

For the Major Program

Table of Contents

List of Figures

List of Tables

Acknowledgment

This thesis was prepared with the support of the U.S. Department of Energy (DOE), under Award No. DE-FG26-99FT40587. However, any opinions, findings, conclusions, or recommendations expressed herein are those of the author and do not necessarily reflect the views of the DOE.

Chapter 1. General Introduction

1.1 Introduction

The search for clean and efficient energy sources is an ongoing process. In the past 150 years the world wide energy demand has increased by a factor of 20. By the year 2100 it could be up to five times what it is now. The five main sources of energy for electrical power production are oil, gas, coal, nuclear and hydroelectric. Based upon energy consumption of commercially traded fuels, oil accounts for roughly 40%, gas 22.5%, coal 27.5%, nuclear 7.5% and hydroelectric 2.5% (BP, 1995). At the current rate of energy consumption the estimated world reserves of the nonrenewable energy sources are 500 years with hard coal and lignite, 40 years with oil, 56 years with natural gas and 40 years with uranium (World Resources Institute, 1997). Aside from the obviously large resources of coal, which make it an attractive fuel, such resources enable other countries without access to domestic petroleum to rely less heavily upon foreign oil. Fortunately, newer technologies have already been developed and are being improved upon to efficiently use coal to generate electricity.

In the past, coal in large lumps was combusted to generate steam for use in electric power plants. These original power plants could only reach a maximum efficiency of 30%. By finely pulverizing the coal prior to burning, the efficiency was increased to 35%. As the technology was advanced, it was realized that by first gasifying the coal with an air and steam mixture at high temperatures and utilizing the hot fuel gas directly in a gas turbine, the efficiency was increased. Furthermore, when the exhaust gas from the turbine was used to generate steam to power another turbine, the efficiency was increased even more. The

combined system is known as an integrated gasification-combined cycle system (IGCC). Today, plants based on the IGCC system are achieving efficiencies of over 40%. Currently, IGCC power plants are used in several countries including the United States, the Netherlands, Spain, Germany, Japan and China. What is even more remarkable is that the highly efficient IGCC system also includes a method for removing toxic and corrosive gases such as H_2S, COS and HCl and also particulates. Such methods are referred to as hot gas clean up or HGCU.

Depending upon the source of the coal it can contain up to 2% volume sulfur in the gaseous form. Conventional power plants can only remove 90% of the sulfur using a cold removal process involving an aqueous agent. But, with an IGCC system it is possible to remove over 99% of the sulfur and still attain an efficiency of over 40%. Because of an IGCC system's higher efficiency and improved sulfur removal capabilities, it releases 30% less SO_x and NO_x than a conventional power plant.

Different types of systems for gasifying coal are available. These systems and their operating temperatures include moving bed gasifiers (400-800°C), fluidized bed gasifiers (400- 1100°C), entrained-flow gasifiers (1200-2000 °C), and molten salt bath gasifiers (1600°C). Following the gasifier in an IGCC system is the HGCU. Within the HGCU particulates, vaporized alkali metals and sulfur compounds are removed since they are corrosive and detrimental to gas turbines and the environment. The process unit used to remove the sulfur compounds is referred to as the hot gas desulfurizer or HGD. Within this unit sulfur compounds such as H_2S and COS are removed by intermixing the hot coal gas with solid metal oxide sulfur sorbents, which react to form metal sulfides.

Supplying the coal gas at temperatures of 800°C and above to a gas turbine can increase the efficiency of the overall power generation system by 6% (Furimsky and Yumura, 1986). Because a higher efficiency can be achieved by not cooling the coal gas before it reaches the turbine, the gas should be cleaned at the gasifier outlet temperature. By just increasing the temperature at which the HGCU operates by 200°C the efficiency will be increased by 1% (Barth'el'emy, 1991). A 1% increase in efficiency will reduce the total CO_2 output by 2%. Thus, the overall efficiency of an IGCC system is strongly dependent on the temperature at which the hot coal gas is cleaned.

There are many solid sorbents currently being tested for use in a HGD. The most widely known sorbent is made by Phillips petroleum and is called Z-Sorb®. The base compound in Z-Sorb® is ZnO. Z-Sorb® works quite well at temperatures below 700°C but tends to vaporize in the highly reducing atmosphere of gasified coal at higher temperatures. Other sorbents that have been studied contain compounds such as CaO, FeO, MnO, $BaCO_3$, CoO, MoO_2, SrO, WO_3, V_2O_3, and CuO. Above 800 °C, compounds such as V_2O_3, WO_3, MoO_2, FeO, CuO, and CoO also become reduced or inactive unless they have other elements included that increase the materials resistance to reduction at higher temperatures. But the addition of non-reactive compounds lowers the overall capacity of the sorbent for sulfur uptake.

For an IGCC system it is advantageous to employ a regenerable sorbent for hot gas cleanup because less sorbent material is needed and no solid waste is generated for disposal. If a once-through sorbent is used, it must be converted to a benign form prior to discarding it. An example would be CaO, which reacts with H_2S to form CaS. If the CaS is buried in a

landfill, it will react with water to form H_2S again. Therefore, it has to be converted to a more stable form such as $CaSO_4$ prior to disposal. Since the conversion will not proceed readily past 40% it is not an effective solution. Another advantage gained with a regenerable sorbent is the recovery of a useful by-product, i.e., SO_2 which can be converted into sulfuric acid or elemental sulfur; both of which are used by many industries and can be sold as a by-product.

While most solid sorbents used for sulfur removal cannot exceed temperatures of 400 to 800°C, calcium oxide can operate effectively in the 800°C to 1400°C range. Calcium oxide can be generated from naturally occurring limestone ($CaCO_3$), dolomite ($CaCO_3 \cdot MgCO_3$), or calcium sulfate hemihydrate ($CaSO_4 \cdot ½ H_2O$). Limestone is commonly used as a sorbent in fluidized bed gasifiers and combustors. Although it works quite effectively, it is used once and then discarded. If the product is in the form of calcium sulfate, it can be used in wallboard material or dumped into a landfill. One of the disadvantages of CaO is that it is friable, thus eliminating it from use in a moving or fixed bed system. In order to overcome this disadvantage Akiti and Wheelock (2002) developed a process for pelletizing limestone or $CaSO_4 \cdot ½ H_2O$ and then coating the resulting pellets with a thermally stable and strong material made of alumina. These new core and shell pellets enabled the use of CaO in a fixed or moving bed HGD process. Prior to developing the pelletization process, Jagtap and Wheelock (1996) discovered a method to efficiently regenerate a CaO sorbent used for capturing H_2S. These two developments made it possible to utilize CaO as a sorbent material that is effective at high temperature, regenerable, attrition resistant and suitable for a moving or fixed bed HGD process.

The overall objective of this research project was to improve the durability and life cycle performance of the core and shell sorbent. To meet this objective, both the core and shell required improvement. Since the reactivity of the CaO cores declined with usage, the reason for this decline required investigation, and a means for preventing the decline needed development. Although a reasonably good shell material had been developed before, its formulation had not been optimized so further improvement was possible.

Another objective was to find a suitable and practical model for representing the sulfidation process involving the reaction of H_2S with an agglomerated pellet of CaO. Such a model was needed to guide further development and application of the sorbent.

1.2 Literature Review

The desulfurization process in a hot gas clean up unit (HGCU) is complicated by the reactions that take place in such a harsh and reactive atmosphere. Since coal gas is highly reducing due to the presence of large concentrations of H_2 and CO, the reduction of various metallic materials to their elemental form can occur upon exposure to the gas. Many other researchers have tested a wide range of elements and compounds as possible sorbents to withstand the reducing nature of the coal gas, but unfortunately the ability of the coal gas to reduce a compound to its elements also increases with temperature. Higher temperatures not only increase the rate of reduction of various compounds, but also increase the rate of sintering. Another problem is the attrition of solid sorbents. The attrition occurs due to the mechanically stressful volume expansions during the regeneration step and to the abrasive

mechanical forces that are exacted upon the sorbent materials in fixed, moving bed and fluidized bed reactors.

This review of metal oxide sorbents begins with materials normally used in the low temperature regime and concludes with high temperature materials. Following the general materials review, an overview of the materials that have been studied at Iowa State will be covered. In addition, studies of the reactivity and sintering of $CaCO_3$ and CaO are included, along with models representing the gas-solid reactions that take place.

1.2.1 *Metal oxide sorbents*

One of the earliest forms of solid sorbent used for removing H_2S is iron oxide. It was first used in the United States in the late 1800's to early 1900's to remove H_2S from 'town gas' (van der Ham etal., 1996). In the 1970's it was used in combination with other materials and studied extensively. During this time it was found to be thermally unstable and very susceptible to attrition.

Although iron oxide has proven to be thermally unstable, it has still been used successfully in Japan in a demonstration plant. A process based upon crushed iron ore was developed by Ishikawayama-Harima Heavy Industries (IHI) and the New Energy & Industrial Technology Development Organization (NEDO) of Japan (Kobayashi, 1990). It uses a two-stage bubbling fluidized bed (BFB), in which Fe_3O_4 in the bottom of the bed reacts with H_2S to form FeS. In the upper part of the bed regenerated sorbent enters and is reduced from Fe_2O_3 to Fe_3O_4 by the reducing gases; it then reacts to form a coal gas lean in H_2S. For the regeneration process the FeS is drawn from the bottom of the desulfurizing bed into another BFB. In the second BFB, FeS is oxidized with air and mixed with recycled gas that is used

as a temperature stabilizer. The resulting SO_2 is then transported to another reactor where it is reduced to elemental sulfur. The performance results from the study revealed that the sorbent is capable of removing 95% of the H_2S from the coal gas at a temperature of 460°C. This was possible only if there was less than 10% H_2O present. The results indicate that the overall performance of the iron ore was stable and consistent for a plant operating at a rate of 200 tons of coal per day. Unfortunately, a higher degree of H_2S removal and much higher temperature stability are needed for effective use in a HGCU, which precludes the use of iron ore by itself.

By adding other components to act as stabilizers and to give the iron oxide better strength and attrition resistance, more effective sorbents have been produced. Such supports were studied by van der Wal (1987) and included SiO_2, Al_2O_3, and TiO_2. The supports were loaded with iron oxide up to 50% by weight using the deposition-precipitation method. Very good results were obtained. By using a SiO_2 carrier, the sorbent was prevented from being reduced to elemental Fe, was not easily deactivated and had a surface area of 200 m^2/g. The sulfidation could be carried out in the temperature range of 300 to 500°C. The sorbent was regenerated by using diluted air with < 0.5 vol% O_2 which resulted in the formation of SO_2 and elemental sulfur within a range of 200-400°C. The maximum capacity was 9 wt% sulfur for a 50 wt% iron oxide loading.

Using the same technique as van der Wal (1987), van Yperen (1994) added MoO_3 as a second component and used aluminum phosphate instead of silica as the support. His results revealed that the Mo reacted with H_2S to form MoS_2. The Mo also prevented iron oxide from forming sulfates when SO_2 was present, while the iron oxide worked to prevent

the MoO_3 from being reduced to its elemental form. The addition of MoO_3 increased the capability of the sorbent to remove H_2S, improved resistance to reduction, and could operate with up to 8 wt% steam. The sorbent was capable of being regenerated with low O_2 concentrations in concentrated SO_2 streams to yield more SO_2 and very little sulfates. Again, the combination of the mixed metal oxides with iron is not useful at high temperatures although the previously described materials proved to be strong and applicable in fluidized bed systems and enabled high sulfur removal. And due to the needed addition of other components to limit the reduction and sulfation of Fe_2O_3, the overall capacity of the sorbents tends to fall. Thus, some of the sorbents contained only 50 wt% Fe_2O_3.

A well-known H_2S sorbent that has been in the commercial market for quite some time is ZnO. Zinc oxide was first used in the petroleum industry as a once-through sorbent, i.e., it was discarded after one use. In the 1980's, researchers began to investigate whether ZnO could work as an effective regenerable sorbent (Flytzani-Stephanopoulos, 1998). It was discovered that there were many drawbacks to using ZnO at high temperatures. Two major effects were the sintering of ZnO and the loss of Zn due to vaporization. Once subjected to the reducing gases in coal gas, ZnO is reduced to its elemental form as liquid Zn and then vaporized at 419°C and above. The results from the sulfidation tests with ZnO indicated that a maximum of only 20% of the available ZnO had reacted due to pore closure. This was attributed to the 1.64 : 1 molar volume ratio of ZnS : ZnO (Jalan et al., 1981; Gibson and Harrison, 1980), but could also have been the result of surface area loss and densification due to sintering effects and the formation of liquid Zn. Since ZnO reacted quite rapidly with H_2S, it was still a very useful sorbent, so researchers began to find ways to improve it.

By adding other compounds to ZnO it was discovered that the detrimental properties of ZnO could be changed. Iron oxide (Fe_2O_3) was initially tested and found not to inhibit the reduction of ZnO; in fact the ZnO was still reduced and vaporized (Flytzani-Stephanopoulus, 1988, 1993) and the material tended to crack. Alumina (Al_2O_3), SiO_2, and Cr_2O_3 were each tested resulting in no improvements of the material. The best results involved the use of TiO_2, which improved the strength and attrition resistance of the material and increased the resistance of the ZnO to reduction (Lew et al., 1989, 1992; Flytzani-Stephanopoulus, 1987, 1988, 1993). During the regeneration phase the TiO_2 also prevented the formation of $ZnSO_4$ (Farha, 1982). The addition of up to 50 wt% TiO_2 helped to decrease the sinterability of ZnS, which was thought to be due to the TiO_2 acting as a physical barrier. During the testing it was discovered that the smaller grains reacted much faster than the larger grains (Lew et al., 1990, 1992), and H_2 concentrations of 1, 10, 20 vol% did not affect the initial surface reaction rate, although at higher conversions the H_2 concentration did affect the rate. Steam was also included in the tests but did not affect the rate of reaction (Lew et al., 1990, 1992). Unfortunately, the initial reaction rate of $ZnTiO_3$ was 1.5-2 times less than ZnO at 873 and 973 K when it contained $\geq$ 25 mol% Ti. During the regeneration and sulfidation cycles it was observed that the ratio of Zn to Ti increased on the surface of the sorbent. It is believed that after multiple cycles this could lead to the formation of ZnO followed by vaporization of Zn (Siriwardane et al., 1992). It should also be considered that the overall capacity drops with an increase in TiO_2 content. Therefore, larger reactors will be needed due to the decreased rate of reaction and lower capacity, and the cost of production will increase.

Phillips Petroleum developed pellets based on $ZnTiO_3$ and pellets based on ZnO with a Ni promoter, commercially known as Z-Sorb®. The pellets were tested in bench scale reactors by General Electric (Ayala et al., 1994). The studies indicated that the $ZnTiO_3$ pellets reduced the bed outlet concentration of H_2S to 20 ppmv while the Z-Sorb® pellets reduced the outlet concentration to 10 ppmv for an overall removal efficiency of 99% after 8 cycles. The zinc titanate ($ZnTiO_3$) pellets exhibited an average loading of 8.9% while the Z-Sorb® pellets had an average loading of 16%. Although the Z-Sorb® pellets exhibited a higher sulfur capacity on a mass basis, the overall bulk density was lower than the $ZnTiO_3$ pellets, thus resulting in a similar bed loading for the two sorbents. But, of all the sorbents that have been commercially made, Z-Sorb® has been the most successful.

During the regeneration of the sorbents at 760°C in air, it was revealed that only the $ZnTiO_3$ pellets mechanically deteriorated. The higher porosity of the Z-Sorb® pellets could explain why it held up better than the $ZnTiO_3$ pellets during the regeneration process, if it enabled the sorbent to better accommodate the large change in volume during regeneration. Another sorbent, called Z-Sorb Three®, exhibited a 50% loss in capacity after 160 hr of operation in a moving bed pilot facility, and the loss was believed due to the effect of steam in the coal gas or regenerator gas (Ayala et al., 1995). The study of Z-Sorb® in a moving bed facility revealed a maximum loading of 30% and an attrition loss of 0.2%.

The ability of ZnO-based materials to remove H_2S to very low levels makes ZnO an attractive material, but the low thermal stability of the material precludes it from use at higher temperatures, i.e., > 700°C. In addition, due to the high concentrations of TiO_2 needed to increase the strength, attrition resistance and reduction potential of the material, the overall

capacity of the sorbent is reduced by a substantial amount. Additional work performed by Pineda et al. (2000) showed that the performance of zinc titanates degraded after multiple cycles in a fixed bed reactor, and that the TiO_2 actually reduced the rate of reaction between ZnO and H_2S. The reduction in performance was attributed to pore volume loss due to sintering. No abrasion resistance tests were performed; therefore, the ability of the sorbent to perform in a large packed or moving bed apparatus is not known.

An element that is capable of enduring higher temperatures than ZnO-based sorbents is Cu. While the Fe and Zn based sorbents are restricted to lower temperatures, generally below 700°C, some Cu-based sorbents can withstand temperatures up to 900°C. However, copper oxide (CuO) by itself cannot withstand the highly reducing atmosphere of coal gas and is quickly reduced to Cu. And it is known that both Cu and CuS sinter rapidly at high temperatures; therefore, the formation of Cu must be avoided while CuS must be stabilized (Flytzani-Stephanopoulos, 1987; Lew, 1990).

Two of the most promising sorbent mixtures of CuO conatain Cr or Ce. The sorbents $CuO\text{-}Cr_2O_3$ and $CuO\text{-}CeO_2$ have been reported to exhibit high reactivity and promising regeneration characteristics (Flytzani-Stephanopoulos, 1998). Studies indicate that complete conversion of CuO takes place at 750°C and the sorbent can be used up to 850°C. The Cu-Cr sorbent has exhibited a capacity of 4.3 wt% while the Cu-Ce sorbent has demonstrated a capacity of 2.2 wt%. During the sulfidation phase the sorbents undergo a reduction process prior to sulfidation, and the sulfidation reaction takes place almost independently of temperature in the range of 650-850°C. The two sorbents, $CuO\text{-}Cr_2O_3$ and $CuO\text{-}CeO_2$, have successfully reduced H_2S levels to less than 1-10 ppmv at 650-850°C with 20 mol% H_2 and

10 mol% H_2O present in the gas stream, and complete regeneration was carried out at 750 °C. No abrasion resistance tests were performed on the sorbents, and the sorbents were treated to only one and a half cycles of sulfidation and regeneration. The ability of these sorbents to perform in industrial reactors over many cycles and under abrasive conditions needs to be explored in greater depth and before conducting meaningful kinetic studies.

The last compounds to be covered are based on Mn, Ce and Ca. Compounds involving these elements are applicable at high temperatures. Manganese (Mn), in the form of either $MnAl_2O_4$ or MnO, is thermodynamically capable of successfully removing H_2S from a gas stream in the temperature range of 127-1127°C (Bakker, et al., 1998). It has been noted that $MnAl_2O_4$ is less favorable than MnO for reaction with H_2S. In addition to reacting with H_2S and COS, MnO also reacts with HCl and HF.

During a study of MnO on different γ Al_2O_3 substrates by Bakker, et al.(1998), it was reported that after 75 cycles of sulfidation and regeneration the surface area of MnO decreased from 122 m^2/g to 25 m^2/g at 1123 K. It was also noted that for a packed bed absorber, H_2O decreased the breakthrough time while CO and H_2 reacted with the H_2O and thus increased the breakthrough time.

The regeneration of the MnS was carried out by using H_2O at 727°C, yielding H_2S as the product gas. Above 727°C, the regeneration gas contained SO_2 and sulfur in addition to H_2S. At temperatures below 550°C, $MnSO_4$ was formed if any SO_2 was present.

The best manganese loading was 6 wt% Mn on γ Al_2O_3, which provided for better stability than a 23% loading, and, in addition, led to a faster regeneration and a more concentrated product gas. During the testing of the sorbent over 100 cycles, the capacity

decreased from a 1.2 : 1 molar ratio of S : Mn during the first few cycles, but no further decrease was observed in subsequent cycles. The final results of the testing indicated that $MnAl_2O_4$ could be used if less than 2 vol% H_2O was present, and the regeneration of MnS was possible if Al_2O_4 was present. No tests were performed for abrasion resistance of the materials, and quantitative measurements of the sorbent strength were not reported. It was assumed that the nonexistence of sorbent breakup in a microreactor after multiple cycles qualified it as a robust sorbent, which is a common assumption among researchers in this field.

In addition to Mn, Ce-based sorbents are also quite effective at high temperatures. Zeng et al. (2000) performed some studies in this area and found that by reducing CeO_2 to Ce_2O_3 the material became a very effective sorbent at high temperatures. Multi-cycle runs were performed with this material in packed bed microreactors with no significant decline in reactivity of the sorbent over many cycles. Unfortunately, no abrasion tests were performed nor were any results on regeneration time reported. Also, it was noted that without pre-reducing the material prior to sulfidation premature H_2S breakthrough occurs. This is a common phenomenon with materials that need to be pre-reduced prior to reaction. The necessity for pre-reduction can lead to premature H_2S spikes in the effluent if it is not carried out sufficiently, especially for fixed bed applications, and can also lower the combustion potential of the gas, producing unwanted declines in power output.

In the search for effective sorbents, it is generally assumed that material performance in a fixed-bed microreactor is indicative of what is possible in an actual industrial system. Any breakup of the materials in a packed or moving bed system will greatly increase the

pressure drop and make the sorbent useless. Therefore, the assumption is a gross overestimation of sorbent performance and utility since the abrasion resistance of a sorbent will be one of the factors determining whether or not it can be used industrially.

The use of CaO in fluidized beds for H_2S removal has been mentioned previously. The high reactivity of CaO and its resistance to reduction, abundant supply and affordability make it a very attractive sorbent. One of the greatest limitations of CaO as a sorbent for H_2S removal is its low resistance to attrition. If used in a fixed or moving bed reactor in its natural form it will eventually be crushed into a fine powder, making the reactor system inoperable. In order to avoid the problem, Akiti et al. (2001) developed a process by which limestone is coated with a strong, protective material by the technique of pelletization.

The limestone tested by Akiti et al. (2001) was first crushed and sieved, followed by pelletization in a bench scale pelletizer. After pelletization, the pellets were coated with a Portland cement or calcium aluminate cement mixture. The coated pellets were steam cured for three days at 100°C. The green strength of the pellets was tested by crushing them between two metal plates using a crushing strength apparatus that measures the maximum force required to fracture the material. All materials demonstrated a similar green crushing strength of approximately 7 N/mm. After sulfidation tests at 880°C with 1.1 vol% H_2S in N_2, the pellets coated with Type 1 or Type 4 Portland cement possessed cracks in the shell. Crushing strength tests were performed post reaction revealing that the weakest pellets were coated with Type 1 cement and had a crushing strength of 1.8 N/mm, while the Type 4 pellets had a crushing strength between 9.3 and 13.8 N/mm.

In order to improve the absorption capacity, limestone was added to the shell material. This resulted in an increase in absorption capacity that was proportional to the amount of limestone. The effect of tumbling time in the pelletizer was studied to see if it affected the strength of the pellets, and the crushing strength results indicated that the strength of the pellets increased significantly with tumbling time, but the weight gained after 60 min of sulfidation with 1.1 vol% H_2S at 880°C decreased with tumbling time. During the crushing strength tests the pellets that were tested were assumed to have a shell thickness of 0.4 mm and a pellet diameter of 4.76 mm, based upon sieve sizes.

In later developments Akiti et al. (2002) prepared and tested pelletized limestone or plaster of Paris (P.O.P.) with a shell material composed of 80 wt% α-Al_2O_3 and 20 wt% limestone. Two types of alumina were combined for the shell, tabular (Alcoa T–64, 9μm) and calcined (Alcoa A–16SG, 1μm). The limestone was crushed and sieved and had a particle size of 44 to 210 μm.

The optimum formulation of alumina and limestone was found by preparing and crushing tablets made of various mixtures. The tablets were prepared by wet mixing, casting and then heat-treating in air at 1100°C for 2 hr. The composition that exhibited the strongest crushing strength consisted of 80 wt% alumina and 20 wt% limestone. Of the 80 wt% fraction of alumina, 60 wt% was composed of T-64 and the other 40 wt% was composed of A-16 SG. The limestone contained 99 wt% $CaCO_3$ according to the supplier.

The main materials used for preparing the actual sorbent were limestone, reagent grade $CaCO_3$ and a commercial grade plaster of Paris. The plaster consisted of 77 wt%

$CaSO_4 \cdot ½ H_2O$, 15 wt% $CaCO_3$, 6 wt% $MgCO_3$, and 2 wt% other minerals. The pelletization procedure involved two steps. For the pellet cores the limestone in the 44 < diameter < 290 μm size range was dry mixed with 10 wt% A–16SG alumina. The limestone cores were pelletized using a 5 vol% lignin (Norlig A) solution in tap water as a binder. The plaster cores were pelletized with water. After creating the desired size of pellets, they were hardened by tumbling in the pelletizer for 1 hr. Following the pelletization of the cores, the shell material was added using the same pelletization technique with the 5 vol% lignin solution as a binder. After the pellets were coated, they were hardened by tumbling in the pelletizer for 2 hr. The pellets were air dried for approximately a day and then heat-treated in air for 2 hr at 1100°C.

The pellets were tested for crushing strength using the same apparatus mentioned earlier. Any batches of pellets that exhibited a crushing strength of 8.9 N/mm or above were characterized further. A crushing strength of 8.9 N/mm is considered the minimum for use in an industrial fixed bed reactor (Gupta, 1999).

Prior to reacting the pellets with H_2S, the $CaSO_4$ was converted into CaO by a cyclic reduction and oxidation process developed by Jagtap and Wheelock (1996). The process used 30 vol% CO for reduction and 20 vol% O_2 for oxidation with N_2 in both cases as the balance of the gas. The pellets were sulfided with 1.1 vol% H_2S in N_2 at 880°C.

During the study of the coated pellets Akiti et al. found that the shell thickness did not have an effect on the rate of reaction due to shell diffusional resistance. This finding was based upon a number of pellets tested with a plaster of Paris core and varying shell thickness. By comparing the results of full conversion runs made with a number of different pellets it

was determined that the time it took to fully react the pellets was not dependent upon the shell thickness.

In addition, Akiti et al. found that the plaster of Paris pellets reacted more rapidly than the limestone pellets. The slower reaction rate of the limestone pellets was attributed to the addition of Al_2O_3, which was thought to react with the limestone and therefore prevent some of the CaO from reacting with H_2S. By studying the rate of reaction with varying concentrations of H_2S an analysis of the results indicated that the rate of reaction was 1^{st} order. The temperature of the reaction was varied to see its effect upon the rate. Over the temperature range of 840 to 920°C the rate did not change significantly. However, at 960°C, a test with a plaster of Paris-based core indicated that the higher temperature slowed down the rate of reaction. The decrease in the reaction rate was thought to be due to enhanced sintering of the core or to a change in the reaction mechanism.

The effects of multi-cycle sulfidation and regeneration were examined by testing both cores and coated pellets. The sulfidation was conducted at 920°C with 3 vol% H_2S in N_2. Each sulfidation test lasted 10 min. After only three cycles with a limestone core the capacity of the pellet had dropped by 50% (Akiti et al., 2002). The drastic reduction in capacity was thought due to excessive sintering. Reagent grade $CaCO_3$ was also tested in pelletized form. The test was performed to see if impurities in the limestone or added Al_2O_3 had affected the performance of the limestone pellet. The test included seven cycles. The first six cycles were conducted for the same amount of time as the limestone pellets, but the seventh sulfidation cycle was extended in time for 65 min to see how long it would take for the pellet to obtain the same weight that was gained during the first 10 min cycle. Based upon the tests

with the reagent grade $CaCO_3$, it was assumed that the impurities and/or Al_2O_3 were not the cause of the excessive loss in reactivity of the limestone pellets. Contrary to the results of tests performed with the limestone and reagent grade $CaCO_3$ pellets, a multi-cycle test conducted with a plaster of Paris-based core and shell pellet indicated no decline in reactivity over 10 cycles. Unfortunately, no other tests were performed with plaster of Paris-based pellets to confirm these results.

One of the objectives of the present research project was to utilize CaO derived from large, natural deposits of minerals such as limestone, gypsum or dolomite for the absorption of H_2S in the high temperature regime. The sorbent had to withstand the abrasive conditions of a packed or moving bed reactor and be effective over many sulfidation and regeneration cycles. The remaining literature review is devoted to the primary chemical reactions of $CaCO_3$ and CaO with H_2S and the physical effects experienced by the sorbent over time. Also included are some basic models, which can be used to achieve a better understanding of the gas-solid reactions that occur .

1.2.2 *Reactions between H_2S and $CaCO_3$*

Limestone, converted to CaO, is currently used as a sorbent for H_2S removal in fluidized beds. It is quite effective, but is used as a once-through sorbent and then discarded into landfills following oxidation to $CaSO_4$. Calcium oxide is very effective for removing H_2S in the temperature range of 560 to 1015°C in a N_2 atmosphere (Fenouil and Lynn 1996), although complications arise as the concentration of CO_2 in the coal gas increases. In fact, if CO_2 is present and the temperature is below its decomposition temperature, 710°C, CaO will react with CO_2 to form $CaCO_3$. The reaction between limestone and H_2S is

$$CaCO_3 + H_2S \rightarrow CaS + CO_2 + H_2O \qquad (1.1)$$

prior to decomposition and

$$CaO + H_2S \rightarrow CaS + H_2O \qquad (1.2)$$

post decomposition.

Several studies have been undertaken to examine the kinetics of $CaCO_3$ reacting with H_2S. A study by Borgwardt (1984a) revealed some valuable information regarding particle size, temperature, H_2 concentration and sintering effects.

The study by Borgwardt(1984a) was conducted with limestone composed primarily of $CaCO_3$ (95 wt%) and $MgCO_3$ (1.3 wt%). The study revealed that particle size had a large effect on the reaction rate. For large particles, > 15 μm, reacted at 750°C, the conversion dropped off rapidly after reaching 10%, but for small particles, with a mean size of 1.6 μm, a high reaction rate was observed up to 60% conversion. A linear correlation was obtained between the rate of reaction at 20% conversion and inverse particle size.

The following reaction rate law was applied in the analysis:

$$\frac{d(CaCO_3)}{dt} = \frac{k(CaCO_3)C_{H_2S}}{D_p} \qquad (1.3)$$

where ($CaCO_3$) represents moles of unreacted limestone. The reaction rate constant obtained at 750°C was k = 0.66 cm^4/min. The effect of particle size, D_p, indicates the dependence of the rate on the surface area. Since the limestone had a porosity of only 8%, the change in surface area with particle size had a large effect (Borgwardt, 1984a).

The effect of temperature on the rate of reaction was studied over a temperature range of 550 to 870°C. An increase in temperature up to 750°C had a positive effect on the rate, but

in the range of 750 to 870°C there was no change in the reaction rate. An activation energy of 43.2 kcal/mol was obtained using the Arrhenius equation in the 550-750°C range. Beyond a temperature of 750°C the rate of reaction leveled off. The drop in rate was thought to be due to three possibilities: 1) sintering, 2) H_2S decomposition and/or 3) product layer diffusion (Borgwardt, 1984a).

Verifying the existence of a sintering effect, was the finding that after a heat-up period of 9 min to a temperature of 850°C, the surface area of 1.6 μm diameter particles decreased from 4.5 to 2 m^2/g. Scanning electron microscope (SEM) micrographs revealed the effect of sintering by showing the coalescence of particles. By using Coulter Counter analysis, the average particle size was shown to change from 1.6 to 3.5 μm in diameter. After pre-sintering 1.6 μm particles for 30 min at 850°C, the particles were reacted with H_2S and a conversion of only 38% was achieved after 5 min compared to 63% for a non-sintered sample.

The decomposition of H_2S in the reactor used by Borgwardt (1984a) was also taken into account. The following reactions were proposed based upon the results:

$$H_2S + CO_2 \rightarrow COS + H_2O \qquad (1.4)$$

$$H_2S \rightarrow H_2 + S \qquad (1.5)$$

At a reactor temperature of 700°C, 12 mol% of the H_2S thermally decomposed and at 900°C the decomposition rose to 42 mol%. The extent of the decomposition of H_2S into sulfur vapor was 2% at 700°C and 24% at 900°C.

The effect of H_2 concentration on the rate of reaction of H_2S with CaO was studied by comparing the rates of reaction of 1.6 um particles over a range of H_2 concentration from

0 to 45 mol% at a temperature of 750°C (Borgwardt, 1984a). Attar (1982) discussed the effect of H_2 concentration and stated that higher concentrations reversed the disassociation of H_2S on the surface of the CaS. Ruth et al. (1972) studied the effects of H_2 concentration during the reaction of dolomite with H_2S and found that 40 mol % H_2 had no effect on the reaction rate. The same dolomite studied by Ruth et al. was also studied by Borgwardt, and he found that H_2 did not affect the reaction rate. The effect of H_2 concentration could be due to its effect on the diffusion of the reactive species of the disassociated H_2S through the product layer. By analyzing the conversion of limestone vs. time, Borwardt (1984a) found that the inflection point where diffusion limitation took over began earlier in time as the concentration of H_2 was increased. The effect of H_2 concentration indicated that the rate was limited by product layer diffusion. When the H_2 concentration was held constant and the particle size was increased from 1.6 to 2.8μm, the extent of conversion after 7 min of exposure was reduced from 20% to 8%. The results fit a model based on product layer diffusional resistance, Borgwardt (1984a). To investigate the effects of surface area, the H_2 concentration was held constant at 15 mol% while the particle size was reduced from 1.6μm to sub-micron size, which resulted in a rise in specific surface area of the particles from 4.5 to 7 m^2/g. The results revealed an increase in conversion of 60% as the specific surface area was increased. Further increases in H_2 concentration did not affect conversion of the sub-micron size particles. It was thought that if the $CaCO_3$ grains within the dolomite were small enough, the H_2 concentration would not really affect the diffusion of H_2S through a thin product layer. For sub-micron size particles diffusional resistance seemed to limit the

reaction of H_2S with dolomite at conversions greater than 90%, whereas the reaction of H_2S with 1.6 μm limestone particles was affected at conversions greater than 50%.

Studies of the reaction of limestone with sulfur vapor were performed by Levy (1982) assuming the following reaction to take place:

$$2CaO + 3/2\ S_2 \rightarrow 2CaS + SO_2 \qquad (1.6)$$

Borgwardt (1984a) performed a similar study with $CaCO_3$. It was discovered that the effluent consisted of equal amounts of SO_2 and COS. The reaction producing these products was proposed to be

$$CaCO_3 + 3/2\ S_2 \rightarrow CaS + SO_2 + COS \qquad (1.7)$$

The rates of reaction of H_2S and S_2 with $CaCO_3$ were compared, revealing that H_2S was the more reactive species.

A similar process studied by Borgwardt (1984a) was the reaction between H_2S and $CaCO_3$ in the presence of $CaCl_2$. A previous study by van Houte et al. (1981) indicated that the reaction rate of H_2S with $CaCO_3$ increased after 2 mol% $CaCl_2$ was added to the solid. Borgwardt's study revealed the opposite effect. His experiments revealed a strong inhibiting effect indicating that amounts as small as 0.1 mol% $CaCl_2$ reduced the reaction rate.

A study of the reaction of H_2S with calcite (trigonal crystals of $CaCO_3$) by Attar et al. (1979), revealed that the surface reaction was limiting initially. After 80 layers of CaS were formed, the rate changed from reaction rate limiting to solid-state diffusion limiting. These results seemed to explain why the reaction rate observed by Borgwardt (1984a) changed from chemical reaction control to product layer diffusion control after 11% conversion. The

volume of 80 molecular layers on a 1μm pellet corresponds to approximately 10% of the volume of a $CaCO_3$ particle.

A study of the sulfidation of $CaCO_3$ derived from limestone was undertaken by Fenouil et al. (1994). Their work dealt primarily with large limestone particles having a surface area of 0.05 to 0.27 m^2/g and a porosity of 8 to 9%. The results from calcinations tests in 100% CO_2 atmospheres and high temperatures (800 to 910°C) revealed no sintering effects after 2 hr of treatment. They also performed sintering tests on CaS particles, which had an average particle size of 1.7 μm and surface area of 1.32 m^2/g. The CaS seemed to undergo rapid sintering in the presence of CO_2 but not when exposed to only H_2 and N_2 atmospheres. The sintering usually took place above 750°C. In addition, the presence of H_2O and CO_2 did not alter the rate of sintering. A proposed mechanism for sintering was based on the reaction

$$CaS + H_2O + CO_2 \rightarrow CaCO_3 + H_2S \qquad (1.8)$$

The formation of small amounts of $CaCO_3$ was thought to have caused a large increase in surface energy that enhanced the sintering effect.

1.2.3 *Reactions between H_2S and CaO*

A study based upon large particles of limestone, dolomitic limestone and dolomite was performed by Fenouil and Lynn (1996). The study was performed above and below the decomposition temperatures of $CaCO_3$. The different sorbents were derived from $CaCO_3$ (limestone), $[CaCO_3 \cdot MgCO_3]_1[CaCO_3]_3$ (dolomitic limestone), and $MgCO_3 \cdot CaCO_3$ (dolomite). For all three sorbents, full conversion was achieved above the decomposition temperature of $CaCO_3$. The reaction rate appeared to be a function of the amount of $MgCO_3$

present. It was discovered that the higher the ratio of Mg / Ca the higher the reaction rate. Unfortunately, the attrition rate of the material increased as the amount of Mg increased. Below the decomposition temperature of $CaCO_3$, 900°C under 1atm of CO_2 (Saliban et al., 1996), the total conversion of CaO with H_2S was only 20% vs. 100% for the decomposed material. It was discovered that 100% of the Ca in the dolomite regions of the dolomitic limestone was converted to CaS, whereas only 20% of the Ca in the limestone region was converted, yielding only 40% overall conversion. At a temperature of 710°C and above, the rate of reaction was thought to be controlled by product layer diffusion for dolomite and dolomitic limestone, (Fenouil and Lynn,1996). The reaction between $CaCO_3$ and H_2S was carried out using CO_2 (87-88 vol%), H_2 (1-2 vol%), CO (4-5 vol%), H_2O (4-5 vol %) and H_2S (0.5-1.85 vol %) over a temperature range of 570-860°C with a particle size ranging from 1 to 2 mm in diameter. Using scanning electron microscopy (SEM) and energy dispersive spectrometry (EDS) element maps, it was discovered that only 10% of the Ca was converted to CaS. In addition, the reaction appeared to have occurred throughout the pellet, indicating that inter-pellet pore diffusion resistance had not reduced the rate of reaction. The rate of reaction was first order with respect to H_2S concentration. The initial reaction rate was thought to be chemically controlled since the conversion doubled after the reaction time was increased from 15 min to 30 min. The activation energy was observed to be 39 kcal/mol. As the temperature increased the reaction rate decreased. It was observed that the CaS layer broke apart above 660°C and rearranged around the $CaCO_3$ grains. Attar and Dupuis (1979) also reported a similar rearrangement of the grains. The decrease in reaction rate was thought to be due to the densification of the reactive material induced by the sintering of the CaS.

The denser CaS layer was thought to inhibit the diffusion of H_2O and CO_2 out of the grains. In the range of 820 to 880°C the reaction rate order appeared to change to 1/2, which is usually indicative of diffusion effects. As the temperature was increased above this range the rate began to increase again. The change in the reaction rate was thought to be due to the activation of solid state diffusion of H_2S through the CaS layer. Morphological surface changes also indicated this same process.

A very thorough report on the sulfidation of CaO derived from limestone was presented by Borgwardt, (1984b). The research emphasized the effect of surface area on the reaction rate of CaO with H_2S and COS. With particles of limestone it has been recorded that upon calcination no reduction in the geometric size occurs. Since the density of $CaCO_3$ is 2.71 and CaO is 3.32 g/cm^3, the calcination reaction should cause a 45% increase in porosity at a minimum and prior to any sintering effects (Borgwardt, 1984b). After CaO has reacted with H_2S to form CaS the reduction in porosity should be 25%, based upon the density of CaS, 2.61 g/cm^3. The experimental conditions and the apparatus used were the same as those used for the reaction of $CaCO_3$ with H_2S by Borgwardt (1984a). The material was derived from limestone containing 95 wt% $CaCO_3$ and 1.3 wt% $MgCO_3$. The surface area of the particles was 2.2 m^2/g, and the porosity and the particle size range were 8% and 1-3 μm, respectively. The gas was composed of 5000 ppm H_2S or COS and 45 mol% H_2 in N_2. All samples used for measuring the rate of reaction and activation energy were pre-sintered at 950°C for 30 min resulting in a surface area of 5.8 m^2/g. During the sulfidation runs the temperature was varied from 600 to 900°C, and the reported reaction rates were based upon

50% conversion of CaO to CaS. The rate of reaction increased with temperature, and an analysis of the results yielded an activation energy of 31 kcal/mol for both COS and H_2S.

Table 1.1 Surface area change as a function of time and temperature prior to reaction with H_2S.

Temperature (°C)	Time (min)	Surface Area (m^2/g)
700	20	40
700	60	32
850	30	27
950	30	6

The reduction in surface area was determined to be a strong function of calcination temperature. To look into the effect of the surface area reduction on the rate of reaction, experiments were carried out at 700°C with 5000 ppm H_2S. The results indicated that the higher surface area samples reacted much faster than the lower surface area samples. Because of the large effects of temperature and surface area on the rate of reaction, the samples were pre-sintered prior to measuring the reaction rate in order to determine the rate constant and order of reaction independent of surface area effects (Borgwardt, 1984b).

Since H_2S thermally decomposes at high temperatures, H_2 must be added to a reaction mixture containing H_2S in order to prevent the decomposition. It has been noted that H_2 can affect the rate of reaction of H_2S with CaO. Borgwardt's (1984b) study revealed that with high surface area samples, greater than 53 m^2/g, the effect of H_2 was not noticeable, but as the surface area dropped, the H_2 had a significant effect on the rate of reaction based upon tests performed with H_2 concentrations ranging from 0-45 mol%. By analyzing the effect of

surface area on the rate of reaction it was discovered that there was an exponential dependence of the rate upon the surface area. The effects of particle size and H_2 concentration on the reaction rate were evaluated, and it appeared that the rate of reaction of the smaller particles was not affected by varying the H_2 concentration, whereas the rate of reaction of the larger particles was affected. Borgwardt argued that if H_2 did slow down the rate of reaction then an increase in particle size should not have such a dramatic effect on the rate of reaction.

1.2.4 *The regeneration of calcium sulfide*

The regeneration of a sulfided calcium-based sorbent can be carried out by various reactions and techniques. Although different reaction paths can be used to convert CaS to CaO, for use in an industrial environment the conversion method must be efficient, economical and benign towards CaO. Proposed processes usually involve either an oxidizing step followed by thermal decomposition or an oxidizing step followed by a reducing step. The oxidation step usually involves treatment with either SO_2 or O_2 in N_2 or air. There are two CaS reactions that can take place in the presence of O_2:

$$CaS + 2O_2 \rightarrow CaSO_4 \qquad (1.9)$$

$$CaS + 3/2O_2 \rightarrow CaO + SO_2 \qquad (1.10)$$

Using O_2 as the oxidizer Qui et al. (1998) demonstrated a process which first converted part of the CaS to $CaSO_4$ by reaction 1.8 and then reacted the remaining CaS with the $CaSO_4$ according to reaction 1.10 at 850-1000°C.

$$CaS + 3CaSO_4 \rightarrow 4CaO + 4SO_2 \qquad (1.11)$$

The oxidation step was performed with 5.5 vol% O_2 over a temperature range of 750 to

900°C. The experiments were carried out using limestone which was first crushed and sieved to produce particles in the size range of 0.09-0.12 mm. The particles were pre-calcined at 900°C for 120 min under a flow of N_2. Following calcination, the particles were sulfided with 5000 ppm H_2S in N_2 in a fixed bed reactor at 900°C for 310 min. A total flow rate of 600 mL/min was used because it had been shown previously that this flow rate would eliminate film diffusion resistance. During the oxidation tests it was observed that the rate of $CaSO_4$ formation increased with temperature. Also with an increase in temperature it was found that SO_2 was generated as a by-product by way of reaction 1.9. The generation of SO_2 began at a temperature of 900°C. Davies et al. (1994) also reported the same phenomenon. The solid-solid reaction 1.11 was used to convert the $CaSO_4$ and CaS into CaO. The mechanism of the reaction is a point of controversy, and two different mechanisms have been proposed. Yang and Shen, (1979) believed the reaction to take place via a gaseous intermediate (SO_3).

$$CaSO_4 \rightarrow CaO + SO_{3(g)} \qquad (1.12)$$

$$CaS + 3SO_{3(g)} \rightarrow CaO + 4SO_2 \qquad (1.13)$$

The gaseous intermediate seemed to explain the high reaction rate that was observed; a rate that seemed too high for a solid-solid reaction. Davies and Hayhurst (1996), however, did not observe the decomposition of $CaSO_4$ until a temperature greater than 1200°C was reached. They proposed a different reaction mechanism involving a liquid phase formed by a $CaSO_4$ and CaS eutectic. Using SEM and EDAX, Davies and Hayhurst (1996) observed evidence of a liquid phase in the temperature range of 850-1000°C.

Qiu et al. (1998) observed that a temperature of ≥ 1000°C was optimum for the solid-solid reaction while a temperature of 850°C was optimum for the oxidation step. When using the two-step process, only two cycles were required to achieve a 98% conversion of CaS to CaO.

Although most proposed regeneration techniques are similar to the process proposed by Qiu et al. (1998), Jagtap and Wheelock (1996) demonstrated a process by which the CaS is first oxidized, with an oxidant such as air, so that reactions 1.9 and 1.10 can be initiated. Most of the CaS is converted to $CaSO_4$ through reaction 1.9. The $CaSO_4$ is then reduced using one or more of a number of possible reducing gases.

The reducing gases studied by Jagtap and Wheelock were CO, CH_4, and C_3H_8. The reactions taking place with the various reducing gases included the following:

$$CaSO_4 + CO \rightarrow CaO + CO_2 + SO_2 \qquad (1.14)$$

$$CaSO_4 + \tfrac{1}{4}\, CH_4 \rightarrow CaO + \tfrac{1}{4}\, CO_2 + \tfrac{1}{2}\, H_2O + SO_2 \qquad (1.15)$$

$$CaSO_4 + 1/10\, C_3H_8 \rightarrow CaO + 3/10\, CO_2 + 4/10\, H_2O + SO_2 \qquad (1.16)$$

All experiments were carried out in a TGA with N_2 making up the balance of the gas mixture. The CaS used had a particle size of 5.92 μm and was pressed with a die into tablets that were 6.35 mm in diameter and had a thickness of 1-2 mm. The tablets were then used either whole or crushed and sieved. The cyclic oxidation/reduction process was conducted so as to allow 1 min for each phase of the cycle before switching to the next gas.

The effect of varying the O_2 concentration on the rate of conversion was studied at a temperature of 1050°C with O_2 concentrations of 5, 10, 20 and 30 vol%. A concentration of 20 vol% O_2 apparently yielded the fastest rate of conversion.

The effect of varying the reducing gas concentration was also studied. For this study 10 vol% O_2 was used during the oxidation step. The optimum concentration of CO was determined to be 30 vol% after testing 5, 10 and 30 vol% concentrations. The optimum concentration of CH_4 was 5 vol% after evaluating concentrations of 5, 20, 30 and 40 vol%. And a 2 vol% concentration of C_3H_8 was discovered to be the optimum after experimenting with 1, 2, 3, and 5 vol% concentrations.

The effect of temperature was studied over the range of 960 to 1100°C. An optimum temperature of 1050°C was found to yield the overall best results for CO. As the temperature was raised above 1050°C the rate was observed to decline. The tests with methane yielded an increase in rate over the entire temperature range up to and including 1100°C.

The tests with propane were conducted only at temperatures of 960 and 1050°C, and the rate at 1050°C was much higher than at 960°C. Generally, the fastest regeneration required 40 min when using the optimum reducing gas concentration, a temperature of 1050°C and a 20 vol% concentration of O_2.

Some very interesting aspects of this study were the results from multi-cycle sulfidation and regeneration tests. The materials used as a sorbent were limestone, reagent grade $CaCO_3$ and CaO. The $CaCO_3$ and CaO particles were small enough that they were first pelletized followed by crushing and screening. The reacting gases were 10 vol% SO_2, 15 vol% CO, and 75 vol% N_2 with the assumption that the reduction of SO_2 to COS would take place prior to reaction with CaO by the following reaction:

$$SO_2 + CO \rightarrow COS + O_2 \qquad (1.17)$$

After six cycles of sulfidation and regeneration there was no apparent decline in the rate of sulfidation. In fact, the apparent rate of sulfidation appeared to increase after a number of cycles. The regeneration time also decreased after a few cycles, indicating an increase in the rate of the regeneration reactions.

1.2.5 *General sintering effects*

The effect of sintering on the reactivity of CaO has been studied by a number of researchers. Sintering decreases the reactivity of CaO due to the accompanying reduction in surface area. Based upon Borgwardt's (1984b) extensive work on the effect of surface area and the reactivity of CaO with H_2S, it is very apparent that any loss in surface area will decrease the reactivity.

Sintering generally occurs in the range of the Tannemann temperature which is approximately one half of the melting temperature of a material. Sintering occurs when there is an excess of surface energy, which creates a driving force for material diffusion to occur. There are three main driving forces for sintering: 1) the surface curvature of particles, 2) the applied pressure from an external source, and 3) the effects of a chemical reaction taking place (Rahaman, 1995). Polycrystalline materials will sinter by diffusional transport while amorphous materials will sinter by viscous transport of material.

In all, there are approximately six different sintering paths for polycrystalline materials (Rahaman, 1995). Three of the paths lead to coarsening of the material which results in a surface area loss and a change in pore size distribution, while the other three paths lead to a denser material, in addition to surface area loss and a redistribution of pore sizes. A single particle exhibits a surface energy or surface tension. These properties are represented

by the Kelvin equation, which relates the partial vapor pressure of a grain material to its reference value for the standard chemical potential of a flat surface:

$$p_{vap} = p_o \exp\left(\frac{\gamma_{sv} K \Omega}{k_b T}\right) \qquad (1.18)$$

In eq 1.18, Ω is the volume of an atom, K represents the curvature of the grain and is positive for convex surfaces, k_B is the Boltzman constant and γ_{sv} is the specific surface energy.

When particles are packed together, the boundaries where the particles touch create an imbalance of surface energy. The boundary between particles or grains of material is called a grain boundary. A decrease in surface area creates a difference in chemical potential between the core material and the material at the boundary. The gradient in chemical potential causes mass transport to the grain boundary to take place. The decrease in surface area ΔA_{sv} and increase in grain boundary area ΔA_{gb} can be related to the total change in energy of the grains:

$$\Delta E = \gamma_{gb} \Delta A_{gb} + \gamma_{sv} \Delta A_{sv} \qquad (1.19)$$

where the grain boundary and surface area tension are denoted by γ_{gb} and γ_{sv}, respectively. In order to minimize this change in energy, material is transported to the grain boundary where a neck forms. If more than two grains are in contact a pore is formed between the grains. During sintering, if matter diffuses via a surface, lattice surface, or vapor mechanism, only the surface area decreases, whereas if the transport occurs by grain boundary, lattice grain boundary, or plastic flow, the density of the material will increase.

The equation describing solid state diffusion is:

$$D_s = D_o \exp\left(\frac{-Q}{RT}\right) \tag{1.20}$$

where D_o is the solid-state diffusion constant and Q is the solid state activation energy. There are several different forms of diffusion in solids. The different types of diffusion include lattice, grain boundary, surface, defect, and chemical (see Figure 1.1).

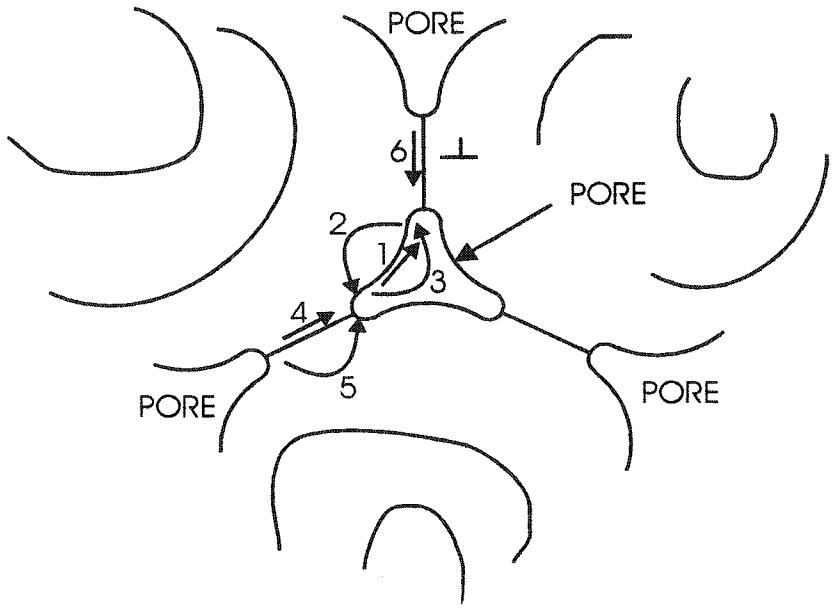

Figure 1.1. (1) Surface diffusion, (2) Lattice diffusion (surface), (3) Vapor transport, (4) Grain boundary diffusion, (5) Lattice diffusion (grain boundary), (6) Plastic flow. (After Rahaman, 1995).

When the density of a material is increased by sintering, material is mainly transported from within the grain. The activation energy for either grain (4) or lattice (5) diffusion is much higher than for surface diffusion (1) or evaporation condensation (3). Due to the higher activation energies, grain boundary and lattice diffusion generally dominate at higher temperatures while surface and evaporation-condensation dominate at lower temperatures (Rahaman, 1995).

The mechanism of sintering can also change according to heating rate, chemical reactions both solid-state and gas-solid, applied pressure, impurities and defects. When considering the packing of spheres, the dominant mechanism for sintering can vary also. The packing coordination of the spheres, the pressure under which they were packed and also the size distribution of the spheres all have major effects upon the mechanism of sintering. As particles sinter, the necks between the particles begin to widen due to the imbalance in surface energy at the junction between the spheres. The angle between the spheres, which represents the curvature, will change until an equilibrium value is reached.

$$\cos\left(\frac{\psi}{2}\right) = \frac{\gamma_{bg}}{2\gamma_{sv}} \tag{1.21}$$

The dihedral angle between the grains (Figure 1.2) represents the interaction between the grain boundary energy and the surface energy.

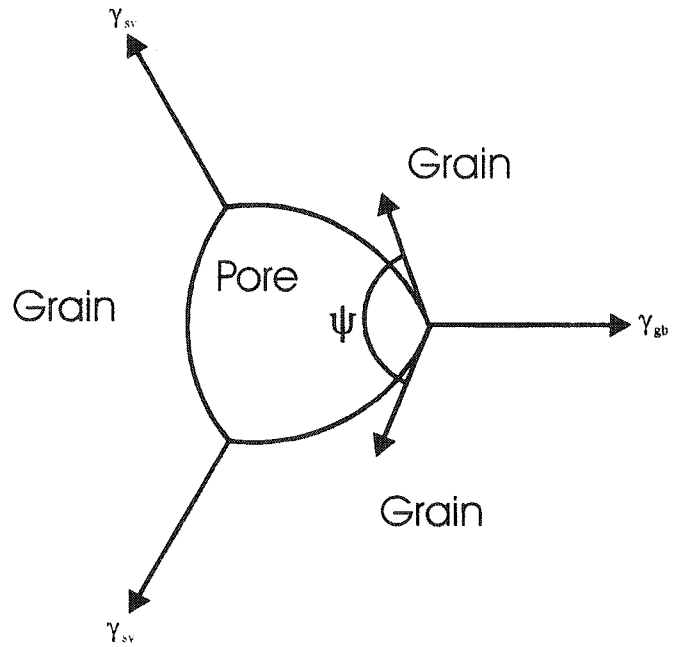

Figure 1.2. Three grain intersection forming a pore.

After a neck has formed, the surface morphology will be dependent upon the dihedral angle and the pore coordination number, r_c (Lange, 1989). It has been shown that there is a critical pore coordination number, r_c , that will determine whether a pore shrinks to an equilibrium value or closes in on itself. According to Kellet and Lange (1989) all pores shrink, but some stop at an equilibrium volume. During sintering some grains will shrink and coalesce into larger grains, a process termed coarsening. As particles are packed they form what is called domains, and domains in turn combine to form agglomerates (Goodwin, 1975). The smallest pores are contained in the domains, followed by the pores formed by the connected domains. The largest pores are formed within the agglomerates. The formation of agglomerates is thought to have a large effect on the limit of the sinterability of packed grains. Another physical factor that limits the sinterability of materials is large grain sizes. Since large grains have a larger radius of curvature the surface energy per unit volume is much less than for smaller grains, which leads to a decrease in the driving force for sintering.

1.2.6 *Sintering of CaO*

Since Borgwardt's (1984b) work on the reduction in the rate of reaction of H_2S with CaO due to a loss of surface area, there have been other studies that investigated the effects of CaO sintering. Most of the research has addressed the effects of temperature and chemical reaction. For example, Borgwardt (1989) investigated the effects of temperature and different impurities on the sintering of reagent grade $CaCO_3$, limestone (96 wt% $CaCO_3$), and $Ca(OH)_2$ over a temperature range of 700 to 1100°C. The material was first decomposed at 700°C under a N_2 flow for 3.5-10 min. The surface area of the samples was ~ 1 m^2/g prior to decomposition. Following decomposition, the surface area of the $CaCO_3$ was 104 m^2/g,

limestone (102 m^2/g), and $Ca(OH)_2$ (76.7 m^2/g). The $CaCO_3$ consisted of 10 μm particles in 80 μm agglomerates. The limestone particles were 2 μm and 10 μm in size, and the $Ca(OH)_2$ particles were 2 μm in size. Borgwardt used a sintering model developed by German and Munir (1976) for his analysis. The modeling results indicated lattice diffusion as the dominant mechanism of sintering, which is a densifying mechanism. A study of the porosity change during the sintering process was conducted using the 2 μm particles of limestone. Below 900°C the porosity of the particles, 48%, did not change. At this temperature the pores in the samples were either 60 or 170 angstroms in diameter. Above 900°C a reduction in 60 angstrom pores was evident while the larger pores remained unaffected. The study indicated that $CaCO_3$ had the highest activation energy for sintering while $Ca(OH)_2$ had the lowest. The sintering took place mainly in the domains, and at latter stages in the agglomerates, which is supported by the theory that smaller particles with a higher density of contact points will sinter more quickly than larger particles with a lower density of contact points.

It has been shown that CO_2 acts as a catalyst for the sintering of high surface area CaO powders (80-120 m^2/g) (Glasson, 1958; German and Munir, 1975a,b, 1976). Even at low temperatures, 610°C, large reductions in surface area have occurred with only 0.2 Pa of CO_2 (German and Munir, 1975c). The same powders did not lose any surface area from heat treatment at 900°C under a vacuum. Beruto et al. (1984) studied the effects of 1.33 kPa of CO_2 on the surface area loss and porosity change of aggregates consisting of 0.01μm particles of CaO at 686°C. The CaO was derived from single calcite crystals that were decomposed under vacuum at 686°C to yield rod shaped particles with a diameter of 0.01μm and a length

of 0.1μm. The particles contained mesopores of ~ 5 nm and macropores of 1-2 μm. After sintering for different times, it was discovered that a decrease in the mesopore volume resulted in an increase in the macropore volume. The high surface area samples did not densify during the initial stages of sintering but did exhibit coarsening effects. The coarsening did not change the mesopore porosity but did reduce the surface area, which points to a surface diffusion mechanism.

Using infrared analysis Beruto et al. (1984) determined that CO_2 chemisorbs onto the CaO surface and reacts with O^{2-} ions to form CO_3^{2-} ions. The CO_3^{2-} ions then diffuse into the lattice, creating an imbalance of the chemical potential at the surface sites of the particles. The activation energy was reported to be 61 +/- 10 kJ/mol for the CO_2 chemisorption step. The overall results indicated that after 16 hr of heating with CO_2, the mesopore volume had decreased by 79% while the overall volume of the particles had decreased by 10%. The effects of CO_2 were seen primarily on the surface area reduction of the samples and the loss of mesopore volume. A growth in the macropore volume was measured in the > 1 μm range of the agglomerates. For samples with a surface area > 90 m^2/g the sintering took place through a surface diffusion mechanism. Below 90 m^2/g an alternative mechanism took over which resulted in a decrease in the rate of surface area loss.

An analysis on the effects of H_2O vapor and CO_2 on the sintering of CaO was performed by Borgwardt, (1989). During Borgwardt's study, 25 mg samples of 10 μm particles of limestone were treated in a sintering reactor to various temperatures, and different H_2O and CO_2 concentrations, either alone or combined. It was discovered that by using a pressure of 7.3 kPa, the sintering of the limestone under pure N_2 began at 440°C instead of

700°C. As the concentration of H_2O was increased the surface area loss also increased, and the same effect was seen with CO_2 except that the rate of surface area loss was not as severe. A mixture of the gases caused a more rapid decline in surface area than H_2O alone caused. In addition to surface area loss, the porosity of the samples declined.

It had been reported earlier by Anderson and Morgan (1964) that H_20 had an effect on the surface area loss of MgO and the effect was thought to occur through surface diffusion transport. Some tests performed by Anderson and Morgan indicated that CaO was more affected by H_2O than by CO_2.

1.2.7 *Modeling of gas-solid reactions*

The gas-solid reaction models which have been applied to the reaction of H_2S or COS with CaO are numerous. Therefore, it is impractical to review all of the models that have been proposed over the years, but in general they can be classified as either nonstructural (macro models) or structural i.e. grain, micro-grain and pore models (Hasler et al., 2003).

The non-structural models are the least complicated since they do not incorporate the grain size of the pellets nor the pore evolution that can take place during the reactions. The model that best represents this category is the shrinking core model (SCM) or sharp interface model (SIM) developed by Yagi and Kunii (1955). All other models in the non-structural class are either volume or homogeneous.

The structural models can be further subdivided into grain and percolation models (Hasler et al., 2003). The grain model, first developed by Szekely and Evans (1970), takes into account the particles that make up an agglomerated pellet. The model incorporates the geometry of the individual particles, pore evolution, the gaseous reactant concentration

throughout the pellet as a whole and the overall pellet geometry. The grain model can be solved analytically for reaction rate limiting, solid-state diffusion limiting or gaseous reactant diffusion limiting, but if the process is a combination of any of the above three cases it must be solved numerically. The percolation models are even more complex and involve concepts such as the statistical physics of disordered media, network modeling of the pore space, discretization, and random walk diffusion processes (Hasler et al., 2003).

Since the SCM is the basic model, researchers typically apply it as an initial analysis of gas-solid reactions. The SCM can be quite effective depending upon the system, and has been successfully applied by many researchers, some of which are noted below.

The SCM is based upon three primary factors that can control the overall pellet reaction rate: gas-film diffusion surrounding the pellet, diffusion of the reactants through the product layer and chemical reaction rate at the interface. When all three factors are combined, the following equation results for a first order chemical reaction rate with respect to H_2S or COS reacting with a solid oxide sorbent (Levenspiel, 1996):

$$t_{Total} = \frac{\rho_{CaO} R}{3k_g C_{H_2S}} X + \frac{\rho_{CaO} R^2}{6D_e C_{H_2S}} \left[1 - 3(1-X)^{2/3} + 2(1-X)\right] + \frac{\rho_{CaO} R}{k_s C_{H_2S}} \left[1 - (1-X)^{1/3}\right] \quad (1.22)$$

The first term accounts for film diffusion, the second term for product layer diffusion and the last term for the rate of chemical reaction. The independent variable X, represents the conversion of CaO to CaS and t represents the total time taken for a specific conversion to take place.

Using energy dispersive spectrometery (EDS) sulfur maps, Fenouil and Lynn (1996) discovered that the reaction between calcined limestone and H_2S could be represented by the

SCM. For the reaction of 0.4 mm particles of CaO with 500 to 18,000 ppm H_2S over a temperature range of 560 to 1100°C, Fenouil and Lynn found that the best fitting model was the one in which the overall rate is controlled by the diffusion of H_2S through the product layer of CaS. This model corresponds to eq 1.21 with only the second term on the right included. However, Fenouil and Lynn noted that they were not able to eliminate the effect of gas film diffusion limitation during the first 5 to 10 min of every reaction. Their results also indicated that temperature did not have a large effect on the rate of reaction.

During a study of the effect of HCl on the rate of sulfidation of CaO derived from limestone and dolomite, Abbasian et al. (1993) found that the SCM also fit their data. Using EDS sulfur maps it was shown that the CaS reaction front formed a sharp interface. The reactions were conducted at 982°C with a 4:1 ratio of H_2 : H_2S in N_2 with either 0 or 1% HCl present. By assuming that the particle volume change during sulfidation was not large, they were able to fit their data to the SCM assuming product layer diffusion control. The correlation was used for conversions up to 60%. Neither HCl nor H_2O had an effect on the modeling of the reaction. In addition, Borgwardt (1984b) found that the SCM could be used to model the reaction between H_2S and CaO with product layer diffusion control as the limiting factor. In general, the SCM is very useful for modeling gas-solid reactions taking place on small, single particles of simple geometry.

Taking a different approach Heesink and van Swaaij (1995) used a variation of the grain model developed by Szekely and Evans (1970) called the grain size distribution model (GSD). The GSD model is a combination of two models, the grain model and the SCM. The GSD model accounts for the variation in grain sizes that make up an agglomerated pellet and

utilizes the SCM to represent the reaction of each individual particle. The GSD model assumes that the reactant concentration is homogeneous throughout the pellet and is not a limiting factor. In addition, the GSD model can also include pore blocking (pore evolution) when calculating the conversion of individual particles. To obtain the particle size distribution, Heesink and Swaaij used mercury porosimetry data to classify the size of the particles making up a pellet. The particle classification is based upon the theory that the size of a pore is proportional to the radius of the grains that surround it. By using the pore size classes obtained by mercury porosimetry, the weight fraction of the grains corresponding to each pore size class was estimated and each class was used to calculate the conversion of a particle based upon the SCM. Following the SCM calculations the conversions of each particle size class were used by weighted averaging to obtain the overall conversion for all size distributions of particles.

The GSD model seemed to work quite well for the reaction between SO_2 and CaO, which accounted for the obstruction of pores by the formation of $CaSO_4$ at ~ 40% conversion. It was also applied to the reaction between H_2S or COS with CaO. And in this case it was also effective, but contrary to other reports, Heesink and Swaaij used a reaction order of ½ as opposed to 1st order for the reaction between H_2S or COS with CaO. Since the order of reaction rate was adjusted, the usefulness of the model for an agglomerated pellet might be questioned. When using small, individual particles the SCM seems to work quite well, but once it is applied to a pellet that is composed of agglomerates, the effect of inter-particle gas diffusion must be taken into account unless the surface reaction rate is very slow in comparison.

Calvelo and Smith (1970) used the grain model or particle-pellet model to analyze the fluorination of uranium oxide according to the reaction

$$UO_2 + 4HF \rightarrow UF_4 + 2H_2O \qquad (1.23)$$

The experiments were conducted on compressed and sintered particles of UO_2 reacted in a stirred tank. They obtained good results by using the model, and experimental constants such as reaction rate and diffusivity (effective) were obtained that were more realistic than when the SCM was applied. The grain or particle-pellet model can be very useful if inter-pellet diffusion is a limiting factor during reaction. The model can also be easily altered according to the specific reactions taking place within each individual particle of the pellet.

Chapter 2. Experimental

2.1 Introduction

The analytical and experimental equipment used for this research is discussed in this section. The instruments listed include items used for chemical as well as physical information. The techniques for sample preparation cover all important steps.

2.2 Materials Analysis

2.2.1. *X-ray diffraction, X-ray fluorescence, scanning electron microscopy (SEM) and energy dispersive spectrometry (EDS)*

In order to obtain and verify the chemical composition of materials such as limestone and commercial grade P.O.P., X-ray diffraction (XRD) and X-ray fluorescence (XRF) were utilized in combination. The XRD enables the verification of the major, minor and trace crystal phases, and the XRF is used for bulk chemical analysis. The XRF is very useful for identifying impurities that XRD will not detect. In addition, any components that are amorphous will be detected by XRF. The XRD instrument was a Siemens D500, and the XRF was a Philips PW 2404.

The surface and structural morphology of the pellets was studied using a JEOL 6100 SEM with a tungsten filament. The SEM micrographs revealed the various particle sizes and configurations within the pellets and also the sintering effects. The SEM was also used for elemental analysis by energy dispersive spectrometry (EDS). The EDS technique was used for elemental spot maps of the pellets, which is useful for analyzing sulfidation reaction fronts and material dispersions.

The specimen preparation for imaging the topography of a pellet was performed by fracturing the pellet in half, mounting it on a 2 cm diameter, 1 cm high polymer cylinder and sputter coating it with a thin (80 Å) layer of gold. For EDS maps, the pellet was subjected to a vacuum for ~ 1 hr followed by encapsulation in a liquid polymer solution under vacuum, then the system was pressurized to 1 atm and heat-treated over night to harden the pellet-polymer mold. The mold was then ground down and polished to expose the inside of the pellet. The same sputter coating technique was applied.

2.2.2 *Particle size analysis*

The particle size distribution of the materials was analyzed with a Horiba CAPA 700 Particle Size Distribution Analyzer. The instrument utilizes liquid-phase sedimentation in conjunction with an optical transmission method. The sedimentation is quantified using Stokes' equation and the amount of absorbency is proportionately related to particle concentration. The instrument uses both gravitational and centrifugal sedimentation. A high-intensity green LED is used to relate the amount of particles in a transmission plane to the concentration and the particle size. The change in absorbance can be related by the equation

$$\log(I_o) - \log(I_i) = K\sum_{1}^{n} K(D_i)N_i D_i^{\,2} \qquad (2.1)$$

where I_o is the intensity of light impinging upon the sample, I_i is the transmitted light intensity, K is the optical coefficient of the cell and particle form, $k(D_i)$ is the absorption coefficient of a particle of diameter D_i, and N_i is the number of particles of diameter D_i. The equations describing both gravitational and centrifugal sedimentation are:

$$D = \left(\frac{18 n_o H}{(\rho - \rho_o) g t} \right)^{1/2} \quad \text{(Gravitational)} \qquad (2.2)$$

$$D = \left(\frac{18 n_o \ln(x_2/x_1)}{(\rho - \rho_o) \omega^2 (t) t} \right)^{1/2} \quad \text{(Centrifugal)} \qquad (2.3)$$

The particle diameter is represented by D, n_o is the viscosity coefficient of the dispersion medium, g is the acceleration of gravity (980.7 cm sec^2), H is the sedimentation distance (cm), ρ is the sample density (g /cm^3), ρ_o is the density of the dispersion medium, t is the sedimentation time, X_1 the distance between the center of rotation and sedimentation plane (cm), X_2 is the distance between the center of rotation and the measuring plane, and $\omega(t)$ is the rotation angular velocity (rad/sec). A constant acceleration or increasing acceleration can be used depending upon the particle size distribution. A particle size distribution may be obtained based upon a length, volume or number.

2.2.3 *Density and porosity measurements*

The porosity of the materials was measured by two techniques. The first technique is based upon Archimedes principle. The pellets were initially weighed after being kept in a desiccator overnight, W_d. Then they were placed in an apparatus and a vacuum was applied for 1 to 2 hr. After the vacuum process, n-decane was poured in through a spout while the pellets were still under a vacuum. After the pellets were completely submerged, air was slowly bled into the system until it reached room pressure. By keeping the pellets under vacuum most of the air trapped in the exterior pores diffused out. After the n-decane was introduced the system was slowly pressurized to atmospheric pressure and during this time the increase in pressure forced the n-decane into all of the open pores. The pellets were removed from the pressurized vacuum system, and placed onto a basket that was completely

submerged in n-decane and the saturated, suspended weight was recorded, W_{ss}. The pellets were taken from the basket and rolled around on kimwipes®, that were saturated with n-decane, to remove any excess liquid on the outside of the pellets. The pellets were weighed again for their saturated weight, W_s. By using the three weights the open porosity, bulk volume and apparent density were calculated by the following equations:

$$V_{op} = \frac{W_s - W_D}{\rho_l} \tag{2.4}$$

$$V_b = \frac{W_s - W_{ss}}{\rho_l} \tag{2.5}$$

$$\rho_a = \frac{W_D}{V_a} \tag{2.6}$$

The true density of the material was measured by gas pycnometry. The instrument used was a Micromeretics model 1305 multi-volume pycnometer. The method is based on the accurate measurement of two known volumes. One volume is the sample cell volume, V_{cell}, and the other is an expansion volume, V_{exp}. By using these two known volumes and the application of the ideal gas law, helium can be used to find the volume of a finely ground powder sample. After calculating the volume of the sample and measuring the weight of the sample, the true density, ρ_t, can be calculated. After a sample was inserted into the sample cell He was allowed to flow into a gas-tight cell until ~ 19.5 psig was reached. After the pressure was measured as P_{1g}, the He was expanded into an additional pre-measured volume, V_{exp}, and that pressure was recorded as P_{2g}. The volume of He displaced was the volume of the sample, excluding all pores. The technique is based on the assumption that no closed

pores remain in the material since it was finely ground. The following equations indicate how the sample volume and density were measured:

$$V_{sample} = V_{cell} - \frac{V_{exp}}{\frac{P_{1g}}{P_{2g}} - 1} \tag{2.7}$$

$$\rho_t = \frac{W_{sample}}{V_{sample}} \tag{2.8}$$

The pressures P_{1g} and P_{2g} represent the pressure of the He gas in the sample cell and the pressure after the gas in the sample cell has been expanded into the expansion cell, respectively. This technique gives the closest measurement of the materials true density as compared to the calculated unit cell volume-based density.

2.2.4 *Surface area and pore size distribution*

Another technique for obtaining a pore-size distribution is by N_2 gas adsorption at liquid N_2 temperatures, which can also be used simultaneously for surface area analysis. Both pore-size distribution and surface area were measured with a Micromeretics 2000 surface area analyzer. The technique for multi-layer, gas adsorption surface area analysis was developed by Brunnauer, Emmett and Teller (BET).

The pore size distribution was obtained for pores smaller in diameter than 3700Å. The measurement technique assumes that all pores are cylindrical in shape, and it is up to the user to decide from the adsorption isotherm whether the pores are cylindrical, bottle shaped, connected-unconnected, etc. There are many different procedures for obtaining the pore size distribution from the adsorption isotherm, but the one used by the Micromeretics software is the BJH (Barret, Joyner and Halenda) method. Webb et al. (1997) should be consulted for specific details on the measurement of surface area and pore size distributions.

All surface area measurements were carried out using N_2 as the adsorbing gas, and all samples were degassed prior to measurement under a vacuum and a temperature of 110°C to remove any adsorbed or absorbed water from the samples. Both powders and pellets were measured by this method.

2.3 Materials and Methods

2.3.1 Pelletization process

The pelletization process involved a small bench scale pelletizer that had a diameter of 25.5 cm and revolved at speeds up to 120 rpm. It was inclined at an angle of 38°. The pelletization process involved charging the drum with ~ 50 g of material followed by hand spraying with a liquid binder solution of 5 vol% lignin and de-ionized water for limestone or water for P.O.P.-based materials. The binder solution was a lignosulfonate material obtained from Lignotech. It contains sulfate groups that have alkali or alkaline earth ions attached. Two types of lignin binder were used: Norlig A, which is a calcium lignosulfonate with a pH of 3.5 containing 16 wt% reducing sugars, 6 wt% total sulfur, 5 wt% sulfonate sulfur and 4 wt% calcium; and an experimental mixture called a High temperature binding agent which was a combination of sodium lignosulfonates, sugar acids and inorganic salts that had a pH of ~ 10.

During the pelletization process, as the material began to form small pellets more powder material was added by hand while the pellets were sprayed. The binder was sprayed ~ 45 cm from the drum. This process was continued until pellets of a desired size were made. The drum was then emptied and the pellets were separated using various meshes. The smaller pellets were reintroduced to the drum and used to form larger pellets. After the

pellets were made, the drum was cleaned out and the pellets reintroduced for a hardening process. This process was used to help improve the sphericity and green strength of the pellets. The hardening process lasted 20 min for P.O.P. pellets and 60 min for limestone pellets.

The coating process was begun by adding the pellet cores to the drum and moistening them with the lignin/water solution. Then the pelletizer was turned on and shell material was added onto the rotating pellets at the same time that the binder was sprayed. The coating process was continued until the pellets were fully coated with a thick shell. The drum was cleaned of excess material and the hardening process was begun. The hardening process took from 60 to 120 min. The hardening process increased the sphericity and green strength of the pellets. It also increased the final strength of the calcined pellets.

To physically mix materials with limestone powder such as graphite, starch or PVA, a slurry was made with 1.0 wt% sodium hexametaphosphate in deionized water. The slurry contained the limestone and a certain concentration of the additive. The materials were mixed in a plastic bowl with a commercial paint mixer for 30 min at 60 rpm. Following the mixing process, the slurry was dried in an oven overnight at 110°C. The dried mixture was then ground into a fine powder with a mortar and pestle. For co-precipitation of $CaCO_3$ and $SrCO_3$, the materials were dissolved in a dilute HCl solution. After dissolution of the solids the pH of the solution was raised to ~ 7. Then the Ca^{2+} and Sr^{2+} ions were co-precipitated as carbonates by adding ammonium carbonate to the solution. The resulting co-precipitate of Ca and Sr carbonates was dried in an oven overnight at 110°C and the powder was ground with a mortar and pestle for pelletization.

Heat treatment was performed at 1100°C in a Lindberg box furnace. The heat treatment involved a 4 hr ramp to a temperature of 1100°C, a 2 hr soak, and a 4 hr ramp down to 25°C. The heat treatment was used to calcine the materials to increase the strength of the shell.

2.3.2 *Materials*

One of the primary materials used was limestone obtained from the Martin Marriett quarry of Ames, IA. The limestone had a pre-calcined chemical composition of 95.75 wt% $CaCO_3$, 1.77 wt% $CaCO_3$-$MgCO_3$, 0.752 wt% SiO_2, 0.216 wt% Fe_2O_3, 0.155 wt% Al_2O_3 with remaining elements < 0.1 wt%. Another material used was plaster of Paris from United States Gypsum in Oklahoma. This material had a pre-calcined composition of 98 wt% $CaSO_4 \cdot 1/2H_2O$, 0.26 wt% $SrSO_4$, 0.20 wt% SiO_2, 0.19 wt% Mg $SO_4 \cdot 7H_2O$, 0.16 wt% $MgCO_3$, with remaining elements < 0.1 wt%. A different type of plaster of Paris was from DAP, Inc. that contained a pre-calcined composition of 78 wt% $CaSO_4 \cdot 1/2H_2O$, 15 wt% $CaCO_3$, 6 wt% $CaCO_3 \cdot MgCO_3$ with remaining elements < 0.1 wt%. There were two forms of dolomite used in the study, the natural carbonate form that is referred to as dolomite [$CaCO_3 \cdot MgCO_3$], and a hydrated form that had first been calcined and then converted into the hydroxide form, which is referred to as dolime [$CaMg(OH)_4$]. Both materials were obtained from Graymont Dolime (OH) Inc. of Ohio and contained 58 wt% CaO, 38 wt% MgO, 0.5 wt% SiO_2, 0.5 wt% metal oxides, and a trace of SrO_2 after calcination at 1000°C and prior to hydration. Two grades of alumina were obtained from Alcoa: T-64 tabular alumina (9 μm) and A-16SG calcined alumina (1 μm). Both had an Al_2O_3 content > 99 wt%. The kaolin was from the Feldspar Corporation and it had a composition of 46.7 wt%

SiO_2, 37.4 wt% Al_2O_3, 0.79 wt% Fe_2O_3, 0.37 wt% TiO_2, 0.33 wt% K_2O, 0.24 wt% P_2O_5, 0.18 wt% CaO, 0.10 wt% MgO, 0.06 wt% Na_2O. The starch was from Fisher Chemical Company and was 100 wt% cornstarch. The poly (vinyl alcohol) was from Polysciences Inc. and was > 99 wt% PVA.

2.3.3 *Crushing strength and attrition resistance tests*

Following the heat treatment, the pellets were subjected to crush strength tests. The apparatus used was an Accuforce EZ250 vertical crush strength stand. The EZ250 employs two flat metal plates for crushing the pellets. One plate is stationary, on top of which is placed a pellet. The upper plate is lowered at a rate of 10 mm/min. The maximum force required to crack a pellet was recorded. The force in newtons, N, was divided by the diameter of the pellet to give a quantitative comparison of strength vs. size.

$$\text{Crushing Strength} = \frac{\text{Force}}{\text{Diameter}} \tag{2.9}$$

An ASTM standard (D 4058-96) for measuring the attrition rate of catalysts was employed for the core and shell pellets. The attrition test for measuring the ruggedness of the pellets utilized an aluminum, cylindrical drum having a diameter of 10 in and width of 6 in. A single, 2 in high radial baffle spanned the full width of the drum. Approximately 100 g of pellets, diameter > 3.96 mm, were charged into the drum, the drum was sealed, and then rotated for 1800 revolutions at 60 +/- 5 rpm. The drum was then emptied and the material was sieved. Any pellets that were retained on the screen but were chipped, were considered attrition losses. The material that fell through the sieve and the chipped pellets were weighed and subtracted from the original weight of the pellets. The attrition loss of the sample was determined by:

$$\%\text{Attrition} = \frac{W_i - W_f}{W_i} \times (100) \qquad (2.10)$$

2.3.4 *Reactor configuration*

The regeneration and sulfidation reactions took place in a quartz reactor tube 2.5 cm in diameter (I.D.) with a heated length of 41 cm, surrounded by a tube furnace capable of reaching a temperature of 1100°C. A gas manifold was used to premix the gases prior to entering the reactor. The reaction was monitored by observing sample weight changes with a Cahn 2000 electrobalance. The apparatus constituted a thermal gravimetric analyzer (TGA) that was connected to a PC for data acquisition. The temperature of the reacting gases was monitored by a type K thermocouple that was encased in quartz tubing and located ~ 1 cm below the sample basket. The thermocouple was also connected to the PC for data acquisition. The samples were placed in a quartz basket that was suspended by a quartz hang-down wire from an electrobalance cantilever bar in a bell jar. The bell jar contained the electrobalance and was constantly flushed with N_2 during the tests to prevent corrosive gases from diffusing in from the reactor tube. The effluent from the reactor tube flowed through a caustic solution that neutralized the corrosive gases.

2.3.5 *Reaction conditions*

The gas supplied for the sulfidation reaction consisted of 1.0 vol% H_2S, 24 vol% H_2 with N_2 as the balance of gas. The sulfidation was carried out at 880°C according to the reaction:

$$CaO + H_2S \rightarrow CaS + H_2O \qquad (1.2)$$

and the equation used for calculating the specific capacity of a pellet was:

$$\%\text{Specific Capacity} = \frac{W_{CaS} - W_{CaO}}{W_{CaO}} \times 100 \qquad (2.11)$$

where W_{CaS} is the weight of the sulfided pellet and W_{CaO} is the weight of the pellet prior to reaction with H_2S.

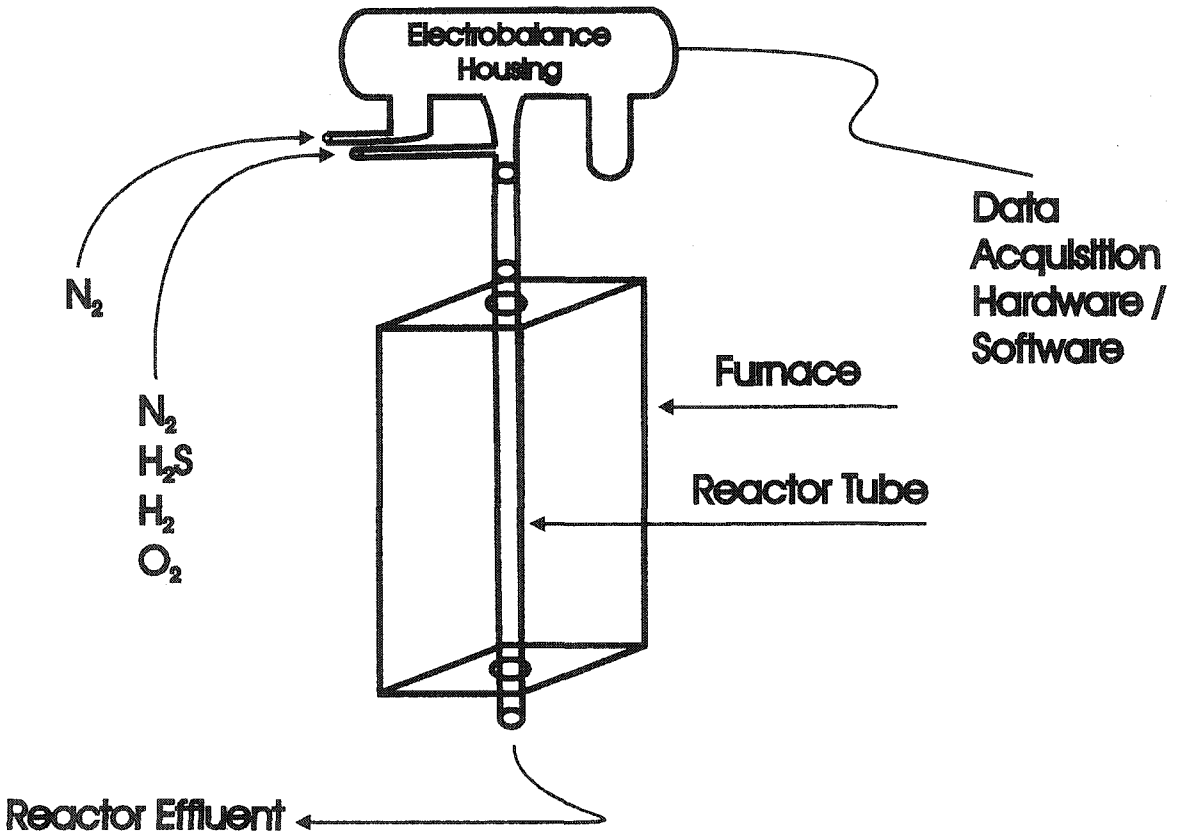

Figure 2.1. Reactor and TGA system for sulfidation and regeneration reactions.

The total gas flow rate was 500 mL/min at approximately 1 atm of pressure for both sulfidation and regeneration. The regeneration reactions were carried out at 1050°C using a gas mixture with 13 vol% O_2 in N_2 for oxidation:

$$CaS + 2O_2 \rightarrow CaSO_4 \qquad (1.9)$$

and 9 vol% H_2 in N_2 for reduction:

$$CaSO_4 + H_2 \rightarrow CaO + SO_2 + H_2O \qquad (2.12)$$

The regeneration reactions typically required three cycles of oxidation and reduction requiring a total time of ~ 15 min.

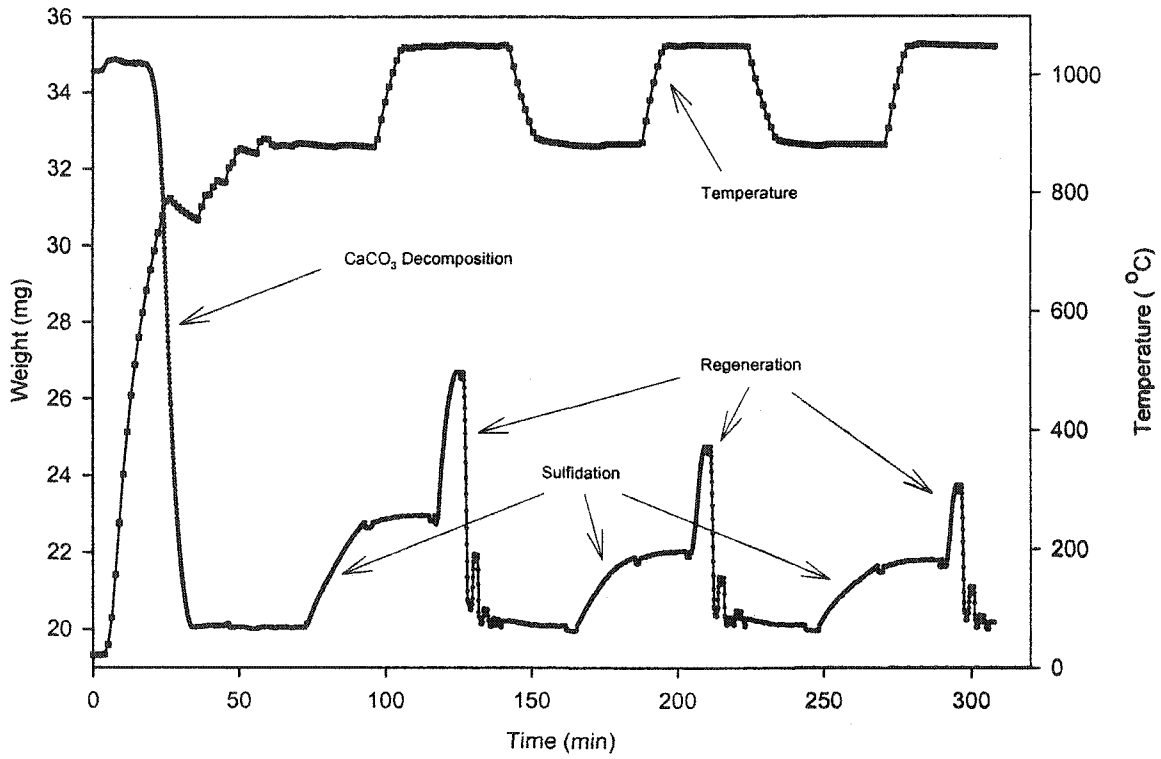

Figure 2.2. Multicycle sulfidation-regeneration of a limestone pellet reacted with 1.0 vol% H_2S, 24 vol% H_2, in N_2 at 880°C and regenerated with 9 vol% H_2, 13 vol% O_2 in N_2 at 1050°C.

Chapter 3. Sorbent Development

3.1 Introduction

The development of a suitable solid oxide sorbent for removing H_2S and COS from gasified coal hinges upon the reusability of the sorbent over multiple cycles of sulfidation and regeneration. In order to obtain high efficiencies with new generation power plants such as an IGCC system, a sorbent that is operable at temperatures exceeding 800°C is needed. Fortunately, calcium oxide is very reactive with H_2S and COS at such high temperatures and is stable under the reducing conditions inherent in gasified coal. The main obstacle presented at high temperatures is the sintering of the CaO. Since the reaction between H_2S and COS with CaO is very dependent upon the surface area of CaO (Borgwardt, 1984b), the sintering of CaO should be kept to a minimum. In addition, the reactivity of CaO is also dependent upon its open pore porosity, which facilitates the mass transfer of reactant and product species in the gas phase. Therefore, the porosity of the CaO sorbent should be increased for better performance.

The development of most sorbents for reacting with H_2S and COS in coal gas are made either through extrusion or agglomeration processes. Due to the complex nature of the sintering process a few key parameters during sorbent processing can be used to affect the sintering and porosity of the sorbent. Such factors are particle size distribution, porosity and purity of the materials.

This chapter covers the analysis and development of an improved CaO-based sorbent originally designed by Akiti et al. (2002). The sorbent development was based upon the agglomeration of particles into spherical pellets ~ 3.5 mm in diameter. The studies in this

chapter are on agglomerated particles (pellets) of limestone, reagent grade $CaCO_3$, dolomite, dolime, two forms of plaster of Paris and limestone cores with different additives. The reactivity of the pellets over multiple cycles as well as the porosity, surface area and density changes were measured and analyzed.

3.2 Results and Discussion

3.2.1 *Comparison between limestone and plaster of Paris*

One of the primary objectives of the sorbent development was to compare the changing physical properties of limestone and plaster of Paris pellets over multiple sulfidation-regeneration cycles. It was previously reported that limestone-based pellets lost sulfidation capacity over multiple cycles while plaster of Paris did not (Akiti et al, 2002). These findings were quite interesting and a study was conducted to investigate the difference.

The study was conducted on the same materials tested by Akitit et al. Since the purity of the material has a large effect on sintering, the materials were analyzed for their chemical composition. The limestone was from Martin Marrietta Aggregates of Iowa, and consisted of 96.75 wt% $CaCO_3$, 1.77 wt% $CaCO_3$-$MgCO_3$, 0.75 wt% SiO_2, 0.22 wt% Fe_2O_3, 0.16 wt% Al_2O_3, with the rest of the impurities < 0.1 wt%. The plaster of Paris (P.O.P.) was from United States Gypsum of Oklahoma, and consisted of 98 wt% $CaSO_4 \cdot 1/2H_2O$, 0.26 wt% $SrSO_4$, 0.20 wt% SiO_2, 0.19 wt% $MgSO_4 \cdot 7H_2O$, 0.16 wt% $MgCO_3$, 0.01 wt% Fe_2O_3, with the rest of the impurities < 0.1 wt%.

The comparison between limestone and P.O.P. pellets was undertaken by reacting 1 g of the pellets with 1 vol% H_2S, 24 vol% H_2 and N_2 at 880°C according to the reaction

$$CaO + H_2S \rightarrow CaS + H_2O \qquad (1.2)$$

over multiple, consecutive cycles in the TGA reactor system described in Chapter 2. The regeneration of the CaS was carried out after each sulfidation reaction, according to the cyclic process discussed in Chapter 2, with 9 vol% H_2, 13 vol% O_2 and N_2 at 1050°C by the reactions:

$$CaS + 2O_2 \rightarrow CaSO_4 \qquad (1.9)$$

$$CaSO_4 + H_2 \rightarrow CaO + SO_2 + H_2O \qquad (2.12)$$

The experiments revealed that the limestone pellets exhibited a loss in specific capacity similar to that described by Akiti et al., but the P.O.P. pellets also exhibited a loss in specific capacity after multiple cycles (Figure 3.1) where specific capacity is represented by the equation:

$$\%\text{Specific Capacity} = \frac{W_{CaS} - W_{CaO}}{W_{CaO}} \times 100 \qquad (2.11)$$

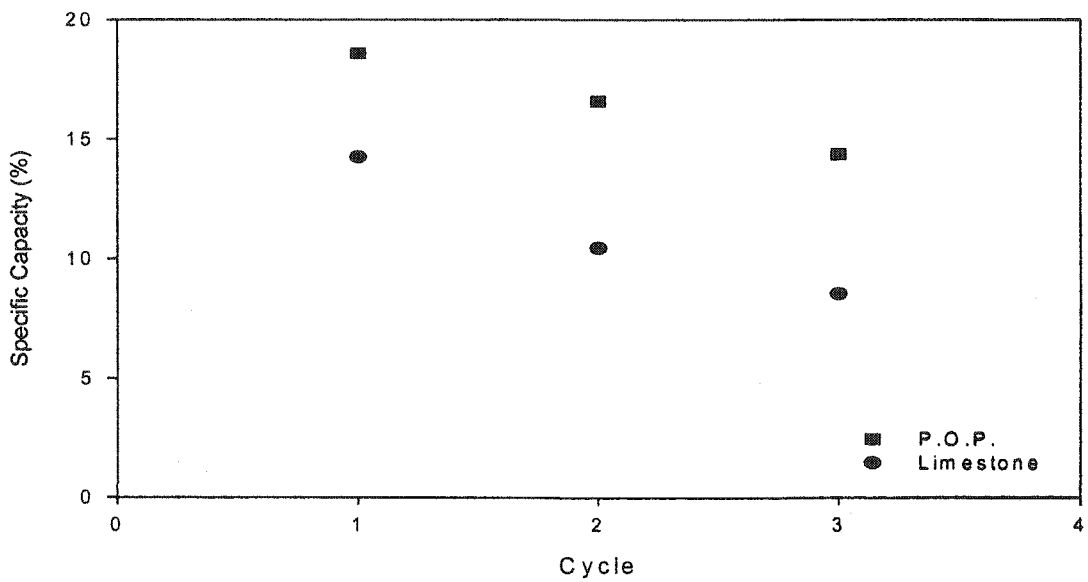

Figure 3.1. P.O.P. and limestone pellets reacted with 1.0 vol% H_2S, 24 vol% H_2 in N_2 at 880°C.

What is also apparent is the higher reactivity (specific capacity) exhibited by the P.O.P. pellets. Since both types of pellets were in the form of CaO after decomposition or regeneration, and they were both very pure materials, there was no apparent reason why one type should react differently than the other. Therefore, an investigation into the physical properties of the two types of pellets was conducted.

The comparison between the two types of pellets was based upon surface area, pore size distribution, open pore porosity and apparent density. The study was carried out by reacting ~ 40 pellets of each type in the reactor system described earlier and following the changes in the pellets. The physical properties were measured after the following stages: post pelletization (stage 1), heat treatment at 110°C under vacuum (stage 2), decomposition at 880°C (limestone) or conversion at 1050°C (P.O.P.) (stage 3), and three cycles of sulfidation and regeneration (stages 4-6).

Because the reaction between H_2S and CaO is dependent upon surface area, this property measurement was a primary focus (Borgwardt, 1984b). The change in surface area at each stage in the process is shown in Figure 3.2. Initially, the P.O.P. pellets had a much higher surface area, which was probablly due to the large volume expansion that the P.O.P. underwent during the pelletization process.

$$CaSO_4 \cdot 1/2H_2O + 3/2H_2O \rightarrow CaSO_4 \cdot 2H_2O \qquad (3.1)$$

Following the hydration reaction, and stage 2, during which the pellets were subjected to 110°C under vacuum, the water of hydration was removed leaving a very porous structure. The limestone pellets did not undergo such a reaction during pelletization, and remained as $CaCO_3$ even after the heat and vacuum treatment. But, once the pellets had been converted to CaO, the surface areas of the pellets were reversed (stage 3). This finding is very

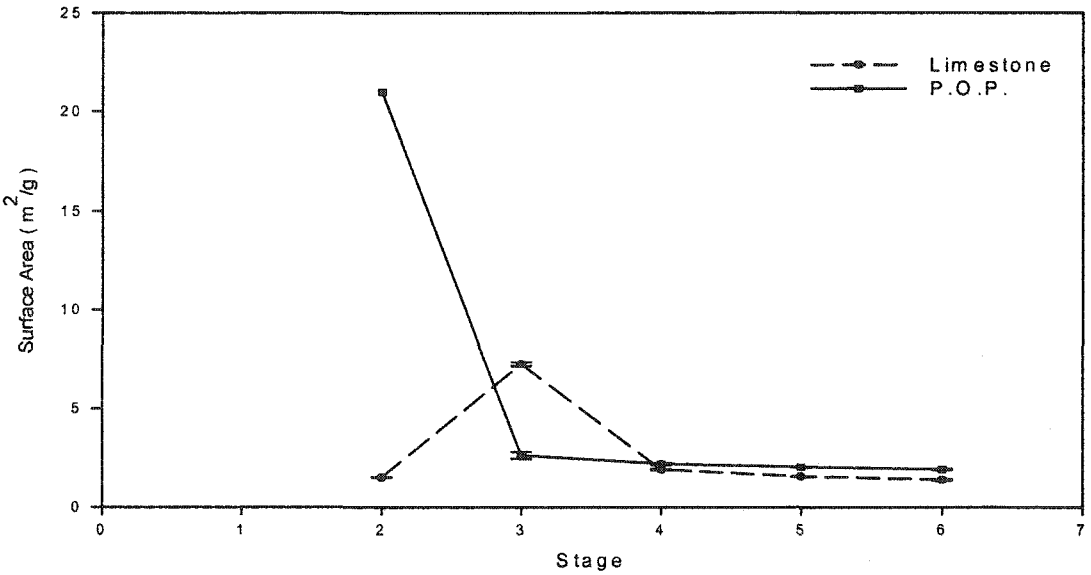

Figure 3.2. P.O.P. and limestone pellets surface area change with stage.

interesting since the limestone at this point had a higher surface area than the P.O.P. pellets, yet the P.O.P. pellets reacted faster during the first sulfidation cycle (Figure 3.1). Since the H_2S-CaO reaction is surface area dependent, this result is quite perplexing. One possibility could be that by the time the CaO pellets had reached the temperature of 880°C they were already sintered, which resulted in a surface area lower than the P.O.P. pellets. According to Figure 3.2 the trend in the reduction of surface area is similar for the two materials at stages 4-6, but what is not apparent, is that the P.O.P. pellets had a surface area that was 13%, 24% and 28% higher than the limestone pellets at stages 4,5 and 6. This larger surface area could be the reason for the higher reactivity exhibited by the P.O.P. pellets.

Another possibility for the lower rate of reaction of the limestone pellets could be due to gas-phase mass transfer limitations throughout the pellet as a whole. With this thought in

mind, the pore size distribution was looked into. The average pore size distribution of the two materials is shown in Figure 3.3.

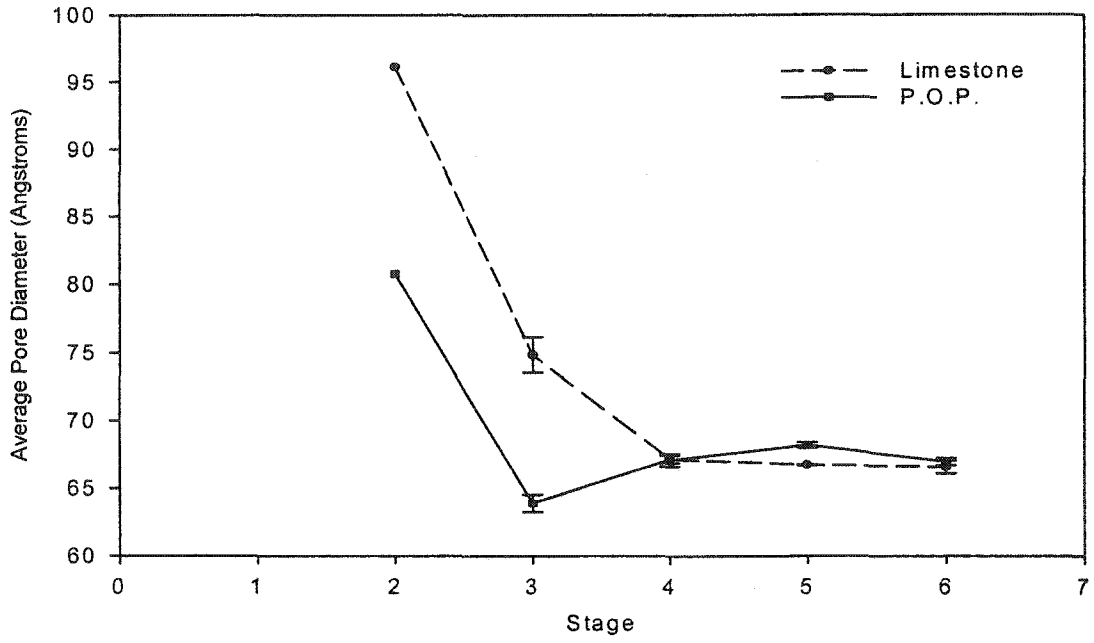

Figure 3.3. P.O.P. and limestone pellets average pore size change with stage.

In this case, the change in averge pore diameter for the two materials follows a similar trend. At stages 2 and 3 it can be seen that the limestone pellets had a larger average diameter, but this distinction was immediately lost after the sulfidation reactions took place. Therefore, no conclusion can be drawn that would point to a pore size effect on the rate of reaction. But, since these measurements were based on N_2 adsorption and BET analysis, only pores up to a diameter of 3700 Å were included in the measurement, so the effect of larger pores was excluded.

Using a different technique based on Archimedes' principle, total open pore porosity and apparent density were measured which enabled the comparison of macro-porosity and sintering effects respectively.

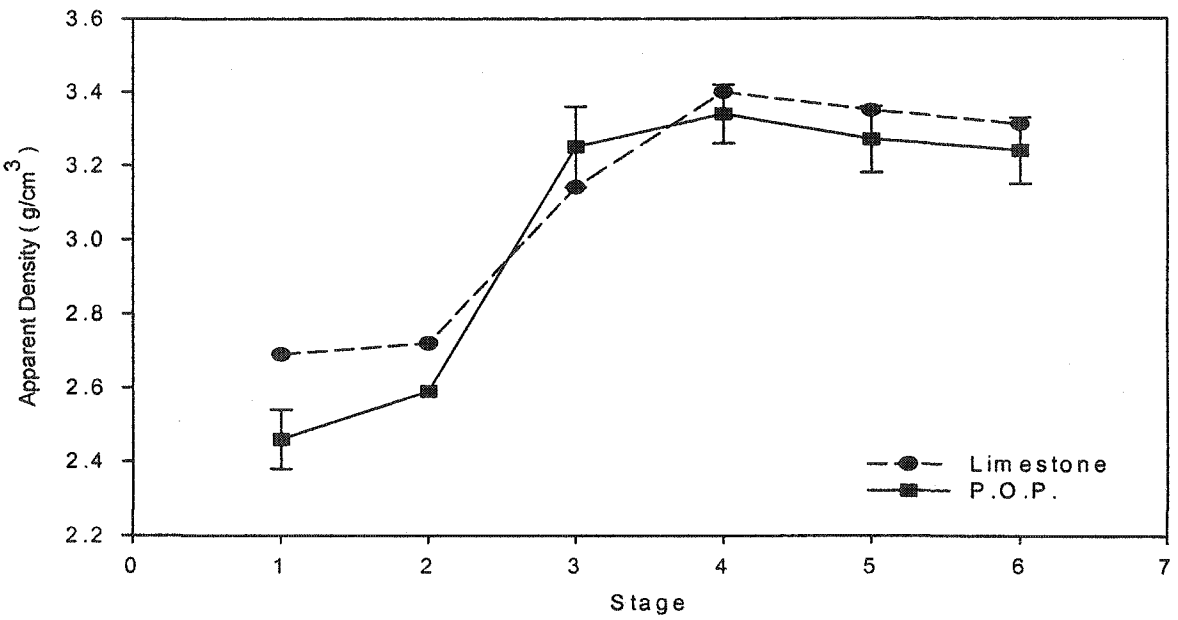

Figure 3.4. P.O.P. and limestone pellets apparent density change with stage.

The graphs in Figures 3.4 and 3.5 show the change in apparent density and percent open porosity, $\%V_{op}$, of the pellets at each stage, respectively. While both parameters indicate that the pellets followed a similar trend, no quantitative differences in apparent densities can be distinguished between the pellets at stages 4-6. Since the materials were quite pure, the apparent densities should have been in the same range so these results are not surprising.

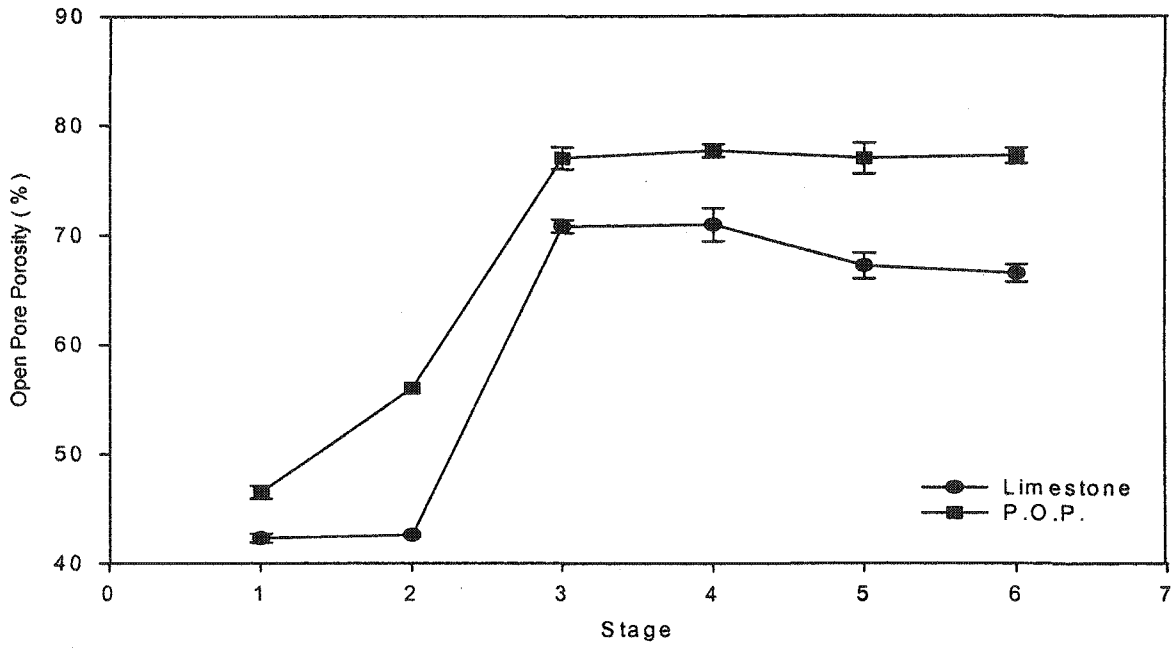

Figure 3.5. P.O.P. and limestone pellets open pore porosity (%) change with stage.

The open pore porosity data showed a similar trend, but in this case, the P.O.P. pellets exhibited a larger $\%V_{op}$ throughout all of the stages. Since the measurement technique for obtaining the $\%V_{op}$ reveals the overall pellet porosity including micro, meso and macro pores, it does not distinguish between any size of pore, and it includes very large pores such as those created by the pores between particle-particle agglomerates. Because the majority of surface area for both pellets lies in the < 780 Å pore size range, the large macro-pores outside of this range will only affect the gas-phase diffusion process.

In order to analyze and compare the effects of surface area and macro-porosity on the sulfidation capacity, the changes in both parameters are compared in Table 3.1.

Table 3.1. Changes in surface area and porosity with stage for P.O.P. and limestone pellets.

	P.O.P.			Limestone		
Stage	Surface Area m^2/g	Porosity 20<D<780Å cm^3/g	Porosity 780Å<D cm^3/g	Surface Area m^2/g	Porosity 20<D<780Å cm^3/g	Porosity 780Å<D cm^3/g
2	21	0.0423	0.463	1.49	0.00360	0.269
3	2.6	0.00418	1.059	7.3	0.0136	0.711
4	2.18	0.00366	1.042	1.89	0.00317	0.701
5	2.02	0.00344	1.054	1.53	0.00256	0.611
6	1.89	0.00316	1.015	1.36	0.00227	0.599

D represents the diameter of pores that contribute to the porosity in that size range.

The data in Table 3.1 represent the changes in physical properties that the two types of pellets experienced. The most distinct correlation was between porosity in the 20<D<780Å range and surface area. It was in this range that a decrease in porosity matches directly with a decrease in surface area. Since a connection is sought between the drop in sulfidation capacity and a physical parameter, the most obvious correlation is with a loss in surface area. Therefore, the change in macro-porosity does not have such a significant effect.

The reason for the more rapid loss in surface area of the limestone pellets is attributed to the higher content of Fe_2O_3. Iron oxide is a fluxing component at high temperatures and could be the root cause for the rapid sintering of the limestone. An observation that supports this idea was the discoloration of the limestone pellets after multiple runs. The limestone pellets would slowly exhibit a large number of reddish-brown dots on the surface, which were thought to be the iron oxide in the material. While the P.O.P. pellets were very white in comparison, and contained approximately one 0.1 mm brown dot per pellet.

3.2.2 *The effects from increasing the porosity of limestone pellets*

Since the sintering of materials at high temperatures cannot be prevented entirely, alternate paths that inhibit or slow down the process was sought. One possibility of slowing down the process is to increase the porosity of a material. The increase in porosity decreases the number density of particle-particle contacts, which reduces the points of contact for sintering to take place. For the preparation of heterogeneous catalysts or solid sorbents, the porosity can be increased by chemical methods such as sol-gel processing or simply by adding an organic material that will be vaporized or combusted at high temperatures leaving behind a porous substrate of the complex of interest.

The work presented in this section is based upon the addition of materials to limestone pellets in order to increase the porosity and the reactivity of the pellets and possibly slow down the rate of sintering during the reaction with H_2S. The materials used in the study were water-soluble starch, poly (vinyl alcohol) (PVA), and graphite.

The initial tests were conducted with starch dry-mixed with limestone powder prior to pelletization. The resulting pellets were difficult to pelletize, irregular in shape and when reacted with H_2S, exhibited a lower capacity than pellets made with only limestone. No explanation can be given for this except that due to the irregular shape of the pellets some areas might have been compacted much more severely during the pelletization process. Since the pellets were irregular in shape, it is possible that as the pellets rolled, ground and tumbled in the drum, they experienced a wider range of compacting forces than spherical pellets. This could possibly result in pellets with densely compacted regions, which could then be more prone to sintering than a spherical pellet.

Since inhomogeneous mixing was thought to be a problem when dry-mixing the powders, a technique was introduced to effectively and quickly mix the powders together. The process involved mixing the limestone and pore-forming material (5 wt%) in a water and 0.05 wt% sodium hexametaphosphate solution. The resulting slurry was then mixed for 30 min with a commercial paint mixer at 60 rpm. Following the mixing process the material was dried in an oven at 110°C, ground into a fine powder and pelletized according to the process described in Chapter 2.

The pellets were tested for specific capacity by running multi-cycle sulfidation and regeneration tests with 1.0 vol% H_2S, 24 vol% H_2, and N_2 at 880°C for 20 min followed by regeneration at 1050°C as described in Chapter 2. A total of three sulfidation and regeneration cycles were used for comparing each type of pellet. The results in the form of specific capacity versus cycle are shown in Figure 3.6 where the limestone results are from three separate tests, the starch and PVA two tests, and the graphite one test.

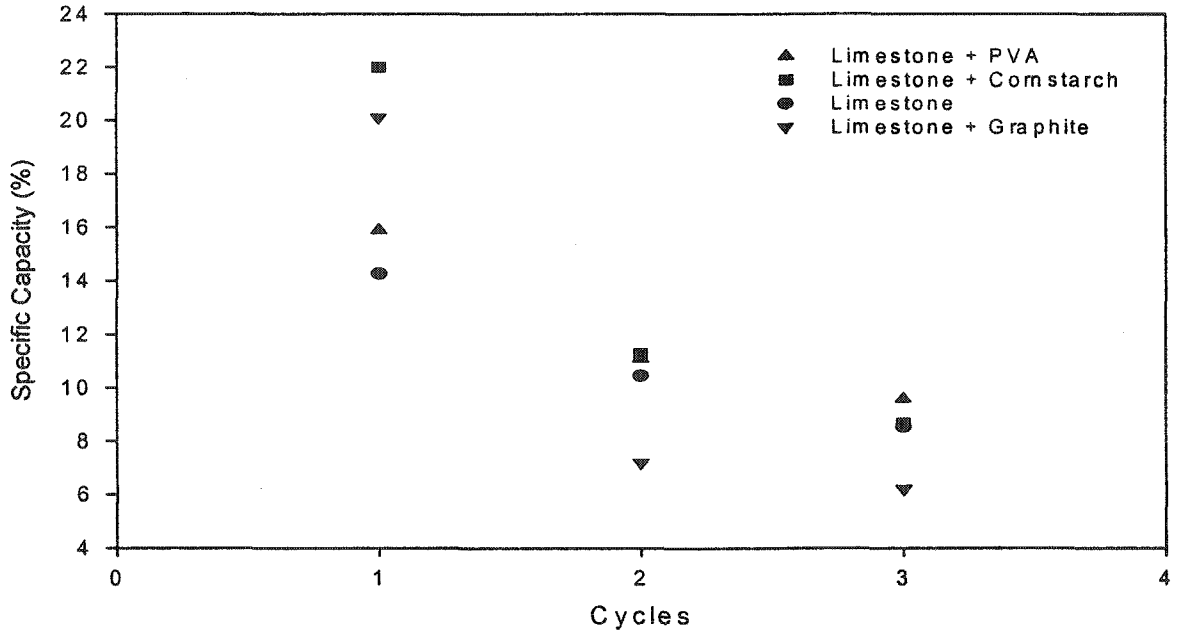

Figure 3.6. Various limestone pellet formulations including starch, PVA and graphite reacted with 1.0 vol% H_2S, 24 vol% H_2 in N_2 at 880°C.

The results indicate that all three forms of pellets with additives exhibited a higher rate of reactivity than limestone during the initial sulfidation test. Similar results were obtained by Pineda et al.(1998), while studying the effects of graphite as a pore modifier on zinc titanate sorbents during reactions with H_2S. But, as the data reveal, the reactivity of the pellets dropped off significantly with each cycle. And the drop in capacity was very similar to limestone. Only the PVA pellets exhibited a slight increase in capacity above the limestone pellets throughout all three cycles, whereas the starch pellets had a comparable capacity and the graphite pellet capacity dropped significantly during the second and third cycles. The reason for the drop in capacity below that of limestone is not known, but the graphical profile of a typical limestone pellet experiment (Figure 3.7) is much different from the graphite pellet (Figure 3.7) during the sulfidation and regeneration cyclic process.

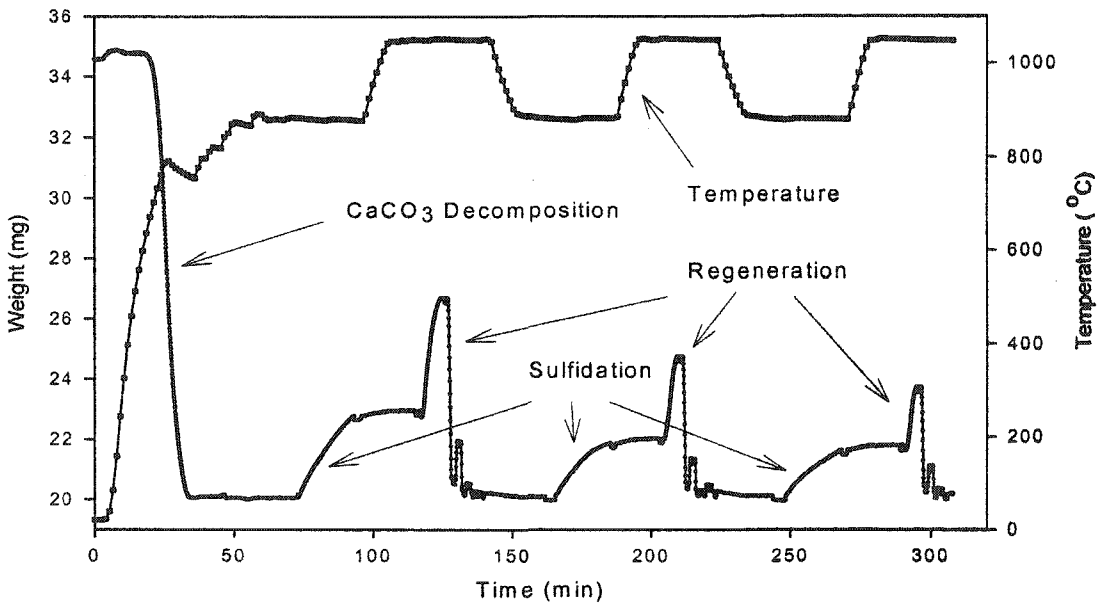

Figure 3.7. Multicycle sulfidation-regeneration of a limestone pellet reacted with 1.0 vol% H_2S, 24 vol% H_2 in N_2 at 880°C and regenerated with 9 vol% H_2, 13 vol% O_2 in N_2 at 1050°C.

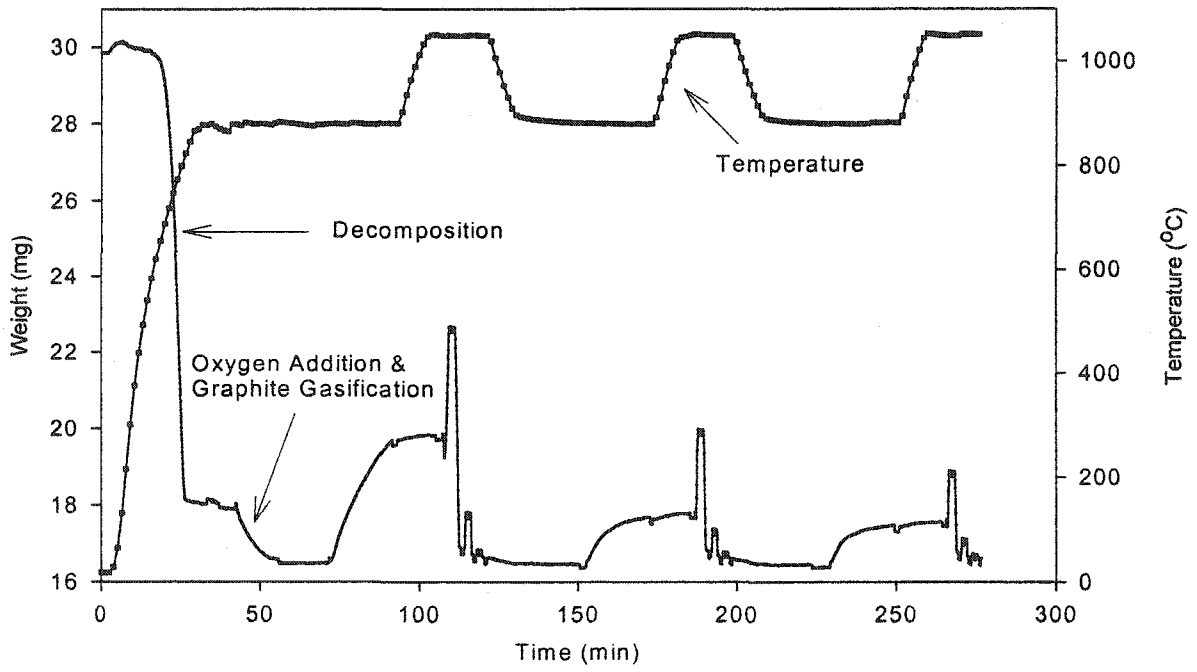

Figure 3.8. Limestone-graphite pellet decomposed, gasified and reacted with 1.0% vol H_2S, 24% H_2 in N_2 at 880°C and regenerated with 9% vol H_2, 13% O_2 in N_2 at 1050°C over multiple cycles.

One major difference between the three modified pellets is that the graphite pellets had to be oxidized prior to reaction to remove the graphite through gasification. For the PVA and starch pellets, the materials were vaporized at relatively low temperatures (~200°C). The oxidation of the graphite can occur through the following reactions:

$$C + 1/2O_2 \rightarrow CO \qquad (3.2)$$

$$C + O_2 \rightarrow CO_2 \qquad (3.3)$$

which are both exothermic reactions at 880°C, -109.4 kJ/mol for CO production and -394.5 kJ/mol for CO_2 production. The oxidation reaction was performed using a very dilute stream of O_2 in N_2 to limit the rate of combustion of the carbon. It is thought that the exothermic oxidation of carbon could increase the sintering of the material and cause a

decrease in the surface area of the pellets, but this does not explain the high reactivity exhibited during the first cycle.

Another result that is not explainable was the similarity between the reaction profile of a starch pellet (Figure 3.9) and a graphite pellet (Figure 3.8). Both types of pellets exhibited a very fast and linear rate of reaction during the first cycle, but the second and third cycles indicated that the rates were dropping off at a rapid pace.

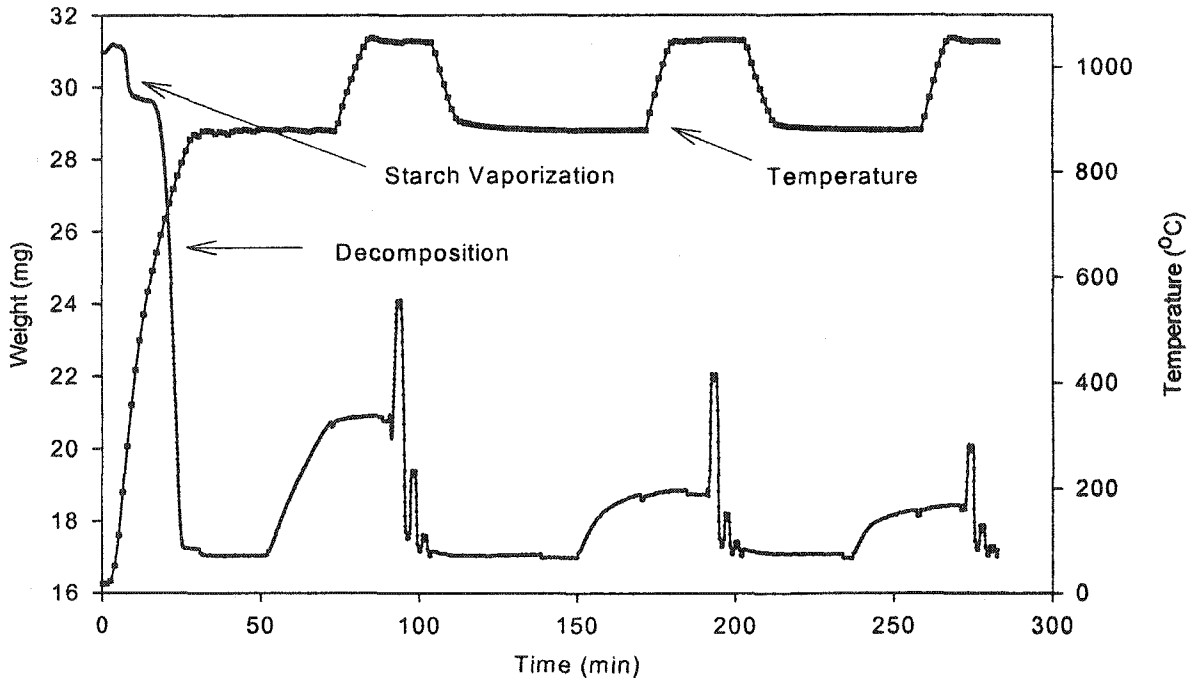

Figure 3.9. Limestone-starch pellet vaporized and reacted with 1.0 vol% H_2S, 24 vol% H_2 in N_2 at 880°C and regenerated with 9 vol% H_2, 13 vol% O_2 in N_2 at 1050°C over multiple cycles.

Of the three types of additives, the PVA additive seemed to provide the best improvement in the capacity of the limestone. Even though the starch additive increased the capacity of the limestone more than the PVA for the first cycle, by the second cycle the capacity was approximately the same for either additive. And by the third cycle the capacity

of the starch pellets had dropped to that of the limestone without an additive, while the PVA pellets still exhibited an improved capacity. In addition, the decrease in capacity of the PVA pellets with each cycle was not as severe as that of the starch or limestone pellets. The reason for the improved performance provided by the PVA is not known. It is possible that the PVA was distributed more uniformly throughout the powder than the starch, or during the pelletization process the starch may have tended to flocculate due to the presence of the lignin solution, thereby preventing a homogeneous distribution. The interaction between the limestone and the different pore modifiers could be very different during the mixing and pelletization process, so without a thorough analysis it is not possible to offer an accurate explanation for the difference in performance.

3.2.3 *The effects of strontium and magnesium on the reactivity of CaO with CO_2*

In addition to increasing the porosity of a material to inhibit sintering at high temperatures, the use of chemical additives can also be employed. The incorporation of the additive can be through a number of processes, some of which are co-precipitation, and the wet and dry mixing of powders. Or natural materials can be used that already contain chemical additives, such as dolomite, which has $MgCO_3$ distributed throughout the material. Regardless of the method used, the chemical additive should be homogeneously arranged throughout the bulk of the material in order to improve its effectiveness.

The research discussed in this section focused primarily on the effects of Mg and Sr additives on the reactivity of CaO with CO_2, but a comparison of all Ca-based materials tested with H_2S is made at the end. The effect of Mg was evaluated by using materials that naturally contain $MgCO_3$ and the effect of Sr was evaluated by incorporating it into the limestone by both wet-mixing and co-precipitation with $CaCO_3$, as discussed in Chapter 2.

The Mg was incorporated into the study due to its prevalence in $CaCO_3$-bearing materials and the Sr was chosen due to a report by R. A. Brown (1965), in which he reported that the addition of SrO (1, 2, 5 wt%) reduced the rate of densification of CaO at temperatures of 800 to 1550°C.

In order to increase the rate at which materials could be tested for sintering effects, the CaO materials were tested with CO_2 in N_2 at 750°C instead of H_2S at 880°C. The reaction with CO_2 was chosen since the decomposition of $CaCO_3$ at 750°C is only a function of CO_2 partial pressure, which can be easily reversed,

$$CaO + CO_2 \rightarrow CaCO_3 \qquad (3.4)$$

whereas the CaS has to be heated to 1050°C and reacted with H_2 and O_2 for regenerating CaO, which takes ~ 45 min for a typical pellet. The performance of the pellets is represented by the total specific capacity achieved after 20 min of carbonation

$$\%\text{Specific Capacity} = \frac{W_{CaCO_3} - W_{CaO}}{W_{CaO}} \times 100 \qquad (3.5)$$

where W_{CaCO_3} is the final weight of the pellet and W_{CaO} is the initial weight of the pellet.

To study the effects of SrO on CaO, the $SrCO_3$ was wet-mixed (2 wt%) with limestone powder (< 44 μm) by using either a commercial paint mixer or by wet ball milling. The $SrCO_3$ was also combined (10 wt%) with $CaCO_3$ by co-precipitation. Following the mixing process the pellets were dried in an oven at 110°C and then ground with a mortar and pestle. The powders were pelletized to provide spherical pellets ~ 3.5 mm in diameter. Specifications for the materials, materials mixing, and reactor system can be found in Chapter 2. During the testing, samples were initially decomposed at 750°C under N_2 and then reacted with a 40 vol% mixture of CO_2 in N_2 at 750°C for 20 min. Following the

carbonation reaction (eq 3.4), the materials were decomposed by flowing pure N_2 through the reactor for ~ 15 min. The results from a typical multi-cycle carbonation-decomposition experiment are shown in Figure 3.10.

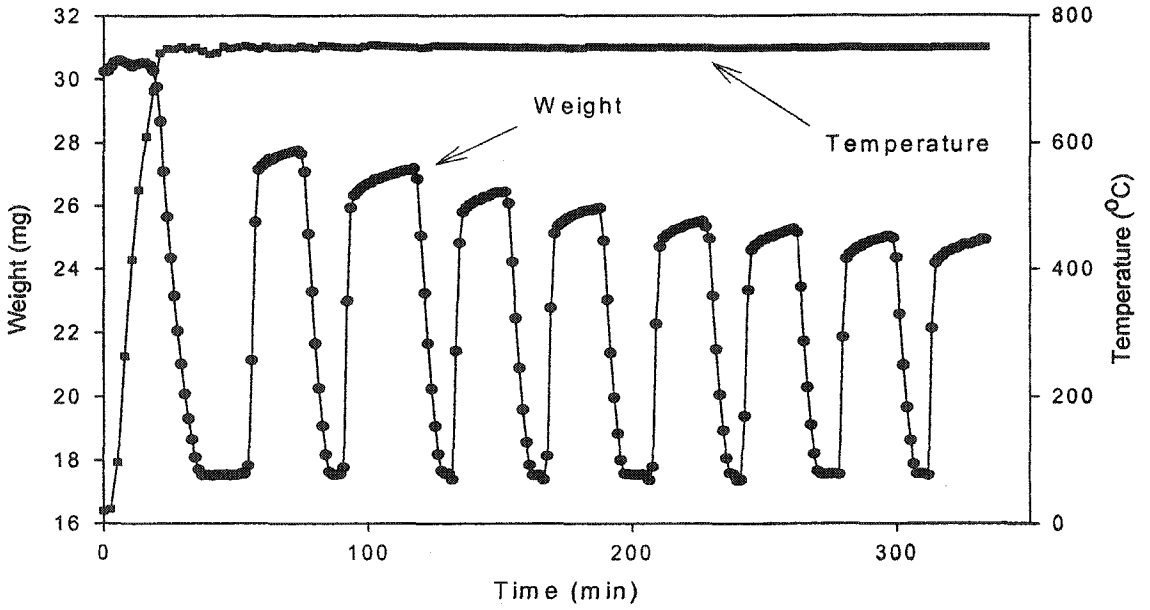

Figure 3.10. Limestone pellet reacted with 40 vol% CO_2 in N_2 at 750°C for 20 min cycles.

The results from similar tests obtained with different materials after eight cycles of carbonation-decomposition at 750°C are shown in Figure 3.11, where each dot represents the average of two pellets tested for each type of material. The results show how the specific capacity of all the materials decreased after each cycle. The limestone, limestone-$SrCO_3$, and $CaCO_3$- $SrCO_3$ pellets all exhibited a rapid decrease in specific capacity over the eight cycles. Some differences between the Sr-containing pellets can be seen for the first cycle with regards to the ball-milled pellets exhibiting a lower capacity, but eventually all of the pellets with Sr ended up with a specific capacity that was more than 20% lower than the

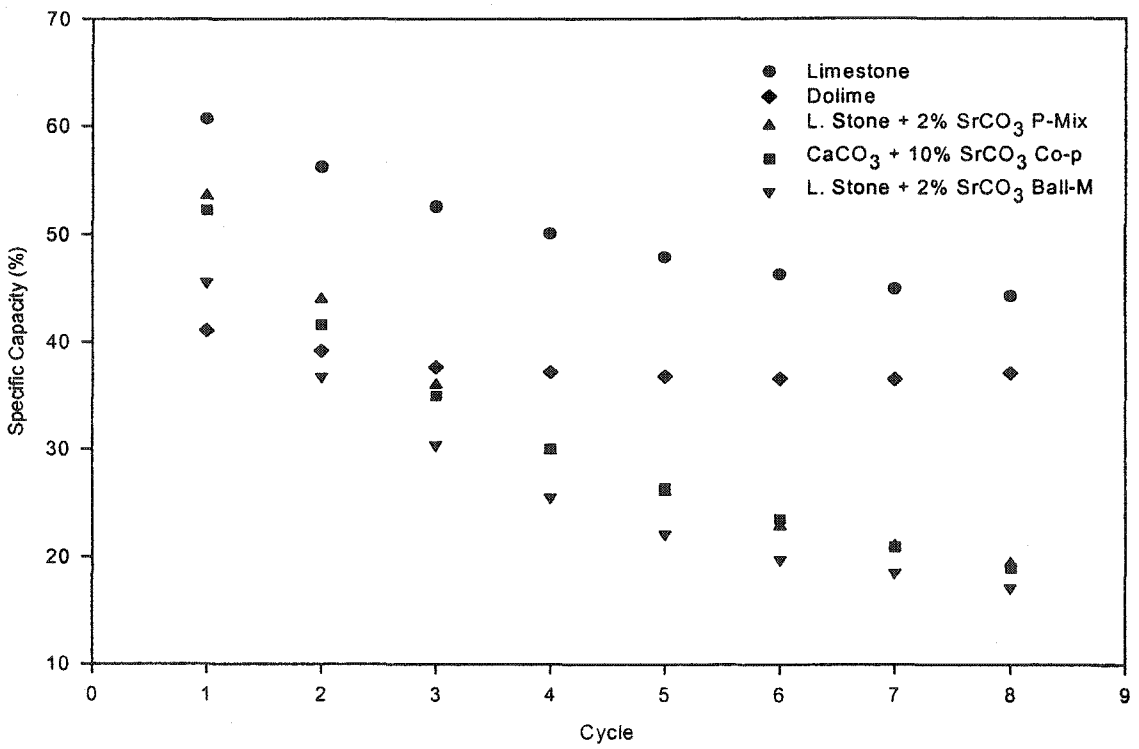

Figure 3.11. Change in specific capacity with carbonation-decomposition cycle for pellets made of: limestone, limestone-2 wt% $SrCO_3$, $CaCO_3$-10 wt% $SrCO_3$ co-precipitate and dolime reacted for 20 min cycles with 40 vol% CO_2 in N_2 at 750°C.

limestone pellets. What is especially interesting is the very low loss in specific capacity exhibited by the dolime sample. Because the dolime sample contained MgO, which did ot react with the CO_2 at 750°C, the CaO was probably stabilized by the inert MgO particles. An extensive report on the reactivity of various dolomites with CO_2 was presented by Bandi et al. (2002) in which they discussed similar findings with regards to the high capacity exhibited by the dolomites after multiple cycles.

Since a decrease in reaction rate at such high temperatures is assumed to be a function of surface area loss, samples in the carbonated form that were tested for eight cycles were fractured and viewed with an SEM to evaluate the pellets for sintering effects

(Figures 3.12-3.15). The SEM micrographs were obtained by focusing on the midsection of each type of pellet.

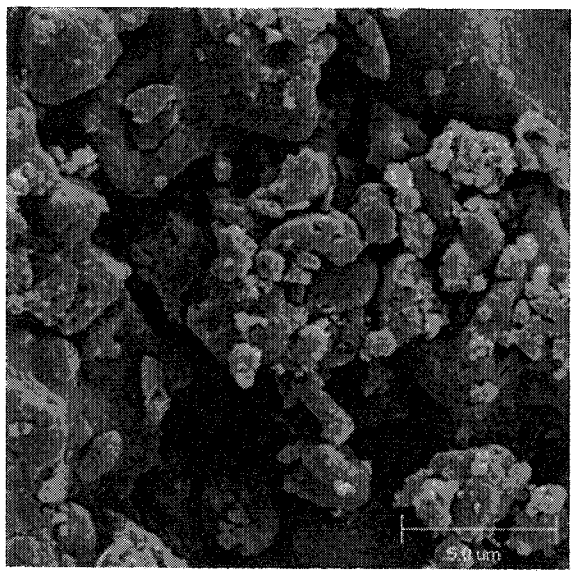

Figure 3.12. Carbonated limestone, 5500X.

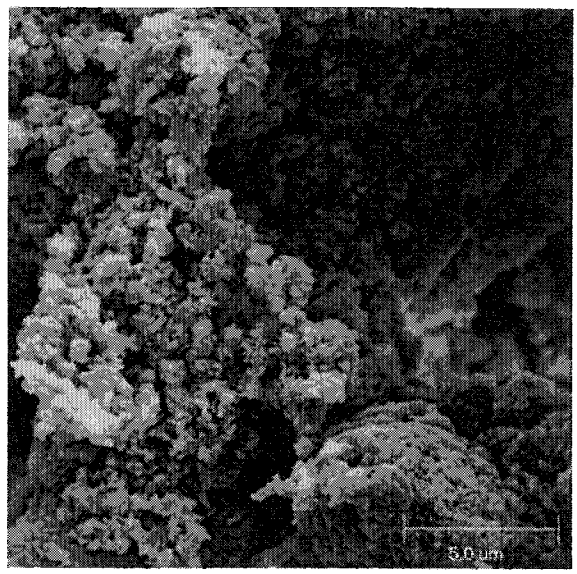

Figure 3.13. Carbonated dolime, 5500X.

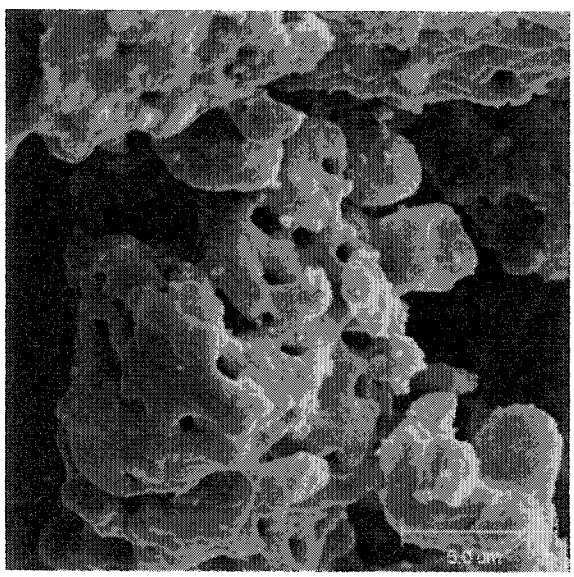

Figure 3.14. Carbonated limestone-$SrCO_3$ wet-paint mixed, 5500X.

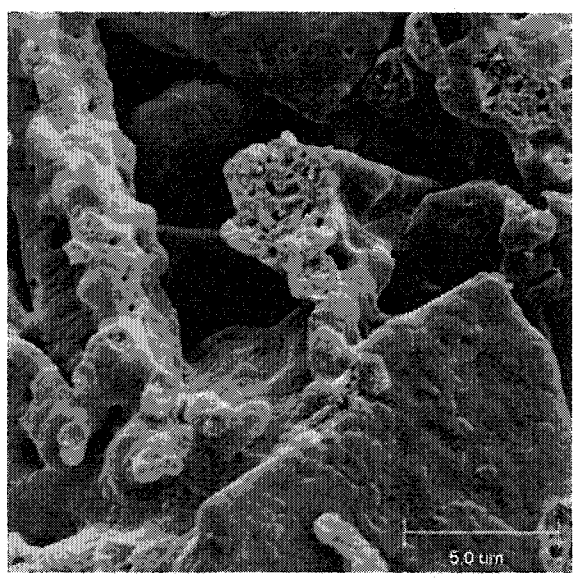

Figure 3.15. Carbonated co-precipitated $(Ca,Sr)(CO_3)_2$, 5500X.

The micrographs reveal the pronounced sintering effects in the Sr-containing samples through the rounded edge appearance of the particles, whereas the limestone and dolomite particles are sharper in appearance. The Sr-containing sample that was wet-paint mixed indicated severe particle coalescence and appeared to be the most sintered of the four samples. The co-precipitated sample contained both large and small particles, of which the larger particles seemed to exhibit some form of structure. It is apparent that smaller particles had begun to coalesce into the larger, structural particles. It is not known whether the larger particles were mixtures of Sr and Ca.

The limestone sample appeared to contain both large and small particles that was the result of pelletizing particles < 44 μm in diameter. The sample looks as though it was beginning to show the signs of sintering. The dolime sample contained a more mono-disperse particle distribution of all the samples and also contained the smallest particles, and yet it did not appear to have undergone any significant sintering at this scale. Since these micrographs were taken from a select area in the center of the pellets, more images were taken of the pellets at a lower magnification and on the outer edges of the pellets.

It can be seen (Figures 3.16-19) how much more sintered the wet-paint mixed Sr-containing pellet was in comparison with the other pellets. The limestone pellet showed some sintering of the smaller particles, while the dolime pellet did not show any effects at this magnification. At this scale the co-precipitated pellet showed some sintering effects but the large, structured particles appeared to be stable, while the smaller particles appeared to have coalesced into larger particles. The larger particles could have been in a more thermally stable form, whereas the smaller particles were probably more affected by their greater surface area to volume ratio.

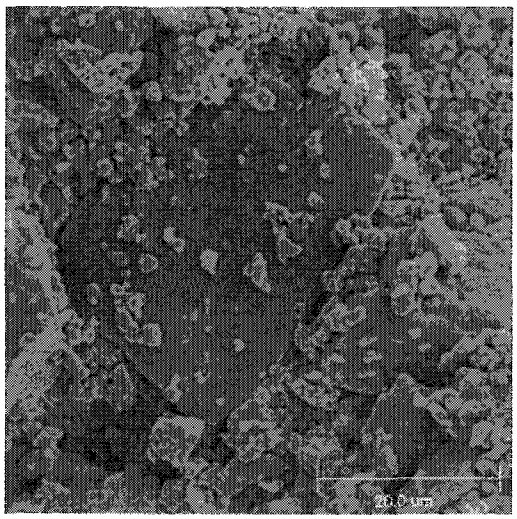

Figure 3.16. Carbonated limestone, 1800X.

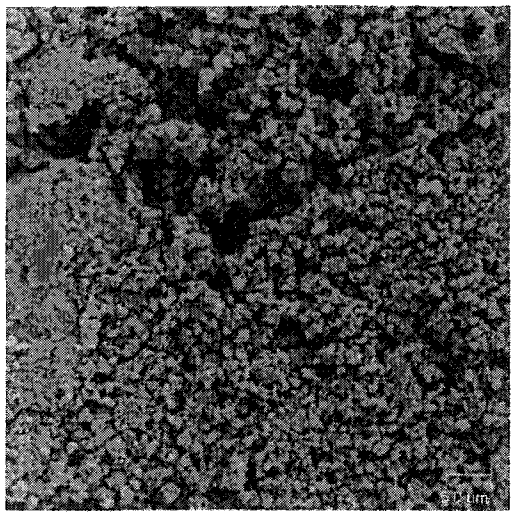

Figure 3.17. Carbonated dolime, 1800X.

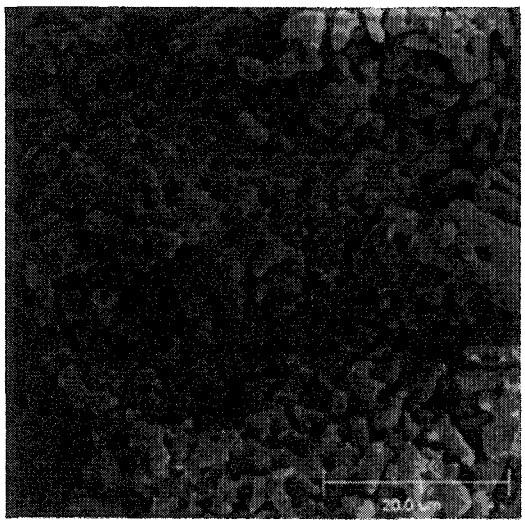

Figure 3.18. Limestone-$SrCO_3$ wet-paint mixed, 1800X.

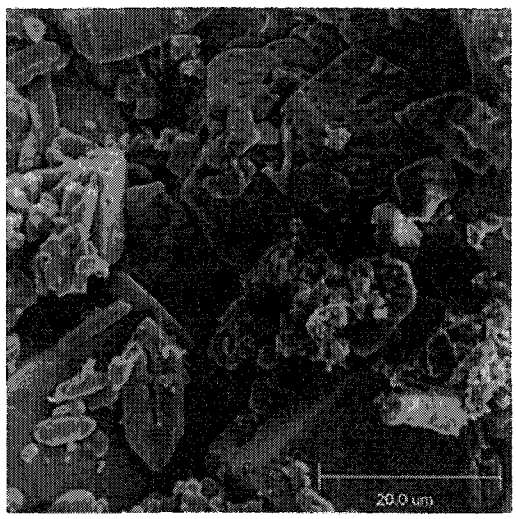

Figure 3.19. Carbonated co-precipitated $(Ca,Sr)(CO_3)_2$, 1800X.

A quantitative comparison of the effect of sintering on the surface area of the different materials was undertaken. The surface area of the samples was measured after a one hour calcination at 750°C under N_2 and after eight cycles of carbonation-decomposition discussed earlier. The results are presented in Table 3.2.

Table 3.2. The surface area (m^2/g) of different pelletized materials after decomposition and eight cycles of carbonation/decomposition. Approximately 2 g of material were used for all measurements.

Conditions	Limestone	Limestone + 2wt% $SrCO_3$ Wet-Paint Mixed	$CaCO_3$ + 10 wt% $SrCO_3$ Co-Prec.	Dolime
Calcination, 1hr 750°C in N_2	13.8	1.36	2.31	50.3
8 Cycles of Carbonation/Decomposition	9.0	0.67	2.03	20.0
% Decrease in Surface Area	35	51	12	60

The surface area change exhibited by the different materials provided a quantitative comparison of the effect of sintering. The measurements indicate the surface area loss due to the eight cycles of carbonation/decomposition. The effects from the initial calcination step are quite large, especially considering that micrometer-sized limestone particles typically exhibit a surface area of roughly 100 m^2/g post calcination (Borgwardt, 1984b). With this in mind, it should be understood that all of the materials presumably underwent quite a bit of surface area loss prior to the analysis.

Although the SEM micrographs were useful, the surface area of the materials indicated that some of the materials had undergone more rapid changes during the reactions than was apparent. The most startling change was exhibited by the dolime sample, which underwent a 60% reduction in surface area. The small particles that made up the dolime pellets could cause such an effect due to the high surface area energy associated with particles as they decrease in size, especially below the micron level. Even though the surface

area of the dolime pellets was reduced significantly, particle coalescence was not apparent at these magnifications.

The co-precipitated pellets underwent the smallest change in surface area, which was not apparent in the micrographs. The small change can be justified by considering the large size of the particles that made up the pellets, which decreased their susceptibility to sintering. The performance of the co-precipitated pellets indicates that the homogeneous mixing of the Ca and Sr ions might have increased the thermal stability of the materials, and the higher initial surface area could also partially explain the higher reactivity with respect to the wet-paint mixed pellets. The surface area change of the limestone and limestone-Sr wet-paint mixed pellets appeared to correlate with the apparent sintering effects as displayed in the micrographs.

These results are surprising since Brown's (1965) work indicated that the SrO provided thermal stability for CaO during high temperature heat treatment. The reason for such a difference could be due to the CO_2 reaction. To look into this possibility, the temperature of $SrCO_3$ decomposition was measured with the same reactor conditions, which revealed that it slowly decomposed at a temperature of 750°C in a N_2 atmosphere. Since a small amount of the $SrCO_3$ decomposed at 750°C during every decomposition cycle, that same amount was also assumed to have reacted during the carbonation cycle (Figure 3.20). The slowly decomposing $SrCO_3$ is evident in Figure 3.20 for a limestone-$SrCO_3$ pellet reacted over multiple cycles. If the $SrCO_3$ was not decomposing, the weight measurement of the pellet would exhibit a flat, linear line between the decomposition and carbonation reactions.

The reactive SrO probably resulted in an increase in surface energy of the sample and subsequently increased the sintering. It might have also induced a fluxing environment. One

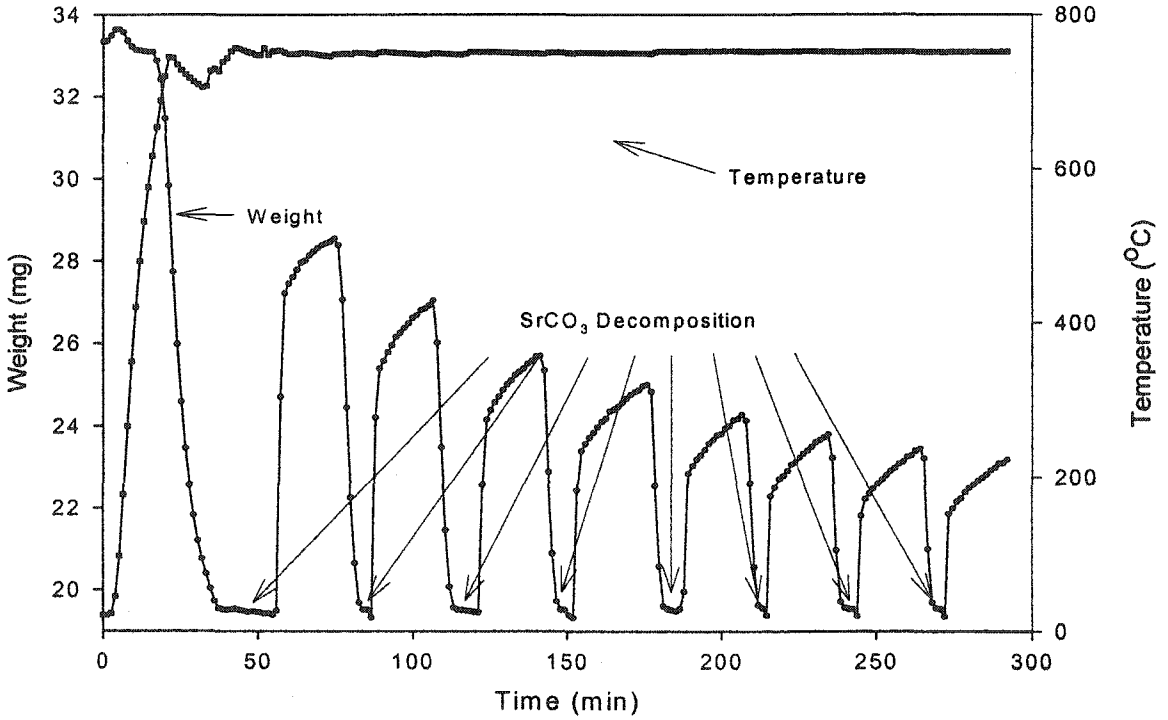

Figure 3.20. Limestone-$SrCO_3$ pellet reacted with 40 vol% CO_2 in N_2 at 750°C for 20 min cycles.

other possibility is that a dispersant, sodium hexametaphosphate, was used during the mixing of the limestone and $SrCO_3$. Since the dispersant is a salt, with a sodium ion, some fluxing could have resulted that promoted sintering of the material.

The dolime sample exhibited the most stable reactivity over the eight cycles. Even though it had a lower specific capacity than the limestone, the drop in capacity over the eight cycles was only ~ 5%, whereas the limestone exhibited a 15% drop. The thermal stability provided by the MgO was probably due to its inertness during the reaction since the temperature of reaction was higher than its decomposition temperature. The MgO could

have possibly acted as a separator, which prevented the mobility and coalescence of the CaO particles. The higher porosity exhibited by the sample could have also been a factor in reducing the rate of sintering due to a much lower density of particle-particle contacts.

Research in this area was also performed by Bandi et al. (2002) on the reactivity of various dolomites, calcites, lanthanites and strontianites with 10 vol% CO_2, 20 vol% H_2O and 70 vol% N_2 at 480°C. The materials were subjected to multiple cycles of carbonation and decomposition during which the temperature was cycled continuously between 480 and 830°C. They found that the MgO in dolomite provided a form of thermal stability for the CaO-$CaCO_3$ particles during the reactions, which enabled the dolomite samples to out perform the calcite samples with respect to stability over multiple cycles. In addition, they tested a form of strontianite [$(Ca,Sr)(CO_3)_2$] that resulted in a decrease in capacity that was more severe than any of the calcite or dolomite samples that were tested. The work of Bandi et al. with strontianite provides further evidence that the Sr does not work well as a stabilizer for CaO during carbonation-decomposition cycling. And the results of Bandi et al. further supports the reactivity theory of Sr posed earlier, since their tests involved decomposition reactions at 830°C, which would definitely decompose the $SrCO_3$ that was in the sample, leaving it reactive towards CO_2 at 430°C and therefore increase the sintering effects. But the Mg that was in the materials was inert and presumably acted as a thermal stabilizer preventing the coalescence of CaO particles (Bandi et al.). All of these results indicate that a potential thermal stabilizer for CaO should be non-reactive with either the CaO or the reacting gases.

Although the CO_2 reaction provided a different technique for comparing the effects of additives on the stability of CaO, the tests were not conclusive. Since the SrO was slightly

reactive at the conditions used for testing the materials, the ability of the SrO to stabilize the CaO during sulfidation is still unproven.

3.2.4 *The effects of magnesium and chemical impurities on the reactivity of CaO with H_2S*

The use of a suitable CaO-based sorbent for removing H_2S from hot coal gas requires that a sorbent be regenerable and remain reactive over 100 + cycles of use. To get an idea of how well a specific material will perform, a first step in the analysis is to test the material over a few cycles of sulfidation and regeneration. A group of six materials were tested for their effectiveness as H_2S sorbents. The results from the tests are presented in this section.

The materials that were tested included: $CaCO_3$, plaster of Paris (P.O.P.) [$CaSO_4 \cdot 1/2H_2O$], dolime [$CaMg(OH)_4$], plaster of Paris with dolomite [$CaSO_4 \cdot 1/2H_2O \cdot CaMg(CO_3)_2$], limestone $CaCO_3$, and dolomite [$CaMg(CO_3)_2$]. All of the materials were tested in pelletized form. The P.O.P. materials were pelletized with deionized water and the rest were pelletized with 5 vol% Norlig A lignin in deionized water. The P.O.P. pellets were converted to CaO from $CaSO_4$ at 1050°C with 9 vol% H_2, 13 vol% O_2 and N_2 according to the regeneration process described earlier in Chapter 2.

$$CaS + 2O_2 \rightarrow CaSO_4 \qquad (1.9)$$

$$CaSO_4 + H_2 \rightarrow CaO + SO_2 + H_2O \qquad (2.12)$$

The $CaCO_3$-based pellets were converted to CaO by decomposition in N_2 during the heat-up period to 880°C. The sulfidation reaction was carried out using 1.0 vol% H_2S, 24 vol% H_2 and N_2 at 880°C according to the reaction:

$$CaO + H_2S \rightarrow CaS + H_2O \qquad (1.2)$$

The performance of the pellets is represented as the total specific capacity achieved after 20 min of sulfidation,

$$\%\text{Specific Capacity} = \frac{W_{CaS} - W_{CaO}}{W_{CaO}} \times 100 \qquad (2.11)$$

where W_{CaS} is the final weight of the pellet and W_{CaO} is the initial weight of the pellet. The results from the multi-cycle sulfidation tests are presented in Figure 3.21. The specific capacity results from the limestone pellet tests were the averages for three different pellets, the $CaCO_3$ test results represent an average of two pellets and the rest of the test results represent single pellets of each type of material.

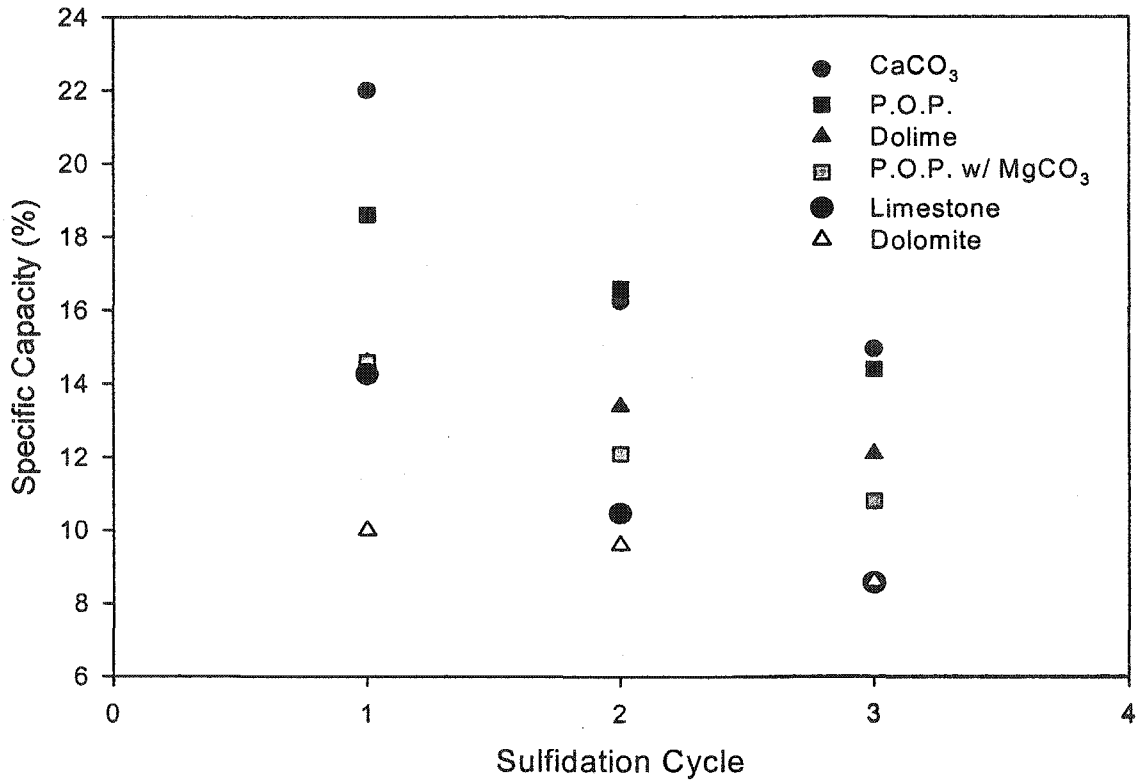

Figure 3.21. Specific capacity of pellets reacted with 1.0 vol% H_2S, 24 vol% H_2 and N_2 at 880°C for three cycles and regenerated with 9 vol% H_2, 13 vol% O_2 and N_2 at 1050°C.

The pellets that exhibited the highest capacity over the three cycles were the pure $CaCO_3$ and P.O.P. The high capacity of the $CaCO_3$ pellets was due to the research-grade

purity of the material, which reduced its tendency to sinter and ensured that every particle of the pellets was reactive. The $CaCO_3$ pellets outperformed the P.O.P. pellet during the first cycle since they had not undergone any severe sintering up to that point. The P.O.P. pellet, on the other hand, had been converted from $CaSO_4$ to CaO by the regeneration process at 1050°C prior to sulfidation. The extra time in this high temperature, oxidizing and reducing environment probably increased the degree of sintering of the P.O.P. pellet. Following the first cycle it is seen how the specific capacity of the $CaCO_3$ pellets quickly dropped down to a comparable level as the P.O.P. pellet. The drop in capacity was due to the sintering that had occurred. The P.O.P. material performed quite well due to its high purity and high porosity that was exhibited by the material throughout the multiple stages, which helped to reduce sintering (Chapter 3, Section 3.2.1).

The next two pellets that performed similarly were the P.O.P. with dolomite and dolime. Both pellets contained Mg, which has proven to be a stabilizer during carbonation reactions and therefore probably applies for these conditions since it is inert with regards to H_2S at these temperatures. In addition, both materials are quite porous and their surface areas were measured to be > 20 m^2/g prior to any high temperature treatment, which is similar to the P.O.P. pellets. The two types of pellets lost capacity in a rate similar to the P.O.P. pellet and their lower specific capacity was due to the Mg content.

The pellets that exhibited the lowest specific capacity by the third cycle were the limestone and dolomite. Even though the overall capacity of the dolomite was low, its drop in capacity per cycle was not very significant and was the lowest of all the pellets tested. The low specific capacity was due to the large amount of Mg in the material, but the Mg was also the reason for the high stability exhibited by the pellet. The limestone pellets exhibited the

fastest rate of reduction in specific capacity per cycle of all the pellets. And this was probably due to a large number of impurities within the limestone, especially iron oxide, which acted as a flux in the material. The drop in specific capacity of the limestone pellets showed the tendency of the material to sinter rapidly at these conditions (Chapter 3, Section 3.2.1).

Since both the $CaCO_3$ and limestone pellets were the only ones that exhibited a rapid decrease in capacity after the first cycle, the initial sintering of both materials seemed similar. This similarity between the two materials, as compared to the others, was most likely due to their lower surface area and porosity, assuming that the $CaCO_3$ pellets were structurally similar to the limestone. Such physical attributes will increase the number density of particle-particle contacts and improve the rate of sintering of any material. A closer examination of the performance showed that the drop in capacity between the 2^{nd} and 3^{rd} cycles was less for the $CaCO_3$ pellets than for the limestone pellets, which is attributed to the impurities found within the limestone material causing it to sinter more rapidly at later stages.

3.3 Summary and Conclusions

The comparison between the performance of limestone and P.O.P. pellet cores during sulfidation and regeneration reactions yielded some interesting results. The comparison dealt mainly with the specific capacity of the pellets over multiple cycles and the resulting changes in surface area, porosity and density. The study revealed that the P.O.P. pellets had a higher capacity and reactivity, higher surface area and porosity, and more stable reactivity over multiple cycles of sulfidation and regeneration than that of the limestone pellets. The higher

reactivity exhibited by the P.O.P. pellets was primarily due to the higher surface area. And the higher surface area and porosity combined to make the P.O.P. pellets less susceptible to sintering. Aside from their lower surface area and porosity, the limestone pellets were more susceptible to sintering due to an impurity of iron oxide, which was thought to act as a fluxing component. The results from this comparison yielded two primary factors that must be considered for future sorbent development. The first factor requires that a suitable sorbent be developed with a high surface area that is stable at high temperatures. And the second factor requires that any impurities within the base component of a sorbent not be fluxing agents at high temperatures.

Since the development of a more reactive and stable sorbent requires a more porous structure with a higher surface area, a study was performed to find a practical method of increasing the porosity of agglomerated limestone powder. The study incorporated a new procedure for mixing the limestone powder with pore modifier additives. Preliminary studies resulted in the finding that soluble cornstarch and graphite did not increase the stability or reactivity of limestone pellets over multiple cycles of sulfidation and regeneration. In fact, the graphite additive resulted in pellets exhibiting a lower capacity after the second and third cycle of sulfidation and regeneration than pellets with only limestone. But poly (vinyl alcohol) (PVA) incorporated as a pore modifier yielded limestone pellets that appeared to be more reactive and stable. These preliminary results indicate that a pore modifier such as PVA can possibly increase the performance of agglomerated limestone pellets for multi-cycle use as a sulfur sorbent at high temperature. But more work needs to be done to prove the usefulness of the PVA.

The effects of chemical elements, such as Sr and Mg, on the stability of CaO at high temperatures during sulfidation and carbonation reactions were investigated. The Sr effect was evaluated using CO_2 as a reactant. This procedure was adopted since carbonation and decomposition reactions could be carried out isothermally by just adjusting the gas composition in the reactor system. The Sr was incorporated into pellets by wet-mixing $SrCO_3$ with limestone powder and by co-precipitating $SrCO_3$ with $CaCO_3$. Both forms of pellets produced results that were worse than pure limestone pellets tested under the same conditions. The decrease in the performance of the Sr-containing pellets is attributed to the slight reactivity exhibited by the SrO towards CO_2. The Sr was originally included in the material to act as a stabilizer, but was not effective since it reacted. Although the Sr did not improve the stability of limestone or $CaCO_3$ during reactions with CO_2, it might still be effective during reactions with H_2S. Such tests should be carried out in future work since the Sr additive was originally incorporated to stabilize CaO during reactions with H_2S.

The testing of Mg-containing materials was performed under the same conditions as the Sr-containing materials but reaction with H_2S was also included. The materials tested with CO_2 were dolomite and dolime. The results with CO_2 revealed that both forms of materials reacted readily with CO_2 and exhibited better stability than limestone. The dolime outperformed the regular dolomite, which was probably due to a more mesoporous structure. For testing with H_2S, only the dolime was used, but a form of plaster of Paris that contained ~ 5% dolomite was also tested. Both forms of materials out performed the limestone, but the dolime pellets exhibited more stability over multiple cycles than the Mg-containing P.O.P. The higher stability was attributed to the larger amount of Mg contained in the dolime.

Pellets made of plaster of Paris and $CaCO_3$ were also tested with H_2S over multiple cycles. The $CaCO_3$ began with a higher specific capacity but, due to a more drastic decrease in reactivity, exhibited a similar specific capacity as that of the P.O.P. pellet by the third sulfidation cycle. The stability of the P.O.P. pellet was attributed to its higher mesoporosity and purity. Since the capacity of the $CaCO_3$ pellets was reduced to that of the P.O.P. pellet by the third cycle, further work should be pursued with the P.O.P. material since it is lower in cost and more practical for industrial applications.

Chapter 4. Shell Development

4.1 Introduction

The efficient and practical application of a HGD unit within a HGCU system requires that the sorbent operate effectively in a given reactor system. The two types of reactors that utilize relatively large sorbents (5-8 mm) are the fixed and moving bed reactors. In contrast to these reactors, fluidized bed and transport reactors are also used for sulfur removal, but utilize small sorbent particles in the micrometer range.

The fixed bed is one of the primary reactor systems that has been tested with solid sorbents. For use in a fixed bed, the sorbents must be strong and attrition resistant, although attrition is not as significant due to the static environment. Even though the fixed bed reactor has proved useful, a number of industrial developers are moving away from fixed bed systems primarily due to the difficulty of temperature control during the oxidative regeneration phase of the sulfided sorbents (Rutkowski et al., 1997). Instead of using a single reactor system, such as a fixed bed, a moving bed system can utilize two reactors with one dedicated to sulfidation and the other to regeneration. The absorber system typically utilizes a counter-current, continuous flow of hot coal gas with intermittent or continuous flow of the sorbent. The regenerator can be operated as a multi-stage, co-current flow reactor that utilizes recycled regenerator gas for temperature control. Because of the two-reactor system, solids-handling equipment is used for transport of the sorbent. The cycling of the solid sorbent between the two reactors requires it to be strong and attrition resistant in order to reduce material loss and reactor plugging.

Whether a solid sulfur sorbent is to be used in a fixed or moving bed system, the particles need to be strong and attrition resistant. A standard measure of strength that a sorbent must exhibit for use in a fixed or moving bed system was proposed by Gupta (1999). He calculated that a sorbent pellet must be able to withstand a crushing force of 8.9 N/mm based on the pellet diameter, for effective use in an industrial fixed or moving bed reactor. To achieve this minimum strength requirement and yet provide a sorbent that was reactive and stable at temperatures from 700 to 1100°C, Akiti et al.(2002) developed a sorbent that contained a CaO-based core and a refractory shell. The core was friable yet highly reactive while the shell was fairly inert towards reaction with H_2S but very strong and attrition resistant. The refractory shell was composed of limestone and alumina.

Since the core-and-shell sorbent developed by Akiti et al. (2002) was very promising during the initial stages of development, further work was conducted to improve its abrasion resistance by optimization of the process conditions for pelletization. Further development of the shell material was carried out by replacing limestone in the shell in order to create a material that was inert towards H_2S, and by replacing the high-grade alumina with a less costly material. This chapter presents the results of crushing strength and abrasion resistance tests of the limestone-alumina shell material in an agglomerated pellet form and the tests of an alternative shell material. Performance results of the core and shell pellets during sulfidation and regeneration tests are also included.

4.2 Results and Discussion

The sorbent materials were tested for mechanical strength and reactivity in the core and shell pelletized form. The mechanical strength was evaluated for application in

industrial reactors and the reactivity was tested to investigate the possible effects that the shell material might impose on the cores during reaction.

The mechanical testing of the shell material was performed on core and shell pellets to accurately reveal the practical strength of the shell material. There were two techniques chosen to test the materials, a vertical crushing strength test and an abrasion resistance test. The crushing strength test evaluated the resistance of the material to compression while the abrasion resistance test evaluated the toughness of the material by subjecting it to collisions and grinding. Both forms of testing apparatus are described in detail in Chapter 2.

The reactivity of the materials was tested by using the reaction system described in Chapter 2. And the same conditions that were used for testing the cores were also used for testing the core and shell pellets.

4.2.1 *Limestone and alumina shell testing*

The first phase of the analysis was conducted on the mechanical properties of the material. The abrasion resistance of the shell material was determined by using core and shell pellets that were heat treated at 1100°C for 2 hr in air. The cores consisted of pelletized limestone particles (< 44 μm), and the shell material consisted of 20 wt% limestone with a particle size range of 44 to 210 μm and 80 wt% alumina of which 60 wt% was tabular (8 μm) and the other 40 wt% was calcined (1 μm), as developed by Akiti et al.(2002). The limestone-alumina shell mixture was prepared by mixing the dry powders and then pelletizing the mixture as described in Chapter 2.

The testing apparatus used were a crush strength analyzer and an ASTM standard catalyst abrasion resistance apparatus as described in Chapter 2. The crushing strength of a

pellet was calculated by dividing the force in Newtons required to fracture the pellet by the average pellet diameter, measured in mm.

$$\text{Crushing Strength} = \frac{\text{Force}}{\text{Diameter}} \tag{2.9}$$

The pellet attrition in percent was calculated by employing the equation

$$\%\text{Attrition} = \frac{W_i - W_f}{W_i} \times 100 \tag{2.10}$$

where W_i is the initial weight of the pellets in grams and W_f is the final weight of the whole pellets; the specifics of the tests are discussed in Chapter 2. Three batches of pellets were used for testing. Approximately ten pellets were chosen at random from each batch for the crushing strength test and 100 g from each batch for the abrasion resistance test. The results are presented in Table 4.1

Table 4.1. Crushing strength of core and shell pellets heat-treated in air for 2 hr. Pellets consisted of limestone cores and limestone-alumina shells.

Batch	Avg. Diameter (mm)	Avg. Shell Thickness* (mm)	Avg. Force (N)	Avg. Force/Shell Thickness* (N/mm)	Avg. Force/ Diameter (N/mm)	% Fail Rate** of Pellets w/ F/D < 8.9 (N/mm)
1	5.9 +/- 0.5	0.95 +/- 0.2	72 +/- 25	75 +/- 30	12 +/- 3	20
2	5.5 +/- 0.2	0.65 +/- 0.08	54 +/- 20	82 +/- 30	9.6 +/- 4	50
3	5.6 +/- 0.4	0.66 +/- 0.14	101 +/- 40	150 +/- 45	17.8 +/- 7	20

* Avg. shell thickness based upon the thinnest regions of the shells and not the overall average thickness for structural comparisons.
** % Fail rate pertains to pellets with a F/D crushing strength less than the minimum of 8.9 N/mm.

The results in Table 4.1 indicate that there is a large variability in the crushing strength of the pellets from a given batch. The variability arises primarily from the irregular shell thickness

that was incurred during the pelletization process. Even though the variability of the shell thickness was quite high, a simple, qualitative correlation was obtained between strength and shell thickness, which is presented in Figure 4.1.

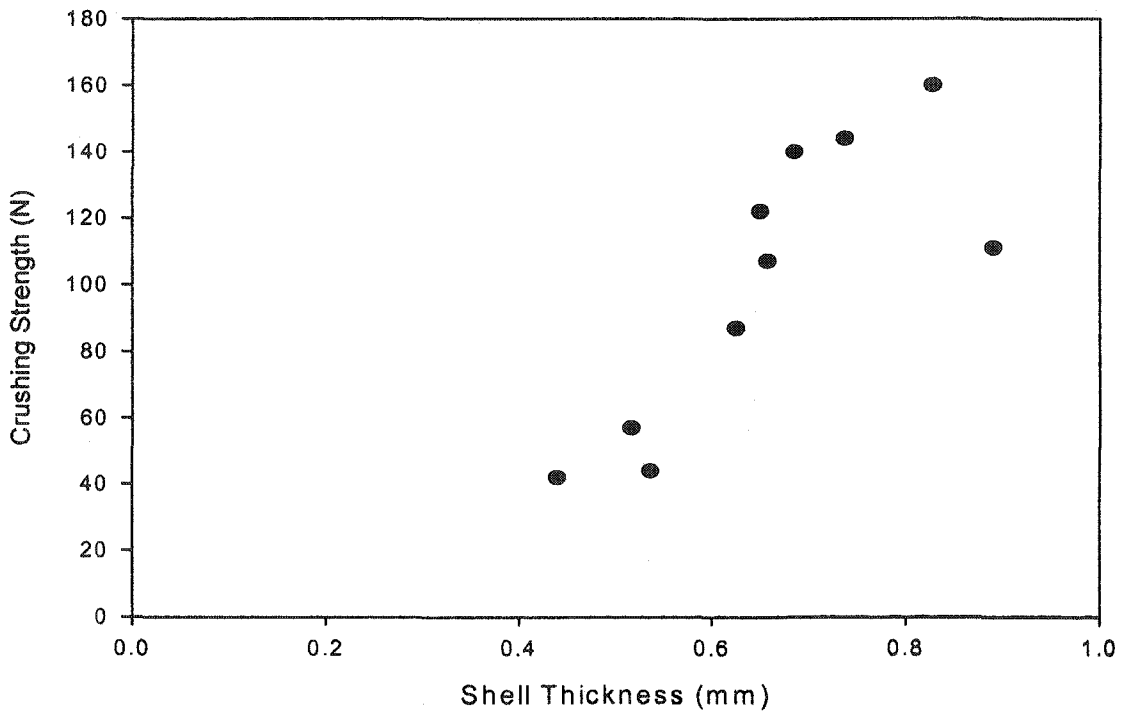

Figure 4.1. Crushing strength results from a batch of limestone core, limestone-alumina shell pellets, heat-treated at 1100°C for 2 hr in air.

The results presented in Figure 4.1 indicate the possible linear rise in strength exhibited by the core and shell pellets as a function of shell thickness. Since the variability in the shell thickness makes it difficult to obtain a good correlation between strength and shell thickness, the results are only useful for qualitative analysis.

Although the vertical crushing strength test is a good technique to evaluate the compression resistance of a core and shell pellet, an abrasion test is also needed for

evaluating the toughness of a material for moving bed applications. Table 4.2 contains the results from three batches of pellets tested for abrasion resistance.

Table 4.2. Abrasion resistance results for limestone core, limestone-alumina shell pellets with a shell thickness < 1.43 mm, heat treated at 1100°C for 2 hr in air.

Batch	Pellet Diameter (mm)	Attrition Loss (wt %)
1	3.96 < D < 4.76	14.9
2	3.96 < D < 4.76	16.8
3	3.96 < D < 4.76	12.4

Even though the pellets incurred a 15 wt% loss, the test is quite destructive and the fact that such a small amount of material was lost is quite significant. And since the abrasion resistance test is more representative of fluidized bed conditions, which are more abrasive than the conditions in a moving bed system, the 15% attrition loss is probably much higher than what the pellets would actually lose in a moving bed system. To look into the effect of using pellets made with cores in the same size range but with thicker shells, three batches of pellets were produced to test such an effect. The pellets were heat treated as before and also tested using the same abrasion system. The results are presented in Table 4.3.

Table 4.3. Abrasion resistance results for limestone core, limestone-alumina shell pellets with a shell thickness of 1.43-2.33 mm, heat treated at 1100°C for 2 hr in air.

Batch	Pellet Diameter (mm)	Attrition Loss (wt %)
4	4.76 < D < 5.66	5.3
5	4.76 < D < 5.66	4.6
6	4.76 < D < 5.66	2.5

The pellets with an overall diameter larger than 4.76 mm experienced an attrition loss that was 28% of that experienced by the smaller pellets. The increase in pellet shell

thickness definitely resulted in an increase in abrasion resistance, and since the testing system is harsher than a typical moving bed system, the pellets are very likely to remain structurally intact in a moving bed system. The improved performance provided by a thicker shell was reflected by Figure 4.1, which indicated that the strength of the pellet is dependent upon the thickness of the shell. Therefore, the compression strength and abrasion resistance both increase with a thicker shell.

Since the pellets in batches 1-6 were prepared by dry-mixing the shell materials, a wet-mixing process was used to try to improve the homogeneity of the limestone and alumina shell mixture. The details for the wet-mixing process can be found in Chapter 2. The core and shell pellets were made with the same type and size of core as used in batches 1-6. A total of five pellets were tested in the > 4.76 mm diameter range for crushing strength. The results are presented in Table 4.4.

Table 4.4. Crushing strengths of core and shell pellets heat-treated in air for 2 hr. Pellets consisted of limestone cores and limestone-alumina shells, with a wet-mixed shell composition, overall diameter > 4.76 mm.

Shell Material Testing in Core and Shell Form						
Batch	Avg. Diameter (mm)	Avg. Shell Thickness* (mm)	Avg. Force (N)	Avg. Force/Shell Thickness* (N/mm)	Avg. Force/ Diameter (N/mm)	% Fail Rate of Pellets w/ F/D < 0.89 (N/mm)
1	5.97 +/- 0.19	1.06 +/- 0.11	84 +/- 8	79 +/- 6	14 +/- 1.4	0

* Avg. shell thickness based upon the thinnest regions of the shells and not the overall average thickness for structural comparisons.

The crushing strength results revealed that the wet-mixed shell pellets yielded an average force/shell thickness of 79 N/mm, which is not very different from the pellets tested in dry-mixed batches 1-3. In fact, the result is lower than the average of batches 1-3, which

was 102 +/- 40 N/mm. What is significant is that none of the pellets from the wet-mixed batch yielded a F/D failure rate greater than 0%, whereas batches 1-3 resulted in 20,50, and 20% failure rates, respectively. The single abrasion test that was performed on the wet-mixed pellets also yielded an interesting finding. Even though the crushing strength of the pellets was not very high, the one abrasion test that was conducted yielded an attrition loss of only 2.0 wt%, which is a factor of 2 less than the average of batches 4-6. Albeit the results are preliminary, the wet-mixing of the shell material appeared to improve the mechanical performance of the pellets.

The incorporation of a thicker shell has proven to increase the strength of the pellets, but a loss in overall pellet sulfur capacity has resulted due to the increased amount of alumina. To test a number of core and shell pellets for reactivity and capacity, four pellets were chosen at random from a batch of pellets and reacted, in the reactor system described in Chapter 2, with a gas mixture of 1.0 vol% H_2S, 24 vol% H_2, in N_2 at 880°C according to the reaction:

$$CaO + H_2S \rightarrow CaS + H_2O \qquad (1.2)$$

The pellets consisted of a P.O.P. core with a limestone-alumina shell, made with the same, dry-mixed, limestone-alumina ratios described earlier. The pellet cores were initially converted from $CaSO_4$ to CaO at 1050°C prior to sulfidation by employing the cyclic process described in Chapter 2 and represented by the reactions:

$$CaS + 2O_2 \rightarrow CaSO_4 \qquad (1.9)$$

$$CaSO_4 + H_2 \rightarrow CaO + SO_2 + H_2O \qquad (2.12)$$

The results from sulfiding the four core and shell pellets are shown in Figure 4.2.

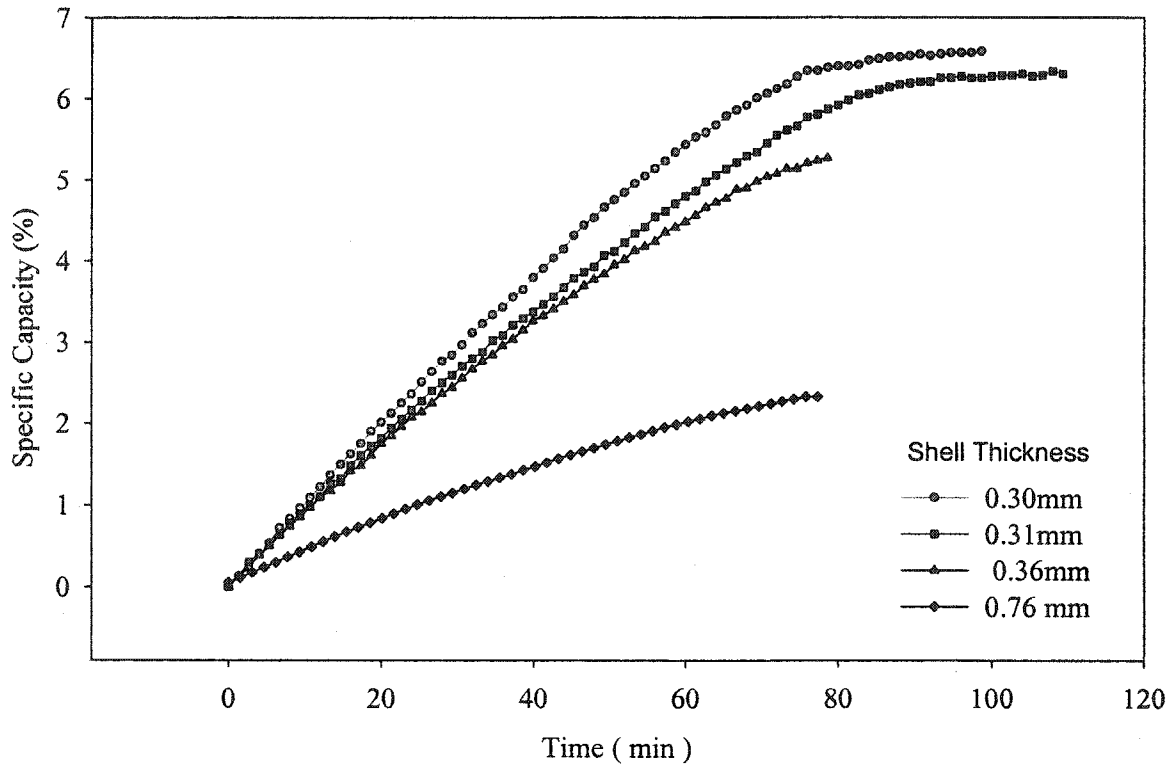

Figure 4.2. P.O.P. core and limestone-alumina shell pellets reacted with 1.0 vol% H_2S, 24 vol% H_2 in N_2 at 880°C. Pellet dimensions are listed in Table 4.5.

The results in Figure 4.2 indicate that as the amount of shell material was increased, the weight contribution of the shell material reduced the overall capacity of the pellets. An interesting result is the linearity that is observed in the reaction rates for the thinnest shelled pellets, 0.30 and 0.31 mm. Although the linearity is not extraordinary, the thicker shelled pellets tend to drop off in reaction rate at a much earlier time, which is counterintuitive. A thicker shell would presumably result in a longer linear portion of the initial reaction rate due to the increased diffusion resistance. Because of these peculiarities, conversions of the pellets were calculated to further investigate the difference. The calculations were based upon the conversion of the P.O.P. pellet cores during the initial conversion.

To accurately reflect the possible conversion taking place during a sulfidation reaction with a P.O.P. core, the total amount of sulfur remaining in a core after the initial conversion of $CaSO_4$ to CaO was tested. Over 20 P.O.P. cores were subjected to the cyclic conversion process described earlier, and the resulting cores of CaO were chemically analyzed for CaS content. The analysis revealed that 2% of the sulfur remained. With this knowledge, the conversion of the core and shell pellets was calculated, which revealed that the four core and shell pellets in Figure 4.2 had exceeded 100% conversion. Since this was not possible, the only other explanation was that the limestone in the shell materials had reacted.

To investigate the reactivity of the shell material, pellets were made by using the pelletization process, but with only the limestone-alumina shell material. Following pelletization, the pellets were heat treated at 1100°C for 2 hr in air and then reacted with 1.0 vol% H_2S, 24 vol% H_2 in N_2 at 880°C. The results revealed that at least 4 wt% of the total CaO present in the shell material had reacted with the H_2S. Previously it was thought that the shell material was inert due to the formation of calcium aluminates (Akiti et al., 2002).

The amount of calcium aluminates formed during the heat treatment and sulfidation-regeneration reactions was investigated. Two types of pellets were analyzed by using XRD: cast pellets formed from a slurry of wet-mixed, limestone-alumina shell mixture and pelletized pellets made with a dry-mixture of limestone and alumina. Both types of pellets were heat-treated in air at 1100°C for 2 hr. The cast pellets were analyzed post heat-treatment and the pelletized pellets were analyzed post heat-treatment and one sulfidation-regeneration reaction. The resulting XRD spectrums are shown in Figures 4.3 and 4.4.

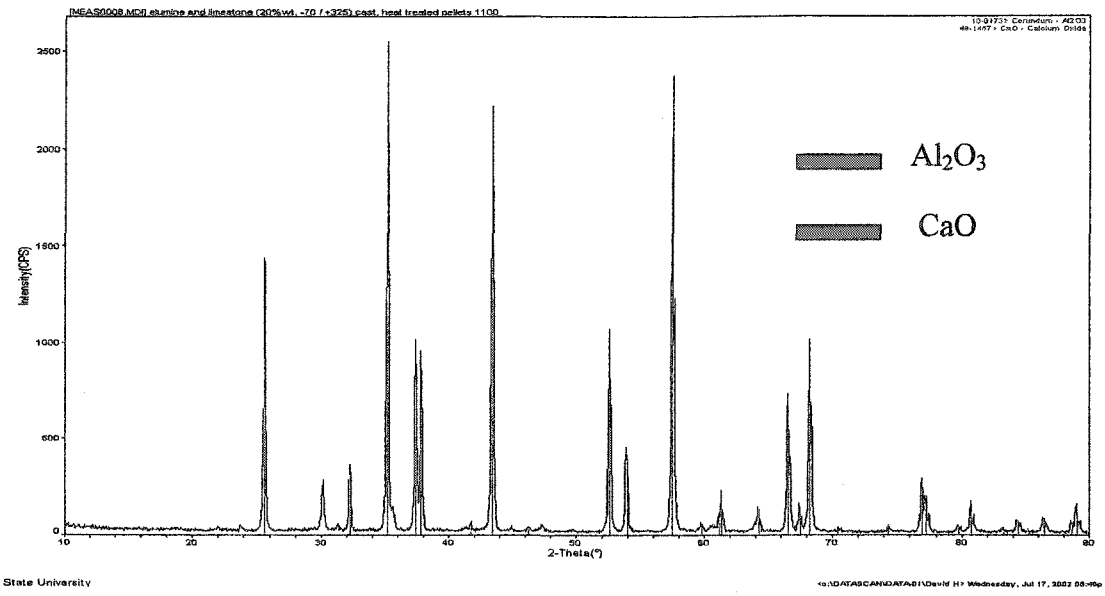

Figure 4.3. XRD spectrum of cast pellets heat-treated in air for 2 hr at 1100°C.

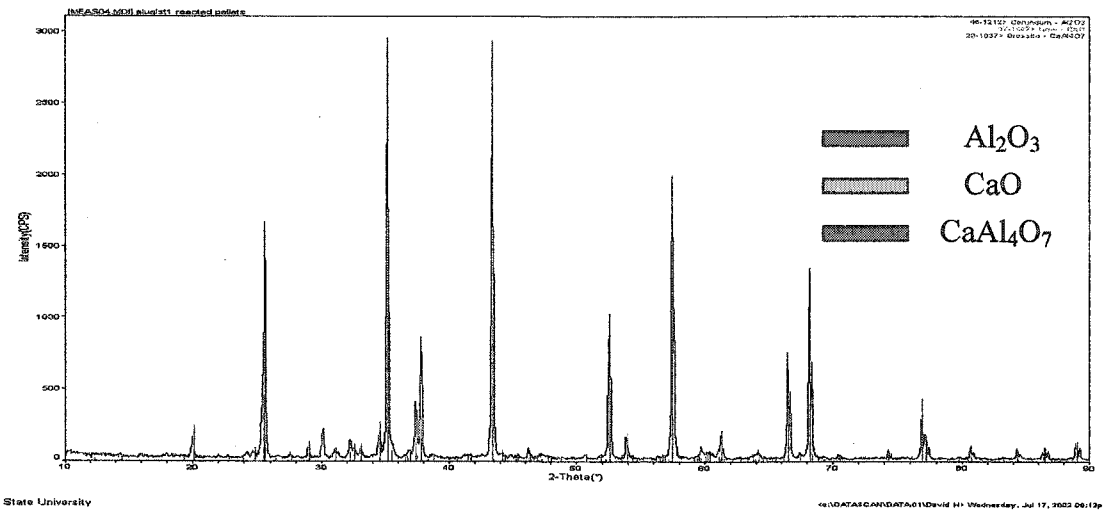

Figure 4.4. XRD spectrum of pelletized pellets, heat-treated for 2 hr in air at 1100°C followed by sulfidation-regeneration.

Figures 4.3 and 4.4 reveal that after the initial heat treatment of the cast pellets, there was a large amount of the CaO phase present and very little calcium aluminate. Since the

XRD technique is only accurate down to ~15 wt% for a crystal phase without a reference material, the calcium aluminate could possibly be present up to ~ 10 wt% and still not have shown up during the analysis. But the XRD results did reveal that the major phases in the shell material post heat-treatment were CaO and Al_2O_3. And it is the free CaO that was available to react with H_2S.

The XRD spectrum of the material after sulfidation and regeneration indicated that a significant amount of the calcium aluminate phase was produced. Whether the phase was increased due to the prolonged exposure to the high temperatures, the highly oxidizing and reducing conditions, the sulfidation reactions or all in conjunction is not known. If the formation of the calcium aluminate increases with time in the reactor system, it can be assumed that the shell material should become stronger over time. But whether the reaction with H_2S and subsequent formation of CaS in the shell material reduces the strength of the shell material during the reaction is not known. Because the formation of CaS in the shell material could lead to pore closures due to sintering effects and, therefore, reduce the rate of reaction, or weaken the shell material by destruction of the $CaO\text{-}Al_2O_3$ bond, these possibilities should be investigated further. Tests were conducted on the four core and shell pellets for crushing strength to investigate whether the materials became stronger because of the reactions and high temperature environment, which might have induced the formation of $CaAl_4O_7$. The results are listed in Table 4.5

To look into the effects of reactor time and other conditions on the shell strength, the crushing strength of the four pellets that were reacted are compared in Table 4.5. Although the tested pellets did not cover a large range in shell thickness, the results are interesting. The pellet crushing strengths exhibited in Table 4.5 indicate that the force/diameter of all the

Table 4.5. Crushing strength of core and shell pellets heat-treated in air for 2 hr. Pellets consisted of P.O.P. cores (converted to CaO) with limestone-alumina shells, with a dry-mixed shell composition and reacted twice with 1.0 vol% H_2S, 24 vol% H_2 in N_2 at 880°C and converted and regenerated three times at 1050°C with 9 vol% H_2, 13 vol% O_2 in N_2.

Pellet	Avg. Diameter (mm)	Avg. Shell Thickness* (mm)	Force (N)	Force/Shell Thickness* (N/mm)	Force/ Diameter (N/mm)	% Fail Rate of Pellet w/ F/D < 8.9 (N/mm)
1	4.3 +/- 0.10	0.32 +/- 0.06	10 +/- 0.5	31 +/- 6	2.0 +/- 0.13	100
2	5.0 +/- 0.15	0.64 +/- 0.08	30 +/- 0.5	47 +/- 6	6.0 +/- 0.2	100
3**	4.37 +/- 0.07	0.24 +/- 0.03	-	-	-	100
4	4.5 +/- 0.13	0.20 +/- 0.04	1	5 +/- 3	0.22 +/- 0.11	100

* Avg. shell thickness based upon the thinnest regions of the shells and not the overall average thickness for structural comparisons.
** Pellet #3 broke apart during the diameter measurements prior to the crushing strength test.

pellets tested fell short of the 8.9 N/mm minimum. The lower strength exhibited by the pellets with the ≤ 0.32 mm shell thickness is not surprising since this range of strength-shell thickness is very similar to the results in Figure 4.1. But the pellet with the largest shell thickness, 0.64 mm, did not exhibit a high crushing strength, which according to Figure 4.1 should have been in the > 80 N range. The limited results of the post reaction pellets indicate that the reaction conditions were not conducive for improving the strength of the shell material and might have actually reduced the strength of the pellets.

4.2.2 *Kaolin and alumina shell development*

The use of kaolin as a possible replacement for alumina was considered due to the refractoriness of the kaolin material. Kaolin is composed primarily of alumina and silica ($Al_2O_3 \cdot 2SiO_2 \cdot 2H_2O$) and is in the category of fireclays. It has found common use in

refractory brick for industrial furnaces and kilns, but it has been replaced over the years with more refined and expensive materials. It is a material that is fairly low in cost and distributed throughout the world.

The kaolin, in powder form, consists of sheets of $n(Si_2O_5)^{2-}$ linked to $(Al_2(OH)_4)^{2+}$ units. The silicon oxides form linked tetrahedra that create a hexagonal structure, and the aluminum hydroxides (gibbsite) form an octahedral structure that fits onto the silica layer (Searle and Grimshaw, 1959). The two structures form a 1:1 layer that distinguishes kaolin from other alumina-silica refractory clays. A unique feature of the kaolin material, aside from its thermal stability, lies in its inability to swell when brought into contact with water (van Olphen, 1977). The non-swelling behavior of the kaolin clay makes it an attractive material for an agglomeration process since excessive shrinkage during subsequent drying will not occur, and most agglomeration techniques require the use of a water-based binder.

The initial experiments were carried out using pure kaolin as a pellet-coating material. The type of kaolin was EPK, and was obtained from the Feldspar Corp. The EPK kaolin had a chemical composition post heat-treatment of 53.7 wt% SiO_2, 43.87 wt% Al_2O_3, 0.9 wt% Fe_2O_3, with the remaining impurities being < 0.4 wt%. The average particle size was 1.36 μm with a surface area of 24 m^2/g. The general pelletization and coating processes are described in Chapter 2. The results from coating P.O.P. cores with pure kaolin indicated that it was possible to coat the pellet cores with kaolin powder and a 5 vol% lignin and water solution, but the subsequent hardening process resulted in the kaolin shells fragmenting and breaking apart. Therefore, a new technique was adopted that involved coating the pellet cores with kaolin, skipping the hardening process, and going straight to the heat treatment at 1100°C for 2 hr. The new technique resulted in weak pellets that exhibited a crushing

strength significantly below the 8.9 N/mm minimum. It was then decided to mix 20 wt% kaolin with the 60:40 ratio of tabular to calcined alumina mixture. The powders were dry mixed by hand and then applied during the coating process. The coated and heat-treated pellets (2 hr in air at 1100°C) exhibited a non-homogeneous coating that resulted in a very low crushing strength. The positive outcome was that the 20 wt% kaolin-alumina mixture passed the hardening process.

To improve the mixing of the materials it was decided to wet-mix the powders in a solution of 1 wt% sodium hexametaphosphate and water. The powders were mixed as a slurry for 30 min at 60 rpm with a commercial paint mixer. Following the mixing process the slurry was dried in an oven at 110°C and then ground with a mortar and pestle. During the coating process, instead of using the 5 vol% lignin and water solution, which had a pH of ~ 3.5, a 5 vol% high temperature binding agent and water solution with a pH of ~ 10 was used. Both types of lignin were from Lignotech. The new technique resulted in a homogenous shell that could endure the hardening process. The hardening process was only carried out for 1 hr, instead of the typical 2 hr. Following the coating process the pellets were heat treated for 2 hr at 1100°C in air and then tested for crushing strength.

Table 4.6. Crushing strength of core and shell pellets heat-treated in air for 2 hr. Pellets consisted of P.O.P. cores and kaolin-alumina shells.

Batch	Avg. Diameter (mm)	Avg. Shell Thickness* (mm)	Avg. Crushing Force (N)	Avg. Force/Shell Thickness* (N/mm)	Avg. Force/ Diameter (N/mm)	% Fail Rate of Pellets w/ F/D < 8.9 (N/mm)
1	5.5 +/- 0.2	0.81 +/- 0.17	86 +/- 35	109 +/- 55	16 +/- 7	20

* Avg. shell thickness based upon the thinnest regions of the shells and not the overall average thickness for structural comparisons.

The strength test results shown in Table 4.6 indicate that the kaolin-alumina shell mixture resulted in pellets that were just as strong, if not stronger than those with the limestone-alumina shell mixture. The results are promising since a strong shell material was synthesized that replaced the reactive CaO component and could potentially replace some or all of the alumina. In addition, even though the hardening process was only performed for 1 hr, the pellets still exhibited a strong shell.

The testing of the reactivity of the pellets was conducted with the same gas mixture and temperature used for testing the limestone-alumina core and shell pellets, which consisted of 1.0 vol% H_2S, 24 vol% H_2 in N_2 and 880°C. The same cyclic oxidation and reduction regeneration technique using 9 vol% H_2, 13 vol% O_2 in N_2 at 1050°C was employed. The results from a single pellet test are shown in Figure 4.5.

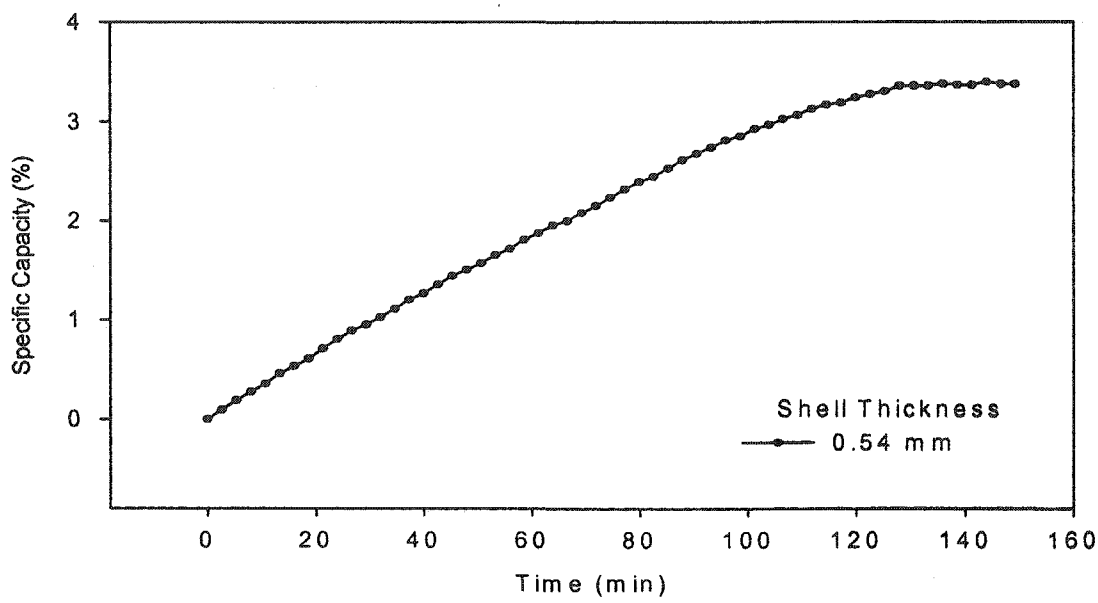

Figure 4.5. A P.O.P. core, kaolin-alumina shell pellet reacted with 1.0 vol% H_2S, 24 vol% H_2 in N_2 at 880°C.

The reactivity of the kaolin-alumina shell pellet appeared to exhibit the same reaction rate profile as the limestone-alumina pellets with the thinner shells, ~ 0.3 mm. But the difference lies in the capacity achieved within the first 40 min. The limestone-alumina shell pellets reached a capacity of ~ 6% during the first 50 min of reaction, while the kaolin-alumina shell pellet only reached a capacity of ~ 1.5%. Since the limestone-alumina shell pellets contained a reactive shell, it is difficult to compare the two types of pellets based upon reaction rates. The strength of the post reaction kaolin-alumina shell pellet was tested and the results are presented in Table 4.7

Table 4.7. Crushing strength of a core and shell pellet heat treated in air for 2 hr, reacted once with 1.0 vol% H_2S, 24 vol% H_2 in N_2 at 880°C and regenerated twice with 9 vol% H_2, 13 vol% O_2 in N_2 at 1050°C. Pellet consisted of a P.O.P. core (converted to CaO) and kaolin-alumina shell.

Shell Material Testing in Core and Shell Form						
Pellet	Avg. Diameter (mm)	Avg. Shell Thickness* (mm)	Crushing Force (N)	Avg. Force/Shell Thickness* (N/mm)	Avg. Force/ Diameter (N/mm)	% Fail Rate of Pellet w/ F/D < 8.9 (N/mm)
1	4.85 +/- 0.10	0.40 +/- 0.02	104 +/- 0.5	260 +/- 13	21.4 +/- 0.5	0

* Avg. shell thickness based upon the thinnest regions of the shells and not the overall average thickness for structural comparisons.

The results in Table 4.7 are preliminary since only one post-reaction pellet underwent testing, but the results are positive. The most significant result is the high crushing strength (F/D) exhibited by the pellet, which was two times the minimum required value. If this value is compared to the results of the kaolin-alumina shell pellets that were heat-treated but not reacted, only 40% of those pellets yielded a F/D value higher than 18.9 N/mm. Whether the

reaction conditions contributed to the increase in strength of the pellet is yet to be determined, but the preliminary results suggest that it is a possibility.

4.3 Summary and Conclusions

The testing of the limestone core and limestone-alumina shell pellets was conducted using crushing strength and abrasion resistance tests. The tests revealed that the original core and shell pellet developed by Akiti et al. (2002), provided a strong and attrition resistant pellet suitable for moving bed applications. Additional tests with core and shell pellets made with thicker shells improved the strength and attrition resistance of the pellets considerably. But the added strength came with a loss in overall sulfur capacity. Sulfidation tests were conducted with core and shell pellets, which indicated that the shells lowered the overall sulfidation capacity. The sulfidation tests also revealed that the limestone in the shell material had reacted with H_2S to a small extent. The effect of the sulfidation and regeneration reactions and the high heat-treatment on the strength of the core and shell pellets was studied. The preliminary results revealed that the crushing strength of reacted core and shell pellets were slightly weaker than pellets that were only heat-treated. Since only a few pellets were tested, more work needs to be done before any conclusive statements can be made.

The improvement of the shell composition was investigated by incorporating kaolin. First attempts using pure kaolin as a shell material proved impractical, therefore kaolin was used as a potential replacement for limestone. The kaolin-alumina mixture proved useful as a shell material if it was first wet-mixed prior to pelletization. The kaolin-alumina shell pellets exhibited an average crushing strength that was higher than the limestone-alumina

shell pellets but no abrasion resistance tests were conducted. One pellet was tested for its reactivity with H_2S and for its crushing strength after sulfidation and regeneration. The sulfidation test indicated that it had reacted at a comparable rate as the thicker-shelled limestone-alumina shell pellets. The crushing strength test, post-reaction, revealed that the pellet was stronger than kaolin-alumina shell pellets that were only heat-treated. Although the results are preliminary, they indicate that kaolin could be a possible replacement for the limestone and maybe some of the alumina.

Chapter 5. Modeling of the Gas-Solid Reaction

5.1 Introduction

In order to design a fixed or moving bed reactor for removing H_2S from hot coal gas, the performance of the solid sorbent must be well known. In general, a model that accurately describes the conversion of a sorbent with respect to H_2S concentration and time is needed. There are several models that have been developed to describe the conversion of a solid sorbent that take into account many different physical parameters of the sorbent. While the extra parameters increase the accuracy of such models, they also increase the complexity.

One of the most useful models that was first proposed to represent the combustion of carbon particles is the shrinking core model (SCM) (Yagii and Kunii, 1955). The model has proven to be very useful for representing the reactions between SO_2, H_2S or COS with CaO. The model includes three primary rate-limiting steps that can occur during gas-sold reactions: 1) gas film diffusion, 2) ash/product layer diffusion and 3) chemical reaction. The three steps are combined in the following equation representing the first order reaction rate for the conversion of a solid, spherical particle:

$$t_{Total} = \tau_{Film} X + \tau_{Ash}\left[1 - 3(1-X)^{\frac{2}{3}} + 2(1-X)\right] + \tau_{Rxn}\left[1-(1-X)^{\frac{1}{3}}\right] \quad (5.1)$$

The τ's represent the characteristic time for total conversion to take place for each particular rate-limiting step.

$$\tau_{film} = \frac{\rho_{CaO} R}{3 k_g C_{H_2S}} \quad (5.2)$$

$$\tau_{Ash} = \frac{\rho_{CaO} R^2}{6 D_e C_{H_2S}} \tag{5.3}$$

$$\tau_{Rxn} = \frac{\rho_{CaO} R}{6 k_s C_{H_2S}} \tag{5.4}$$

The SCM represented by eq 5.1 can be used with any combination of the rate limiting steps to represent the conversion of a solid. Because the model has an analytical solution and it can be used to analyze different forms of reaction rate limitation, it is very useful when it can be applied.

In the following work the SCM was applied to two different types of agglomerated pellets that were reacted with H_2S at 880°C. The first type consisted of CaO pellet cores derived from calcium sulfate hemihydrate and the second type consisted of similar cores coated with an alumina and limestone shell. Both types of pellets were tested and the results were fitted with the SCM. The usefulness of the SCM for application to the agglomerated pellets is discussed together with an analysis of the results.

5.2 Results and Discussion

Since an agglomerated pellet reacting with H_2S can involve many different forms of reaction rate limitation, the inclusion of film, ash and chemical reaction rate were all considered possible rate-limiting steps. Before fitting the SCM to the data, the gas phase mass transfer coefficient and reaction rate were estimated and compared for the experimental reactor conditions. Since gas-film diffusion presents a possible limiting factor, the gas-film coefficient, k_g, was calculated using the Frössling correlation for a sphere in forced convection:

$$\frac{k_g d_p}{D_{H_2S}} = 2 + 0.6 Re^{1/2} Sc^{1/3} \qquad (5.5)$$

where d_p is the average diameter of the pellets tested and the diffusivity, D_{H_2S}, was calculated using the correlation developed by Fuller et al. (1966). The value obtained for k_g was 18.5 cm/s for the following conditions: 880°C, Re (0.79), Sc(1.72) and an average particle diameter of 0.35 cm.

The reaction rate constant was estimated based on the results reported by Borgwardt (1984b) for the reaction between CaO and H_2S at high temperatures. By using Borgwardt's data, an approximate initial reaction rate of 6.58 E-4 mol/min was estimated for the experimental conditions employed in the present work. By comparing the average, initial reaction rate to the rate of gas-film mass transfer $(k C_{H_2S}) / (k_g \pi d_p^2 C_{H_2S})$, for a pellet 0.35 cm in diameter, a ratio of 14.5:1 was obtained for the conditions of 1.0 vol% H_2S, 24 vol% H_2, in N_2, 880°C, 500 mL/min flow rate, and 1 atm of pressure. The estimates of k_g suggest that gas-film limitation was a definite probability in the reactor system used for this study.

Two types of pellets (core and core and shell) were chosen for analysis. Three pellets were selected from a batch of each type for the study. The pellet cores consisted of $CaSO_4 \cdot 2H_2O$ and the core and shell pellets contained a similar core with a shell that consisted of 20 wt% limestone and 80 wt% alumina. The pellets were tested in a tubular quartz reactor and the reaction progress was monitored with a TGA. The design of the pellets and specifics of the reactor system are described in Chapter 2. Prior to any sulfidation reactions, the pellets were first converted to CaO from $CaSO_4$ with gas mixtures of 9 vol% H_2 in N_2 for the

reduction step and 13 vol% O_2 in N_2 for the oxidation step at 1050°C according to the reactions:

$$CaSO_4 + H_2 \rightarrow CaO + SO_2 + H_2O \quad (2.12)$$

$$CaS + 2O_2 \rightarrow CaSO_4 \quad (1.9)$$

The sulfidation reactions were carried out with a gas mixture containing 1.0 vol% H_2S, 24 vol% H_2, in N_2 at 880°C according to the reaction:

$$CaO + H_2S \rightarrow CaS + H_2O \quad (1.2)$$

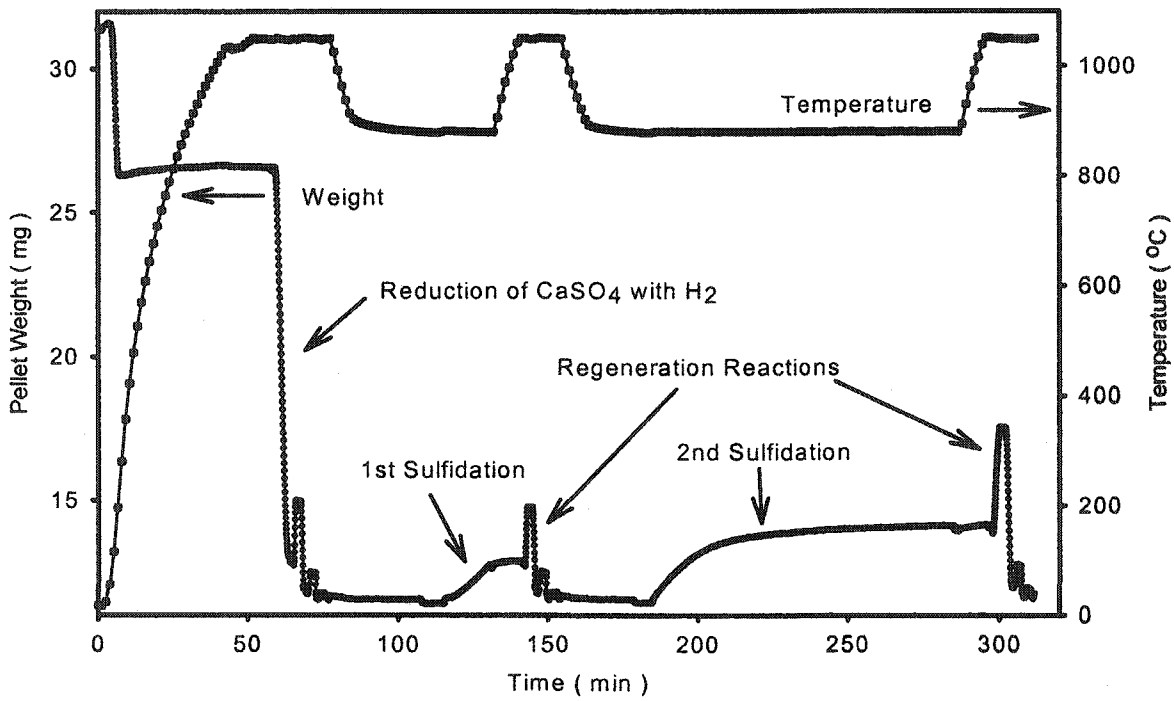

Figure 5.1. Reaction of a P.O.P. pellet core with 1.0 vol% H_2S, 24 vol% H_2, in N_2 at 880°C, and regenerated with 9 vol% H_2, and 13 vol% O_2 in N_2 at 1050°C. Pellet diameter post reaction: 0.272 cm.

After initially testing a pellet core, 0.27 cm in diameter, for its sulfidation capacity over 1.5 hr, it was discovered that the pellet had failed to reach complete conversion. A graphical representation of two cycles of sulfidation and regeneration that is representative of

all the tests in this study is shown in Figure 5.1. For all tests and model fitting, the second sulfidation was used for analysis.

In general, it took approximately 50 min for each of the pellet cores to reach a sulfidation conversion of 79%. To test the effect of pellet size, pellet cores 1 mm in diameter were treated in the reactor, and complete sulfidation of the cores was achieved within 20 min. Therefore, it is believed that inter-particle mass transfer was limiting the rate of reaction of the larger agglomerated pellets. The SCM was first applied for the analysis of the pellet cores. Initial attempts to fit the model did not yield any good results, Figure 5.2.

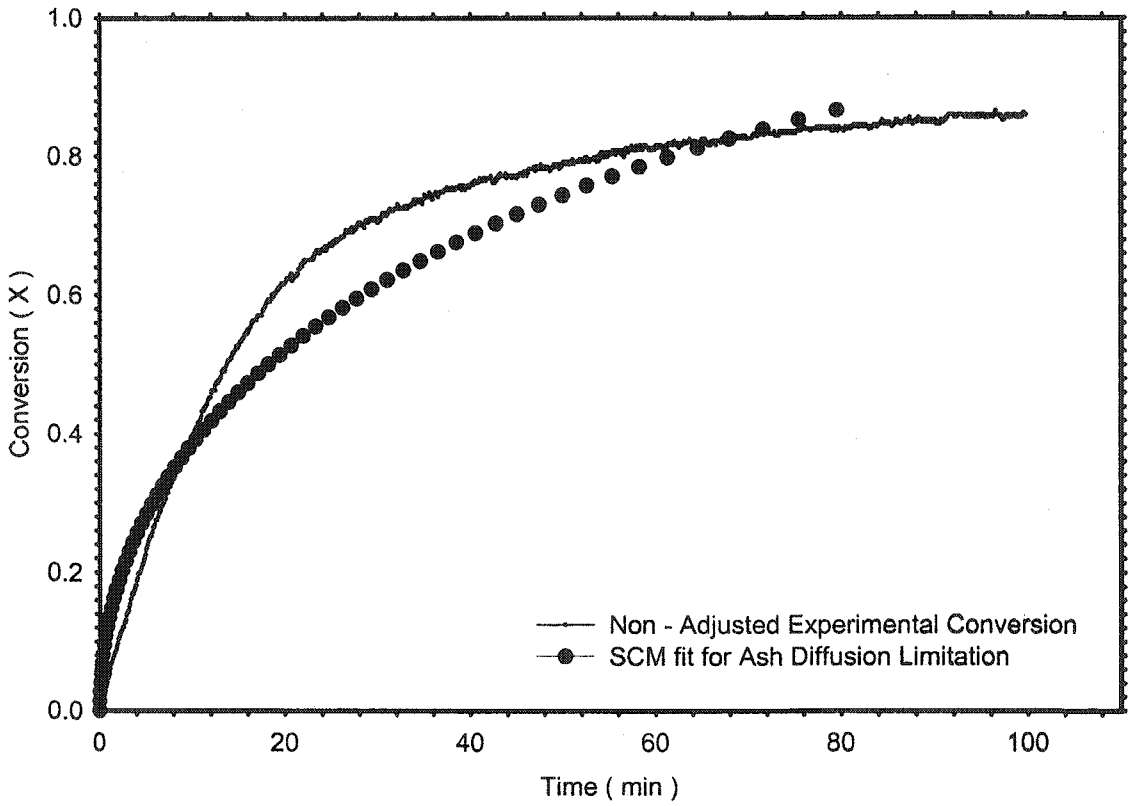

Figure 5.2. Reaction of a P.O.P. pellet core with 1.0 vol% H_2S, 24 vol% H_2, in N_2 at 880°C, and fitted with the SCM for ash diffusion limitation. Pellet diameter post reaction: 0.272 cm.

It was difficult to fit the model since the pellets did not reach 100% conversion in a reasonable length of time. In order for the SCM to apply for a pellet, 100% conversion must be achieved at a reasonable rate and physically the pellet must exhibit the shrinking core reaction phenomena. If these criteria are not met, the rate of reaction of the pellet will not be accurately represented by the SCM, and the calculated coefficients will not yield the correct values of diffusivity and reaction rate. Since the SCM did not fit the experimental data, some consideration was given to the possible shortcomings of the model. Because the SCM does not account for inter-particle mass transfer or solid-state diffusion, it appeared that these might be limiting the overall reaction rate.

To get some insight into the reaction front taking place, pellet cores were sulfided to 35% and 70% conversion and then cross-sectioned and viewed with an SEM so that sulfur dot maps could be obtained using EDS. The results in Figures 5.3 and 5.6 indicate that the pellets reacted in a modified shrinking core manner. It was apparent that there was not a sharp interface between the reacted and unreacted CaO, as prescribed for the SCM. In addition, in Figures 5.3 and 5.4 it can be seen that the reaction front had advanced much further in areas where there were pronounced, radial cracks. This result indicated that the reaction rate was limited by inter-particle mass transfer. Further insight is gained from the image in Figure 5.5, which is an EDS sulfur map of a cross-sectioned core and shell pellet. The pellet had been reacted with H_2S to a conversion exceeding 90%. It is apparent from the sulfur map that the reaction front had apparently reached the core of the pellet. Since the conversion was not complete, it was thought that shell diffusion, solid-state diffusion and inter-particle diffusion combined to reduce the rate of reaction to such an extent that the amount of time for complete conversion to occur would take multiple hours with the

conditions used. Another noteworthy aspect of the sulfur map is the number of areas within the shell that were sulfided, which indicates that some of the Ca in the shell had reacted with the H_2S.

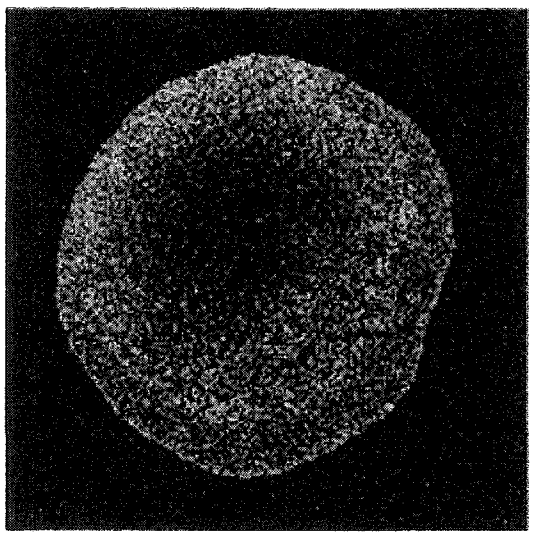

Figure 5.3. EDS sulfur map of a P.O.P. core sulfided to 35% conversion.

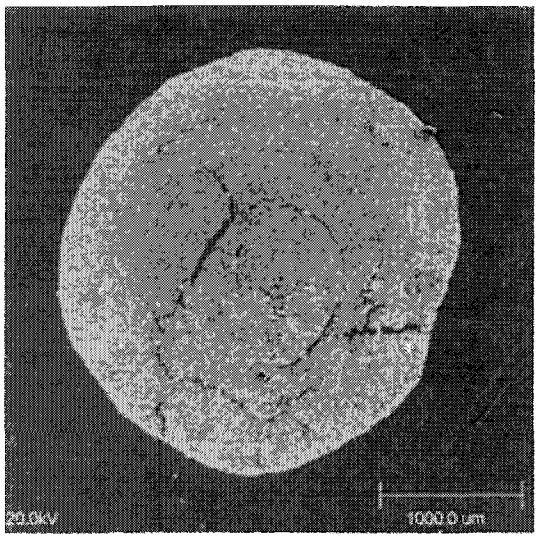

Figure 5.4. SEM micrograph of a core sulfided to 35% conversion.

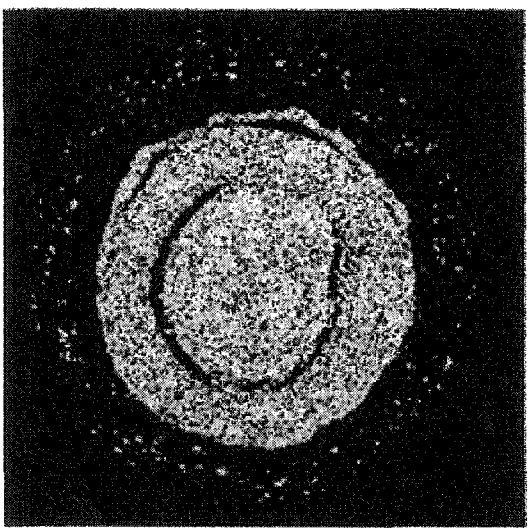

Figure 5.5. EDS sulfur map of a P.O.P. core with a limestone-alumina shell, sulfided to > 90% conversion.

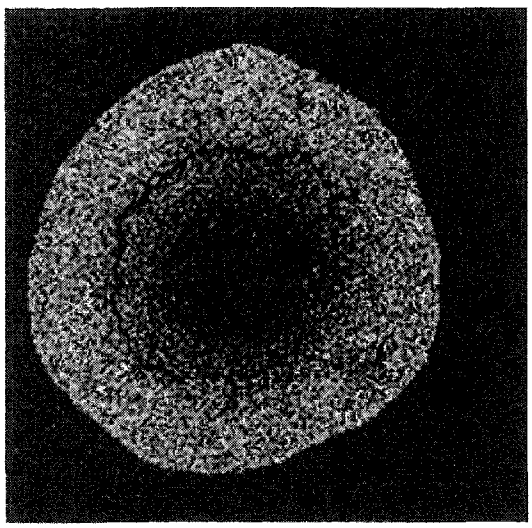

Figure 5.6. EDS sulfur map of a core sulfided to 70% conversion.

Due to the poor lack of fit of the SCM to the sulfidation data, the data was truncated at a value of conversion where the rate of conversion began to level off, which was generally at 79%. The resulting fit of the SCM to the transformed data was quite good with correlations of 0.999.

Since the simplest and most accurate model for designing reactors is always preferable, the SCM applied over a practical range of conversion seemed to offer a good semi-empirical model for the design of fixed and moving bed reactors. After fitting several versions of the SCM, the best results were achieved by fitting the version that accounted for both film and ash layer diffusion control, which gave the overall best fit to the data, Figure 5.7.

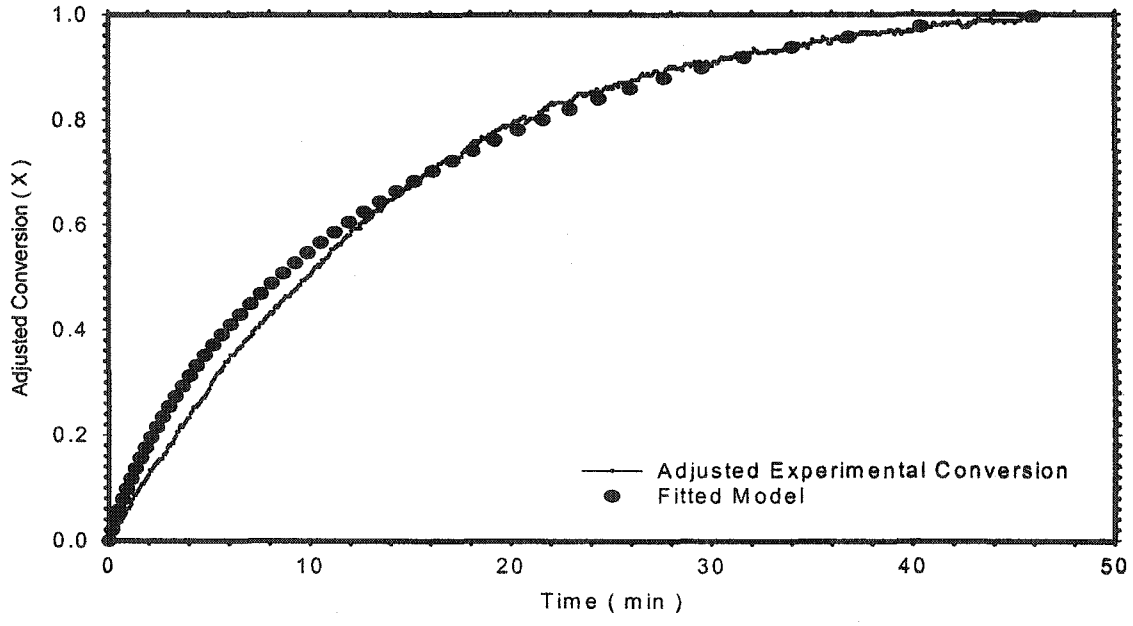

Figure 5.7. Comparison between adjusted experimental data and the fitted SCM for pellet no.2, sulfided with 1.0 vol% H_2S, 24 vol% H_2 in N_2 at 880°C.

This chosen form of the SCM, eq 5.6, has also been used successfully by other researchers for the reaction between CaO particles and H_2S (Borgwardt et al., 1984b; Abbasian et al., 1993; Agnihotri et al., 1999).

$$t = \tau_{Film} X + \tau_{Ash}\left[1 - 3(1-X)^{\frac{2}{3}} + 2(1-X)\right] \qquad (5.6)$$

The values of τ_{film} and τ_{ash} obtained from fitting the model are presented in Table 5.1. The values represent the total time it would take for a pellet to reach 79% conversion if the rate was controlled by film or ash layer diffusion, respectively.

Table 5.1. Results from the application of the SCM for pellet cores using film and ash layer diffusion limitation.

Pellet	Pellet Wt. (mg)	Radius (cm)	K_{film} (min mol/cm^4) C_{H2S}/R	K_{ash} (min mol/cm^5) C_{H2S}/R^2	τ_{film} (min)	τ_{ash} (min)
1	10.8	0.136	4.58 E-6	2.63 E-4	7.91	40.8
2	10.6	0.147	8.05 E-6	1.88 E-4	5.94	46.0
3	12.7	0.140	5.96 E-6	2.20 E-4	11.15	38.4
Average	11.37	0.141 +/- 0.006	6 E-6 +/- 1.7E-6	2.2 E-4 +/- 4 E-5	8 +/- 3	42 +/- 4

By examining the modeling results for τ_{film} and τ_{ash}, it is quite evident that inter-particle mass transfer, represented by τ_{ash}, controlled the rate of reaction and is five times larger than τ_{film} based on an average of all three pellets. This result is not surprising since even micrometer-sized particles have been shown to be limited by ash layer diffusion (Borgwadt, 1984b). A problem with the values of τ_{film} that were obtained is that they do not

correlate well with the particle radii. Since the τ_{film} coefficient is a function of particle radius, it should increase as the particle size increases, which was not the case. To further analyze the results, coefficients denoted as K were calculated to represent the τ coefficients with the H_2S concentration and particle radius factored out. The values of K_{film} and K_{ash} represent constant coefficients that are functions of both gas-film mass transfer and effective diffusivity, respectively.

By comparing the K_{film} values to the pellet radii, it can be seen that as the particle radii increase so do the values of K_{film}. The correlation can be explained through the Frössling equation, which indicates that k_g will decrease as the particle size is increased. Therefore, a decrease in k_g will result in an increase in K_{film}. The same comparison can be made between the K_{ash} values, but in this case, the K_{ash} value is a function of effective diffusivity, D_{eff}, which is not a function of the particle radius. Since the K_{ash} value should be a constant regardless of the particle size, all of the values should be similar, which is also the case as seen in Table 5.1.

Using the averaged τ values a semi-empirical model was formulated and then applied to pellet no. 1 with its radius and the H_2S concentration inserted into the empirical τ's, as shown:

$$t = 10 * X + 52 * \left[1 - 3(1-X)^{\frac{2}{3}} + 2(1-X) \right] \qquad (5.7)$$

The resulting fit of eq 5.7 to pellet core no. 1 (Figure 5.8) indicates that the model represented the data fairly well.

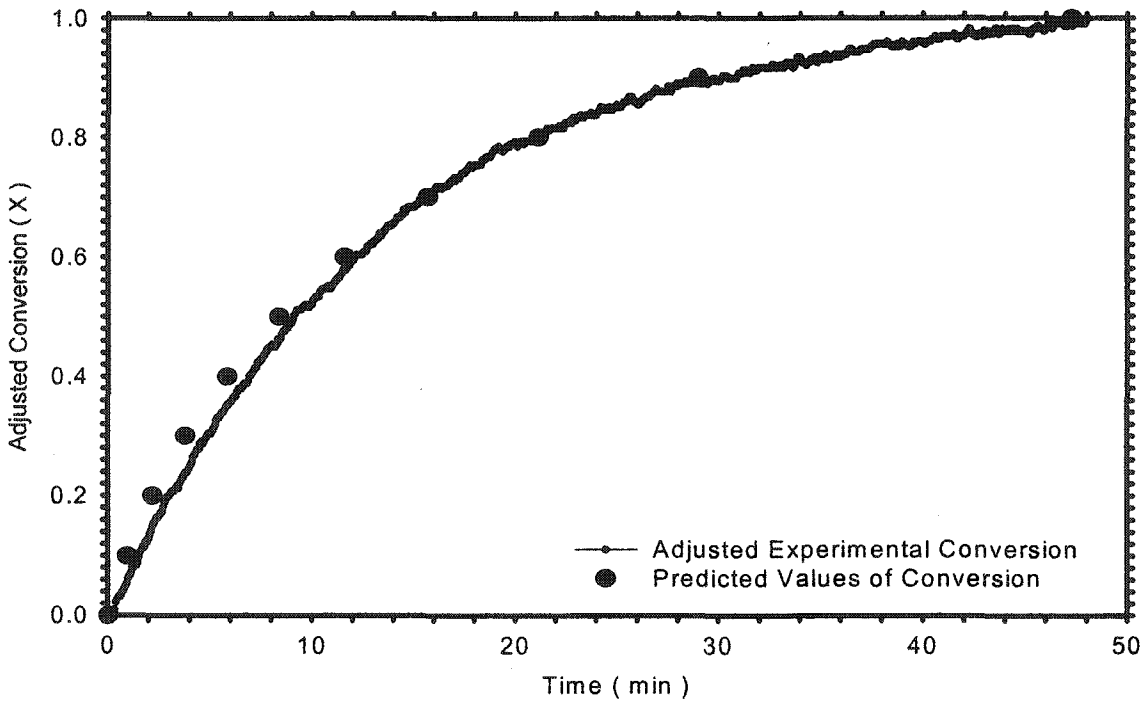

Figure 5.8. Comparison between adjusted experimental data and the fitted SCM for pellet no.1 using the averaged values for K_{film} and K_{ash}, sulfided with 1.0 vol% H_2S, 24 vol% H_2 in N_2 at 880°C.

Since the modification of the SCM worked well for representing the reaction of the three pellet cores, the same technique was tested for its effectiveness on a pellet core made of the same composition as the previous pellets, but reacted with 0.5 vol% H_2S instead of 1.0 vol% H_2S. The average K_{film} and K_{ash} were used for the analysis together with the pellet core radius and different H_2S concentration. These values were used to calculate the adjusted τ's. The results of the model fitting are shown in Figure 5.9, which indicate that even though a different H_2S concentration and pellet were used, there was a fairly good fit between the adjusted experimental data and the values predicted by the model.

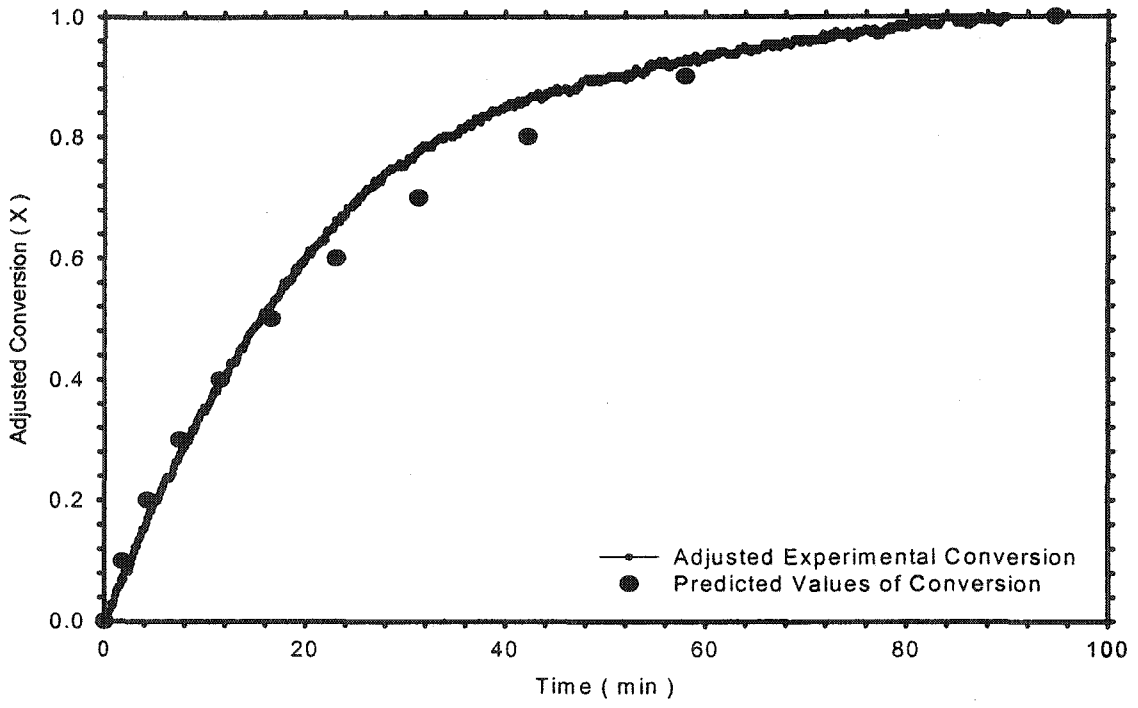

Figure 5.9. Comparison between adjusted experimental data and the fitted SCM for a pellet core using the averaged values for K_{film} and K_{ash}, sulfided with 0.5 vol% H_2S, 24 vol% H_2 in N_2 at 880°C.

Because the SCM provided a unique and accurate way to predict the conversion of pellets in a semi-empirical fashion, the same method was used to evaluate three core and shell pellets. The pellets were evaluated with the SCM for film and ash layer diffusion control for the same reaction conditions as the pellet cores and yielded near unity correlation coefficients. The results from the model fitting are shown in Table 5.2 where the values obtained for the τ's indicate how much more the core and shell pellets were affected by the shell. For this case, the ratio of τ_{film} : τ_{ash} was 3.3, which was the opposite effect that was observed for the core pellets. Since the shell layer added an extra diffusional resistance that was much larger than the film resistance, the values of τ_{film} and K_{film} are referred to as τ_{shell}

and K_{shell}. The reason for the film coefficient being larger was due to the large amount of inert alumina that was contained within the shell. The alumina added an extra form of diffusional resistance to the reaction rate aside from the gas film resistance.

Table 5.2. Results from the application of the SCM for shell and ash layer diffusion limitation to core and shell pellets.

Pellet	Pellet Wt. (mg)	Shell Thickness (cm)	Overall Radius (cm)	K_{shell} ($minmol/cm^4$) C_{H2S}/R	K_{ash} ($minmol/cm^5$) C_{H2S}/R^2	τ_{shell} (min)	τ_{ash} (min)
1	62.3	0.036	0.222	2.80 E-5	4.44 E-5	58.9	20.7
2	54.3	0.030	0.217	3.01 E-5	3.62 E-5	61.8	16.4
3	63.0	0.031	0.227	3.15 E-5	4.50 E-5	67.2	19.2
Average	59.9	0.32 +/- 0.03	0.222 +/- 0.005	2.99 E-5 +/- 1.8E-6	4.19 E-5 +/- 5 E-6	63 +/- 4	19 +/- 2

Unfortunately, the analysis was complicated by the fact that there was limestone within the shell that reacted. Since the shell partially reacted, it could not be dealt with as a complete, inert layer. Therefore, the core and shell pellets actually had two reaction zones, the shell and the core. And, unlike the results from the pellet cores, there was no correlation between the overall pellet radius and the values of K_{shell}, nor were there any correlations between the K_{shell} and τ_{shell} coefficients and the shell thickness. The difficulty of finding a correlation between the pellets and the coefficients was also increased due to the similar shell thicknesses and pellet radii.

To test the semi-empirical SCM on the core and shell pellets the averaged K_{shell} and K_{ash} values from Table 5.2 were used with the dimensions of pellet no. 3 and the

concentration of H_2S factored in. The model was tested using eq 5.6 and the results are shown in Figure 5.10. The results indicate that the model also fits the data of the core and

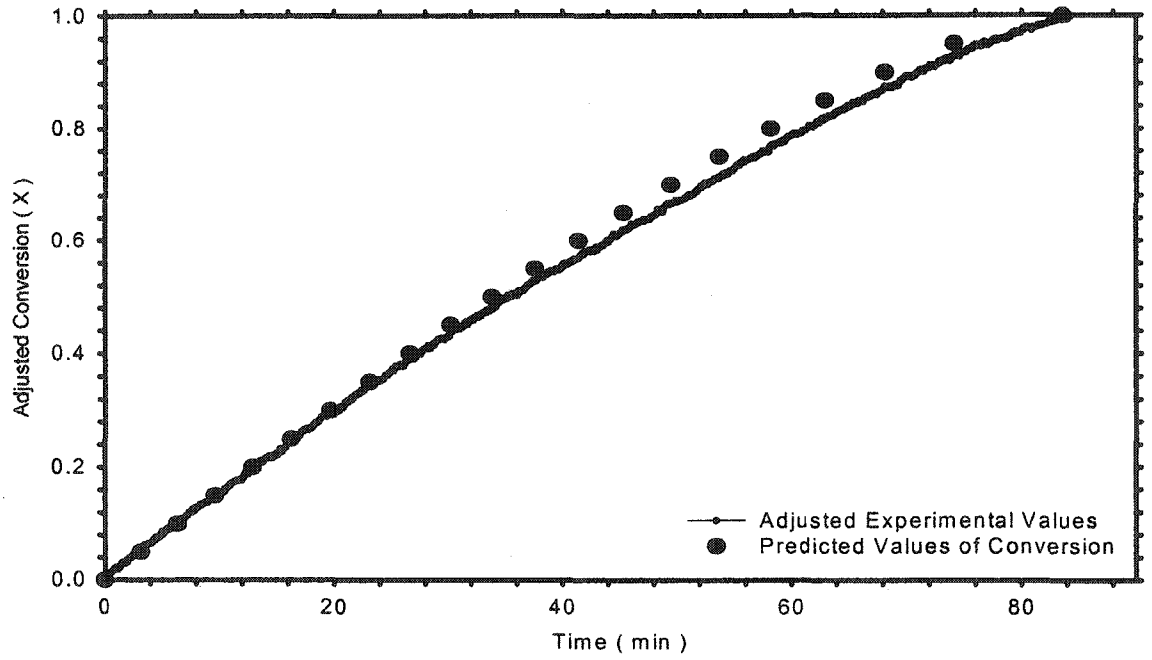

Figure 5.10. Comparison between adjusted experimental data for core and shell pellet no. 3 and the fitted SCM using the averaged values for K_{shell} and K_{ash}, sulfided with 1.0 vol% H_2S, 24 vol% H_2 in N_2 at 880°C.

shell pellets with similar accuracy as the pellet cores. The linear rate of reaction is very apparent in Figure 5.10 and can be attributed to the extra diffusional resistance created by the shell.

5.3 Summary and Conclusions

The applicability of the SCM to core and shell pellets has proved useful. Initially, the pellets were not accurately fitted with the SCM due to a slow rate of reaction at high conversions. Therefore, the conversion data for the pellets were truncated at a value that seemed sufficient for practical use in reactor analysis, and after refitting the model to the

adjusted data, the SCM proved to represent the experimental results quite effectively. The SCM worked well for agglomerated pellet cores when including gas film and ash layer diffusion resistances. Since the SCM was a success with the pellet cores it was applied to core and shell pellets. The same form of the SCM was applied to the pellets after their conversion data were adjusted. The results indicated that the SCM successfully described the rate of reaction of core and shell pellets. The model was then tested on a pellet core, which had been reacted with a different H_2S concentration, and the model still provided an accurate result. These findings resulted in a suitable semi-empirical form of the SCM that could be used successfully to model agglomerated core and core and shell pellets. The resulting model can possibly be used for reactor design if pellets similar to those tested are used.

Chapter 6. General Conclusions

6.1 General Discussion

Since the overall objective of the project was to improve the performance of the core and shell sorbent, areas of study were concentrated on performance enhancers of the core material, durability tests, and a new shell composition. Two primary sources of CaO were compared for their reactivity and physical properties. The results indicated that the reaction between H_2S and CaO was more dependent upon surface area than macro-porosity, and that plaster of Paris pellets provide a more reactive and stable sorbent than those made with limestone powder.

The addition of pore-modifiers to limestone pellets was investigated by wet-mixing the materials prior to pelletization. Preliminary studies with modifiers such as graphite and cornstarch indicated that they either reduced or did not alter the thermal stability of limestone pellets over multiple cycles of testing with H_2S. But preliminary results with poly (vinyl alcohol) (PVA) indicated that it might work to increase the thermal stability of the limestone pellets by introducing more porosity.

There were also studies of the effects of chemical elements on the reactivity of CaO with CO_2 and H_2S. The incorporation of $SrCO_3$ revealed that it reduced the stability of CaO during reaction with CO_2 over multiple cycles, whereas materials that naturally contained Mg, such as dolomite, exhibited a much higher stability than limestone. The same thermal stability effect was exhibited by Mg-containing materials during reaction with H_2S. The materials that exhibited the highest specific capacity were derived from $CaCO_3$ and plaster of

Paris. Of these two materials the one derived from plaster of Paris was apparently more thermally stable.

By testing the original core and shell material developed by Akiti et al. (2002) for durability, it was discovered that the original shell composition provided a strong and abrasion resistant pellet suitable for moving bed applications. A new technique of wet-mixing the shell material powders prior to pelletization indicated that the durability of the pellets could be improved. The discovery that limestone in the shell material reacts with H_2S has prompted some new questions regarding the strength of the pellets during reaction if used in a fixed or moving bed.

The replacement of limestone with kaolin in the shell mixture has provided some promising, preliminary results. The kaolin-alumina shell mixture has been used successfully to coat both limestone and plaster of Paris cores. The coated pellets have exhibited high crushing strength qualities post heat-treatment. A single pellet containing a plaster of Paris core and kaolin-alumina shell was successfully reacted with H_2S and it exhibited a high crushing strength post reaction.

The modeling of both core and core and shell pellets was successful using the shrinking core model (SCM). The model was suitable after the pellet data were adjusted to represent a practical limit of sulfidation. The resulting semi-empirical SCM was tested, and yielded accurate results when applied to pellets reacted under different conditions. The application of the model for these particular pellets appeared adequate for the design of a fixed or moving bed reactor.

6.2 Recommendations for Future Research

Since the research on the reactivity of the CaO-based sorbents indicated that surface area and porosity not only enhanced the reactivity of the material but also increased its thermal stability, these two physical parameters should be considered during future work on potential sorbents. Because the decline in capacity of limestone has been attributed to its sintering, additives which create more porosity should be investigated. Additives should be easy and practical to apply, such as wet-mixing PVA with limestone. Also, reacting the limestone with acetic acid or other compounds that will expand the material and create a more meso-porous structure can possibly be used to increase the surface area.

Additives such as Mg should be tested for incorporation into limestone by wet-mixing methods to investigate its effects. In addition, tests with wet-mixed Sr-limestone or co-precipitated Sr-$CaCO_3$ should be carried out with H_2S to look into its thermal stability effects.

The preliminary results with kaolin indicate that it might be a possible replacement for limestone in the shell mixture. Further testing on the replacement of alumina with some kaolin should also be conducted. Also, kaolin is not the only clay that could be applicable as a suitable shell material, therefore other clays such as bentonite should be considered.

Although the SCM was applied successfully, a model that is more theoretical than semi-empirical should be considered in order to better understand the reaction and diffusion processes that take place in an agglomerated pellet. A model that is suitable for such a case is the particle-pellet model. This model incorporates inter-particle gas phase diffusion resistance and also the individual conversion of particles within a pellet as a whole. Since solid-state diffusion is limiting for full conversion of the particles, the overall conversion of a

pellet takes an infinite amount of time, which the particle-pellet model takes into account. Other factors that can be incorporated within the particle-pellet model are pore loss, surface area loss and particle coalescence due to sintering. In addition, the influence of heat generation during the exothermic sulfidation reaction can be included which will affect the reaction rate, gas and solid-state diffusion rates and the sintering of the material. Furthermore, since a pellet is subjected to a cyclic sulfidation and regeneration process, the regeneration process also needs to be considered. Since the regeneration process involves exothermic reactions and a significant temperature change, its effects on the sorbent material in terms of sintering and the resulting pore and surface area loss and particle coalescence can be substantial.

Such parameters further complicate the model but should improve its accuracy. Even though the solution of the particle-pellet model with or without the added factors is more complicated than the solution of the SCM, it should lead to a better understanding for future sorbent development.

6.3 References

Abbasian J.; J. R. Wangerow; A. H. Hill. "Effect of HCl on Sulfidation of Calcium Oxide," *Chem. Eng. Sci.*, **48** (15), 2689-2695, (1993).

Akiti, T.T. Jr.; K. P. Constant; L. K. Doraiswamy; T. D. Wheelock. "A Regenerable Calcium-Based Core–in–Shell Sorbent for Desulfurizing Hot Coal Gas," *Ind. Eng. Chem. Res.*, **41**, 587-597, (2002).

Akiti, T.T. Jr.; K. P. Constant; L. K. Doraiswamy; T. D. Wheelock. "Development of an Advanced Calcium-Based Sorbent for Desulfurizing Hot Coal Gas," *Advances in Environmental Research,* **5**, 31-38, (2001).

Anderson, P. J.; P. L. Morgan. "Effects of Water Vapour on Sintering of MgO," *Trans. Faraday Soc.*, **60**, 930, (1964).

Attar, A. F., Interim Report for U.S. EPA Research Grant No. R809274, North Carolina State Univ., Raleigh, NC, Dec., 1982.

Attar, A.; F. Dupuis. "The Rate and the Fundamental Mechanisms of the Reaction of Hydrogen Sulfide with the Basic Minerals in Coal," *Ind. Eng. Chem. Proc. Des. Dev.*, **18**, 607-618, (1979).

Ayala, R. E.; A. Feitelberg; A. Furman. "Development of a High Temperature Moving-Bed Coal Gas Desulfurization System," Proceedings of Twelfth Annual International Pittsburgh Coal Conference, pp.1053-1058, 1995.

Ayala, R.E.; T. Chuck; E. Gal; R. P. Gupta. "Development of Sorbents for High-Temperature Desulfurization in Moving-Bed Systems," Proceedings of the Coal-Powered Systems 95 – Advances in IGCC and PFBC Review Meeting, Vol. II, 637-645, (1994).

Bakker, W. J. W.; J. C. P. van Rossen; J. P. Janssens; J. A. Moulijn. "Hot Gas Cleaning, Sulfiding Mechanisms in Absorption of H_2S by Solids," In Desulfurization of Hot Coal Gas, A.T. Atimtay, D.P. Harrison, Eds.; NATO ASI Series, Vol. G 42, Springer-Verlag, New York, pp.159-178, (1998).

Bandi, A; M. Specht; P. Sichler; N. Nicoloso. "In suit Gas Conditioning in Fuel Reforming for Hydrogen Generation," 5th International Symposium on Gas Cleaning at High Temperature, Morgantown, WV, Sept., 2002.

Barth'el'emy, N. M. Improved Heat Recovery and High-Temperature Clean-up for Coal-Gas Fired Combustion Turbines, Master of Science Thesis, Dept. Chem. Eng. Univ. Cal. Berkley, 1991.

Beruto, D.; L. Barco. "CO_2-Catalyzed Surface Area and Porosity Changes in High-Surface-Area CaO Aggregates," *J. Amer. Ceram. Soc.*, **67**, 512-515, (1984).
Borgwardt, R. H. "Sintering of Nascent Calcium Oxide," *Chem. Eng. Sci.*, **44**, (1), 53-60, (1989a).

Borgwardt, R. H. "Calcium Oxide Sintering in Atmospheres Containing Water and Carbon Dioxide," *Ind. Eng. Chem. Res.*, **28**, 493-500, (1989b).

Borgwardt, R. H. "Reaction of H_2S and Sulfur with Limestone Particles," *Ind. Eng. Chem. Proc. Des. Dev.*, **23**, 742-748, (1984a).

Borgwardt, R. H. "Surface Area of Calcium Oxide and Kinetics of Calcium Sulfide Formation," *Environmental Progress*, **3**, (2), 129-135, (1984b).

British Petroleum (BP). "BP Statistical Review of World Energy," BP, London, June, pp.3,19, 1995.

Calvelo, A.; J. M. Smith. "Intrapellet Transport in Gas-Solid Non-Catalytic Reactions," *Chemeca '70*, No. 3,1, (Proc.) Conf., Australia, (1970).

Davies, N. H.; A. N. Hayhurst. "On the Formation of Liquid Melts of CaS and $CaSO_4$ and their Importance in the Absorption of SO_2 by CaO," *Combust. Flame*, **106**, 359-362, (1996).

Davies, N. H.; K. M. Laughlin; A. N. Hayhurst. "The Oxidation of Calciium Sulfide at the Temperatures of Fluidized Bed Combustors," Proc. 25^{th} Symp. (Int) Combust., Irvine, CA, 211-218, 1994.

Farha, F. E. Jr., L.E. Gardner. "Hydrodesulfurization of Organic Sulfur Compounds and Hydrogen Sulfide Removal with Incompletely Sulfided Zinc Titanate Materials," U.S. Patent No. 4, 313,820, 1982.

Fenouil, L. A.; S. Lynn. "Kinetic and Structural Studies of Calcium-Based Sorbents for High-Temperature Coal-Gas Desulfurization," *Fuel Sci. & Tech. Int'l.*, **14**, 537-557, (1996).

Fenouil, L. A.; G. P. Towler; S. Lynn. "Removal of H_2S from Coal Gas Using Limestone: Kinetic Considerations," *Ind. Eng. Chem. Res.*, **33**, 265-272, (1994).

Flytzani-Stephanopoulos, M; Z. Li. "Kinetics of Sulfidation Reactions Between H_2S and Bulk Oxide Sorbents," In Desulfurization of Hot Coal Gas, NATO ASI Series, A.T. Atimtay, D.P. Harrision, Eds; Vol. G 42, Springer, New York, pp.179-211, (1998).

Flytzani-Stephanopoulos, M. "Alternate Sorbents Development," Keynote Lecture at DOE/METC Workshop on "Status and Direction of Research and Development for High Temperature Sulfur Removal Sorbents," Morgantown, WV, Jan. 28, 1993.

Flytzani-Stephanopoulos, M.; T. U. Yu; S. Lew. "Development and Testing of Desulfurization Sorbents," Topical Report to Texaco, Under Subcontract, DOE Coop. Agreement No. DE-FC21-87MC23277, Dec., 1988.

Flytzani-Stephanopoulos, M.; G. R. Gavalas; K. Jothimurugesan; S. Lew; P. K. Sharma; M. J. Bagajewicz; V. Patrick. "Detailed Studies of Novel Sorbents for Hot Coal Gas Desulfurization," Final Report to DOE, DE-FC21-85-MC22193, Oct., 1987.

Furimsky, E.; M. Yumura. "Solid Adsorbents for Removal of hydrogen Sulphide from Hot Gas," Erdol und Kohle-erdgas-Petrochemie, **39**, (4), 163-172, (1986).

German, R. M.; Z.A. Munir. "Surface Area Reduction During Isothermal Sintering," *J. Amer. Ceram. Soc.*, **59**, (9-10), 379-383, (1976).

German, R. M.; Z. A. Munir. "Morphology Relations During Surface-Transport Controlled Sintering," *Metall. Trans. B*, **6B**, (2), 289-294, (1975a).

German, R. M.; Z. A. Munir. "Morphology Relations During Bulk-Transport Sintering," *Metall. Trans., A*, **6A**, (12), 2229-2234, (1975b).

German, R. M.; Z. A. Munir. "Geometry of Sintering Wires," *J. Mater. Sci.*, **10**, (10), 1719-1724, (1975c).

Gibson, J. B.; D. P. Harrison. "Testing of Novel Sorbents for H_2S Removal from Coal Gas," *Ind. Eng. Chem. Proc. Des. Dev.*, **19**, 231, (1980).

Glasson, R. R. "Reactivity of Lime and Related Oxides: I," *J. Appl. Chem.*, **8**, (12), 793-797, (1958).

Goodwin, J. W. "The Rheology of Dispersions," Colloid Science, Vol., 2, D. H. Everett (Sen. Reporter), The Chemical Soc., London, UK, pp.246-293, (1975).

Gupta, R. Personal Communication, Center for Engineering and Environmental Technology at Research Triangle Park, NC, (1999).

Hasler, D. J. L.; L. K. Doraiswamy; T. D. Wheelock. "A Plausible Model for the Sulfidation of a Calcium-Based Core-in-Shell Sorbent," To be published in *Ind.Eng.Chem.Res.*, Levenspiel Commemorative Edition, 2003.

Heesink, A. B. M.; W. P. M. van Swaaij. "The Sulphidation of Calcined Limestone with Hydrogen Sulphide and Carbonyl Sulfphide," *Chem. Eng. Sci.*, **50**, (18), 2983-2996, (1995).

Jagtap, S. B.; T. D. Wheelock. "Regeneration of Sulfided Calcium - Based Sorbents by a Cyclic Process," *Energy and Fuels,* **10**, 821-827, (1996).

Jalan, V.; D. Wu. "High Temperature Desulfurization of Fuel Gases for Molten Carbonate Fuel Cell Power Plants," National Fuel Cell Seminar, San Diego, CA, 1980; also in Giner, Inc., "Final Report to Argonne National Laboratory," Contract No. 31-109-39-5804, Waltham, MA, 1981.

Kellet, J.; Lange, F. F. "Thermodynamics of Densification: I, Sintering of Simple Particle Arrays, Equilibrium Configurations, Pore Stability, and Shrinkage," *J. Amer. Ceram. Soc.*, **72**, (5), 725-734, (1989).

Kobayashi, A. "Test Results of Yubari Hot Gas Desulfurizattion Pilot Plant," Coal Conversion Technologies Dept., IHI Co., Ltd, Japan, 1990.

Lange, F.F. "Powder Processing Science and Technology for Increased Reliability," *J. Amer. Ceram. Soc.*, **72**, (1), 3-15, (1989).

Levenspiel, O., The Chemical Reactor Omnibook, Oregon State Univ. Bk. Stores, Corvallis, OR, 1996.

Levy, A. "Utilization AR & TD Contractor's Review Meeting," U.S. Dept. of Energy, PETC, Pittsburgh, PA, March, 1982.

Lew, S.; K. Jothimurugesan; M. Flytzani-Stephanopoulos. "High-Temperature H_2S Removal from Fuel Gases by Regenerable Zinc Oxide-Titanium Dioxide Sorbents," *Ind. Eng. Chem. Res.*, **28**, 535-541, (1989).

Lew, S.; A. F. Sarofim; M. Flytzani-Stephanopoulos. "Sulfidation of Zinc Titanate and Zinc Oxide Solids," *Ind. Eng. Chem. Res.*, **31**, 1890-99, (1992).

Lew, S. "The Reduction and Sulfidation of Zinc Titanate and Zinc Oxide Solids," Ph.D. Dissertation, MIT, Cambridge, MA, (1990).

Pineda, M.; J.M. Palacios; L. Alonso; E. Garcia; R. Moliner. "Performance of Zinc Oxide Based Sorbents for Hot Coal Gas Desulfurization in Multicycle Tests in a Fixed-Bed Reactor," *Fuel*, **79**, 885-895, (2000).

Qiu, K.; O. Lindqvist; T. Mattisson. "Regeneration of Calcium Sulfide under Alternating Oxidizing and Inert Conditions: Kinetics and Mechanism," *Ind. Eng. Chem. Res.*, **37**, 923-928, (1998).

Rahaman, M. N., Ceramic Processing and Sintering, Marcel Dekker, Inc., New York, 1995.

Ruth, L. A.; A. M. Squires; R. A. Graff. "Desulfurization of Fuels with Half-Calcined Dolomite: First Kinetic Data," *Environ. Sci. Technol.*, **6**, 1009, (1972).

Rutkowski, M. D.; R. Zaharchuk; S.C. Jain; M. G. Klett. "Assessment of Hot Gas Cleanup Systems for IGCC and PFBC Advanced Power Systems," Final Report, January 1997, DOE Contract No. DE-AC01-94FE62747 / Task 18, Parsons Power Report No. 9607, Parsons Power Group Inc., 2675 Morgantown Road, Reading, PA, 19607-9676, USA.

Searle, A. B.; R. W. Grimshaw. The Chemistry and Physics of Clays and other Ceramic Materials, Interscience Publishers, Inc., New York, 1959.

Silaban, A.; M. Narcida; D.P. Harrison. "Characteristics of the Reversible Reaction Between CO_2(g) and Calcined Dolomite," *Chem. Eng. Comm.*, **146**, 149-162, (1996).

Siriwardane, R. V., J. A. Poston, S. D. Woodruff, "Sulfur Capture Mechanisms," Proceedings Of the Twelfth Annual Gasification and Gas Stream Cleanup Systems Contractors Review Meeting, Vol. II, Morgantown, W.V., 498-501, (1992).

Szekely, J.; J. W. Evans. "A Structural Model for Gas-Solid Reactions with a Moving Boundary," *Chem. Eng. Sci.*, **25**, 1091-1107, (1970).

van der Haam; A. G. J.; R. H. Venderbosch; W. Prins; W. P. M. van Swaaij. "Survey of Desulfurization Processes for Coal Gas," In Desulfurization of Hot Coal Gas, NATO ASI Series, A.T. Atimtay, D.P. Harrision, Eds; Vol. G 42, Springer-Verlag: New York, pp.117-136, (1996).

van der Wal, W. J. J. Desulfurization of Process Gas by means of Iron Oxide-On-Silica Sorbents, Ph.D. Thesis, Univ. Utrecht, the Netherlands, 1987.

van Houte, G.; C. Rodrique; M. Genet; B. Dehmon. "Kinetics of the Reaction of Calcium Sulfite and Calcium Carbonate with Sulfur Dioxide and Oxygen in the Presence of Calcium Chloride," *Environ. Sci. Tech.*, **15**, 327, (1981).

van Olphen, H. Clay Colloid Chemistry for Clay Technologists, Geologists, and Soil Scientists, John Wiley & Sons Inc., New York, 1977.

van Yperen, R. On the High-Temperature Desulphurization of Coal Gas; the Development of a Regenerable Absorbent, Ph.D. Thesis, University of Utrecht, the Netherlands, (1994).

Webb, P. A.; C. Orr. Analytical Methods in Fine Particle Technology, Micromeretics Instrument Corp., Norcross, GA, USA, 1997.

World Resources Institute (WRI), 'World Resources 1996-1997: A Guide to the Global Environment,'Ch.12, Date Accessed: 05/16/2003, http://www.wri.org/wri/wr-96-97/em_txt3.html.

Yagi. S.; D. Kunii. "Combustion of Carbon Particles in Flames and Fluidized Beds," Proceedings of the 5th Symposium (International) on Combustion, Reinhold, Hew York, pp.231-244, (1955).

Yang, R. T.; M. S. Shen. "Direct Evidence for the Existence of Gaseous Intermediates in the Calcium Sulfide-Calcium Sulfate Reaction," *AIChE. J.*, **25**, 547-548, (1979).

Zeng, Y.; S. Kaytakoglu; D. P. Harrison. "Reduced Cerium Oxide as an Efficient and Durable High Temperature Desulfurization Sorbent," *Che. Eng. Sci.*, **55**, 3893-4900, (2000).